UNIVERSITÀ DEGLI STUDI DI TRIESTE

XXXVII CICLO DEL DOTTORATO DI RICERCA IN

Earth Science, Fluid-Dynamics, and Mathematics. Interactions and Methods

Paleogene Mass-Transport Deposits (MTDs) from Submarine Landslides in the Julian Basin (Italy-Slovenia): mechanisms of transport, emplacement and tsunamigenic potential

Settore scientifico-disciplinare: **GEO/02**

DOTTORANDO / A
Andrea Gianese

COORDINATORE
Prof. Stefano Maset

SUPERVISORE DI TESI
Prof. Gian Andrea Pini

CO-SUPERVISORI DI TESI
Prof. Marco Franceschi
Prof. Kei Ogata

ANNO ACCADEMICO 2023/2024

Paleogene mass-transport deposits (MTDs) from submarine landslides in the Julian Basin (Italy-Slovenia): mechanisms of transport, emplacement and tsunamigenic potential

Link to the Geological Map: [https://figshare.com/s/57ea5f990e10f17cdfc5]

Abstract

Submarine landslides are significant geological phenomena characterized by the rapid downslope movement of sediment on the sea floor, often triggered by factors such as seismic activity, oversteepened slopes, rapid sedimentation, or overpressure of interstitial fluids. These events can generate substantial Mass Transport Deposits (MTDs) and Mass Transport Complexes (MTCs). The increasing sophistication of seismic and acoustic imaging technologies has revealed the widespread presence of these large remolded sediment accumulations along continental margins, underscoring their environmental, economic, and social importance.

Scientifically, research on MTDs and MTCs gives insights on the emplacement mechanisms of deep-water massive sedimentary deposits of density flows, the flow transformations during the process, and the triggers of mass-wasting events. Additionally, characterizing these sedimentary bodies in exposed sedimentary successions may serve to provide valuable stratigraphic markers, aiding in the delineation of basin morphologies and the analysis of possible syn-sedimentary tectonic movements, thereby providing deeper insights into the geological history and dynamics of sedimentary basins. Economically, they impact hydrocarbon exploration and production, while societally, they pose geohazard risks such as tsunami generation, as evidenced by catastrophic events like the 1998 Papua New Guinea tsunami (Tappin, Watts, and Grilli 2008) and the 2011 Tohoku earthquake-induced underwater landslides (Tappin et al. 2014).

In this context, the study of “fossil” MTDs (that is ancient bodies cropping out in mountain chains) has become a useful tool to better understand submarine landslide processes and deposits, integrating present-day MTDs geophysical and drillcore studies, with meso-scale to macro-scale outcrop observations and insights about mass-transport internal anatomy. However, challenges arise when attempting to compare data from these two different approaches, primarily due to resolution limits, scaling issues, and the scarcity of comparable geodynamic settings.

The Julian Basin, situated within the Julian Prealps and the Tolmin Mountains of Eastern Friuli and Western Slovenia, provides a peculiar geological setting for investigating ancient MTDs. This basin, predominantly characterized by mixed carbonate and terrigenous sedimentation, hosts numerous MTDs, referred to as "megabeds (MB)" or "megabreccia units”. This work concerns the megabeds pertaining to a sequence dated from Late Paleocene to Early Eocene. The over twenty-five MTDs (Feruglio, 1925) are embedded in a carbonate, siliciclastic, and mixed turbidites succession (Catani and Tunis 2001).

The MTD deposits are interpreted as sourced from the Friulan-Adriatic-Dinaric Carbonate Platform (Vlahović et al., 2005), which constituted the basin's passive margin extending to the southwest, south and southeast. Their origin is attributed to catastrophic resedimentation events within a deep, narrow, and elongated trough filled with turbiditic deposits. These mass-transport processes are remarkable in scale, with some lithosomes extending over 70 kilometers and reaching thicknesses exceeding 250 meters, with volumes up to 25 cubic kilometers (Catani and Tunis 2001; Tunis and Venturini, 1992).

This study focuses on the MTDs as the fossil counterparts of massive submarine landslide events. The research employs a multidisciplinary approach, integrating large-scale remote sensing, particularly the processing of extensive lidar-derived Digital Terrain Models (DTMs) and the creation and analysis of 3D photogrammetric models of outcrops, with ground-based and meso- to microscopic-scale sedimentological, stratigraphic, and structural analyses of rock sampled directly from the slide bodies. A significant outcome of this study is the correlation scenario of the sedimentary bodies within the turbiditic deposits to the southern and southeastern margin of the Julian Basin, specifically within the catchment areas of the Iudrio and Isonzo (Soča) rivers, extending towards the Bainsizza plateau. Remote sensing modeling techniques, utilizing different methods and tools, have enabled the correlation of geological features despite challenges posed by dense vegetation and significant tectonic overprinting. The resulting geological interpretation presents the most plausible current scenario for mapping and reconstructing the evolution and correlation of the megabeds within the Paleogene sequence based on our data.

Furthermore, the development and analysis of 3D photogrammetric outcrop models, created from multiple image datasets to maximize resolution, have elucidated numerous internal anatomical features of the MTDs. These features reflect the dynamics of transport and deposition within the mass-transport events. Notably, within Megabed No. 3 (MB3, or Monte Ioanaz Megabed, as named by Feruglio 1925), an internal erosive contact surface was identified and reconstructed, indicating a resumption of flow within the mass-transport complex itself. This finding supports the hypothesis that this megabed represents a composite deposit, characterized by superimposition of multiple events; they may all represent superimposition of multiple sequential processes within one event.

The calcarenitic portions of Julian Basin MTDs, known as Pietra Piasentina, are exploited as ornamental stone, with the main quarries of the area located within Megabed No. 3. The identification of internal erosive surfaces within MB3 not only advances the understanding of the sedimentary dynamics that formed these extensive deposits but also has practical implications for

geological mapping in the mining sector, potentially guiding predictions of calcarenitic unit development directions within the megabeds.

Additionally, the 3D models have facilitated the study of flow evolution within the mass-transport complexes, particularly focusing on the breccias that constitute the lower parts of the MTDs. These breccias contain clasts ranging from pebbles to olistoliths, some with volumes reaching up to hundreds of cubic meters. By interpreting the 3D models, we gained insights into the degree of destruction of flyschoid substrate blocks within the basal breccia unit of well-exposed MTDs—specifically, MB11 in Vernasso Quarry. The analyses revealed the presence of big flyschoid and marly olistoliths also in the uppermost part of the breccia unit at the interface between U2-U3 of the MTD.

Another critical aspect investigated in this study is the tsunamigenicity of the MTDs, a topic that remains contentious. The research focused on the finer-grained, topmost unit of selected MTDs to identify potential sedimentological and geochemical signatures indicative of tsunami-induced backwash deposition. Specifically, the uppermost marly part in the Lastivnica megabed (Anhovo Quarry) contains fine-grained thin-bedded turbidites (TBT) distinct from the surrounding lithology. Elemental analyses using portable X-ray fluorescence (p-XRF) and Inductively Coupled Plasma (ICP) techniques revealed compositional differences between these deposits and the enclosing megabeds. In particular, the content of siliciclastic mineral phases was found to be higher compared to the host rock, indicating a greater continental contribution relative to the enclosing marly deposits. Scanning Electron Microscope (SEM) investigations of heavy minerals confirmed these analyses, indicating not only a different deposition process geologically contemporaneous with the deposition of the MTD but also the contribution of a different sediment source. However, the so-called "smoking gun" that is the definitive proof to associate these deposits and their possible continental contamination with a tsunamigenic trigger, was not found.

Despite the absence of this evidence, the analyses on the MTD top showed intriguing findings regarding the deposition processes within the uppermost unit and its organic carbon content.

Thin sections from various stratigraphic heights of the uppermost Lastivnica unit exhibited traction structures within deposits that were thought to be massive, suggesting the possible presence of ponding effects. Moreover, an attempt of image analysis of organic carbon content was performes and compared Total Organic Carbon (TOC) analyses of the same samples, showing interesting responses and future potential.

Table of Contents

1- Introduction

1.1 - Why do we study (subaqueous) MTDs?

Subaqueous mass transport deposits (MTDs) are sedimentary units and bodies generated by the gravitational downslope movement of sediments in underwater environments, including marine and lacustrine settings (Hampton et al., 1996; Mulder & Cochonat, 1996; Alves et al., 2022). These gravity-driven processes encompass a spectrum of phenomena such as submarine landslides, slumps, slides, debris flows, mud flows, and rockfalls, which can transport substantial amounts of sediment across continental margins into deep-sea basins (Nardin et al., 1979; Lee, 2005; Urgeles & Camerlenghi, 2013), and play an important role in shaping seafloor morphology and sediment distribution into depositional basins (see, e.g., Embley, 1980; Lastras et al., 2003; Alves and Cartwright, 2010; Kneller et al., 2016). Understanding the mechanisms and characteristics of MTDs is crucial for interpreting past geological events and predicting future sedimentary processes in these dynamic environments. Investigating MTDs is essential also due to their impact on geohazards, hydrocarbon exploration, and environmental issues, such as the global carbon cycle.

Submarine mass movements pose considerable risks to coastal communities and offshore infrastructure from a geohazard perspective (see Masson et al., 2006; Festa et al., (Eds.) 2014). Indeed, large-scale submarine landslides have the potential to trigger tsunamis comparable in magnitude to those caused by seismic activity (Harbitz et al., 2014; Satake, 2012). Historical events such as the 1998 Papua New Guinea tsunami, induced by an earthquake-triggered landslide that claimed over 2,000 lives (Tappin et al., 2008), and the Tohoku earthquake in 2011 (Tappin et al., 2014; Kawamura et al., 2012, 2014), which also trigger underwater landslides, highlight the necessity for comprehensive studies on these phenomena to enhance our understanding of their mechanisms and potential impacts. By integrating geological, oceanographic, and engineering perspectives, researchers can develop more effective risk assessment models and mitigation strategies to protect vulnerable regions from future disasters. Furthermore, advancements in remote sensing technology and numerical modeling can aid in predicting the behavior of such landslides and their subsequent effects on coastal communities.

In addition to their tsunami-generating potential, MTDs can disrupt undersea infrastructure (e.g. telecommunication cables and pipelines), due to their extensive runout distances and destructive

force (Carter et al., 2014). The 1929 Grand Banks event off the coast of Newfoundland serves as a classic example, where an earthquake-induced submarine landslide and associated turbidity currents led to multiple cable breaks, providing early insights into the dynamics of such currents (Heezen & Ewing, 1952; Piper et al., 1999). As offshore development expands—with increasing installations of oil and gas facilities, wind farms, and communication networks on the seabed—it becomes increasingly important to understand and mitigate the risks posed by MTDs (Carter et al., 2014).

From sedimentological and geological perspectives, mass-transport deposits represent fundamental events in the evolution and shaping of continental margins and deep-sea systems. They are primary agents in the redistribution of sediments from continental shelves to deeper ocean areas, influencing basin stratigraphy and depositional patterns (Piper et al., 1997; Alves et al., 2014). MTDs can constitute a significant proportion of sedimentary deposits on continental slopes and affect the distribution of sedimentary facies (Huhn et al., 2019; Nardin et al., 1979).

Their complex internal structures and depositional properties present both challenges and opportunities for hydrocarbon exploration; indeed, MTDs can act as reservoirs or seals within petroleum systems, potentially enhancing exploration potential of basins (Weimer & Shipp, 2004; Cardona et al., 2016). However, their heterogeneous nature and overconsolidation potential can also pose risks to drilling operations (Shipp et al., 2004). Understanding geomechanical properties of MTDs is crucial for mitigating these risks and optimizing extraction strategies, as it allows for better prediction of their behavior under stress and as fluid migration pathways (Alves, 2015).

Moreover, MTDs have significant implications for the global carbon cycle and environmental processes. They play a crucial role in the preservation of organic material and the subsequent storage of organic carbon in marine environments. The emplacement dynamics of MTDs, involving rapid sedimentation rates and swift burial of organic-rich material, create favorable conditions for the accumulation and long-term preservation of organic carbon (Gan et al., 2022; Meilijson, 2023). This fast sequestration process plays a fundamental role, as it effectively prevents the oxidation of carbon and its release back into the atmosphere, influencing biogeochemical cycles (Meilijson, 2023). Moreover, the interplay between sediment composition and microbial activity further influences the degradation rates of organic carbon, highlighting the complexity of these systems and their responses to environmental changes. Understanding these processes is essential for assessing past and present carbon cycle in marine systems.

Slope collapses and the related mass transport processes can be triggered by gas hydrate dissociation (Piper et al., 1997; Maslin et al., 1998; Liu et al., 2024), in turn caused by sea level change or seismic events. This relation is threefold, since the dissociation of gas hydrates can be

triggered by large scale slope collapse and MTDs can be the loci of gas hydrates accumulation (Bhaumik et al. 2024)

Present-day submarine landslides and associated mass transport deposits are studied using mainly geophysical techniques, while fossil MTDs outcropping in different parts of the world can be investigated with direct observations in the field.

Despite advancements in geophysical imaging techniques, such as high-resolution seismic reflection profiling, which have enhanced our ability to identify and characterize these deposits (Bull et al., 2009; Alves, 2015), the combined approach with geophysical data interpretation, borehole core studies, and outcrop perspectives is essential for a comprehensive understanding of MTDs complex dynamics:

- geophysical data provide insights into the overall morphology and areal extent of MTDs, but often lack resolution regarding their internal structures due to inherent limitations in imaging techniques (Ogata et al., 2014a)
- The study of borehole cores, enhanced by the present-day availability of x-ray CT scan data and image analysis of half-core cuts, is a fundamental tool for understanding the geophysical data and to characterize smaller scale structures inside the MTDs (Tripsanas et al., 2008; Strasser et al., 2011; Kanamatsu et al., 2014; Bahk et al., 2017). They are, however, strongly limited by the small dimension of the observable sections and the poor availability of cores.
- conversely, outcrop studies allow for detailed observations of micro- to meso-scale structures, sediment transport dynamics, depositional mechanisms and kinematic evolution, which are crucial for understanding the initiation and transport processes involved in landslide events (Ogata et al., 2014a, 2014b; Ogata et al., 2019).

This synergic approach helps to bridge the knowledge-gap in the characterization of submarine landslides at different scales and aids in improve forecasting and mitigating geohazards (Ogata et al., 2014b; Ogata et al., 2019), as well as the understanding of deep-sea systems, carbon cycle in the Earth's oceans and MTDs resource potential.

2 - State-of-the-art

2.1 - Terminology overview

The study of mass-transport processes ("en-masse" processes), led to various classifications (e.g., Nardin et al. 1979; Shanmugam 1996; Tappin 2010; Varnes 1958) with subsequent creation of numerous terms and definitions, sometimes used as synonyms (Shanmugam and Wang 2015).

In this chapter, an analysis of some of these terms is conducted with the effort to clarify their usage within the context of this thesis work.

2.1.1 - Submarine Landslide

Landslides are defined as downward and outward movements of slope-forming materials, wherein shear failure occurs along one or several surfaces (Eckel, 1958; Schuster & Krizek, 1978). Submarine landslides represent the marine counterpart of subaerial mass-movements. They are some of the most significant natural events on Earth, occuring in various settings, including both active and passive continental margins (Urgeles & Camerlenghi, 2013; Camerlenghi & Pini, 2009; McAdoo et al., 2000) within submarine canyons (Harishidayat et al., 2024; Micallef et al., 2012; He et al., 2014) and submarine deltas (Coleman et al., 1978). These events can move up to a thousand times more material than their analogues on land (Hampton et al., 1996). They can occur on low slopes with gradients below 2 degrees and can travel distances exceeding 1,000 kilometers (Urgeles & Camerlenghi, 2013) (Fig.2.1).

The term "megaslide" is sometimes use to identify large-scale landslide events that transport massive volumes of sediment downslope. These events can lead to the formation of megabeds (see definition below) when the displaced material settles as a basin-wide marker (Ogata et al., 2019). The Paleogene megabeds in the Julian-Slovenian Basin, for instance, are the result of catastrophic carbonate platform collapses, indicating a megaslide origin (Ogata et al., 2019).

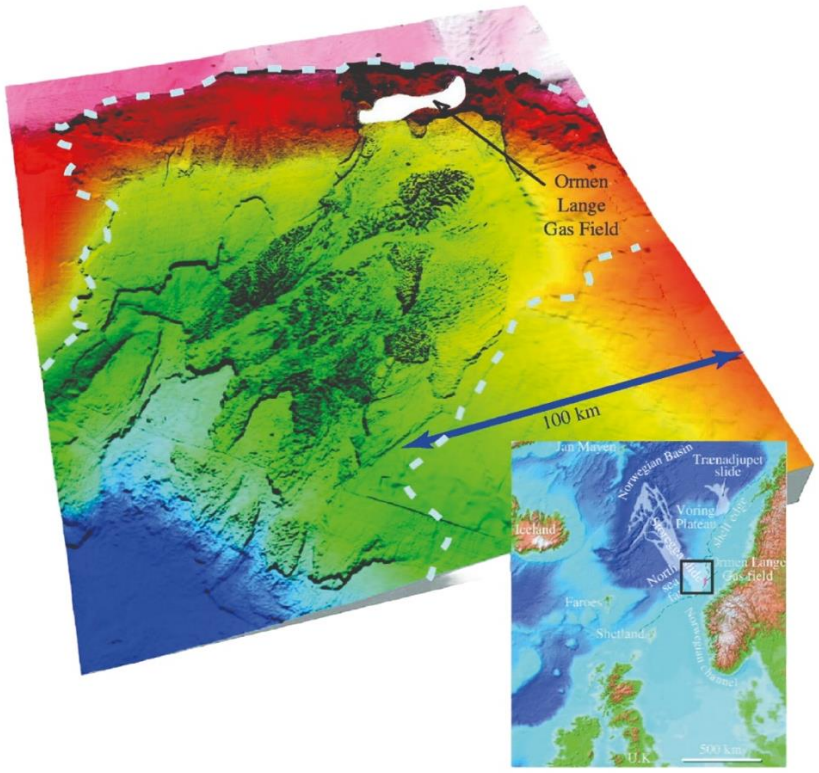

Figure 2.1 Storegga submarine landslide (modified from Bryn et al., 2005)

2.1.2 - Mass-Transport Deposit (MTD)

The term "mass-transport deposit" (MTD) refers to sedimentary deposits formed by the rapid movement of materials, typically resulting from gravitational forces acting on unstable slopes or submarine landslides (Hampton et al., 1996; Lamarche, 2008), which include processes like creep, slides/slumps, mudflows, and debris flows. These deposits often exhibit characteristics such as chaotic bedding, disrupted strata, and a lack of sorting, reflecting rapid movement and deposition (Shanmugam, 2000). However, not all MTDs are chaotic; some may feature folded but coherent bedding, while others, such as slides, can preserve large portions of apparently undisrupted bedding. These may be challenging to identify in the subsurface, as they may display dips only slightly steeper than the surrounding strata but often with subtly or entirely different strike directions. Non-

cohesive flows, such as turbidity currents, concentrated density flows, and hyperconcentrated density flows (Mulder & Alexander, 2001), are not included. However, it should be clarified that, although turbidity currents and mass-transport deposits (MTDs) are different in terms of processes, a turbidity current can represent the final evolutionary stage of the movement of a mass-transport deposit toward the depocenter of a sedimentary basin (Mulder & Alexander, 2001). Indeed, field-based research demonstrates that fluid overpressure can aid in the transition from discrete, coherent movement to uniform, cohesive flow in mass transport processes. This transformation goes with the gradual disintegration of sediment blocks and the seafloor (e.g., Ogata et al., 2012; Ogata et al., 2014a, 2014b). These data are coherent with the concept of mass-transport process evolution, progressing from sliding and slumping to blocky flow, debris flow, turbidity flow and deposition (Mutti et al., 2006; Festa et al., 2016).

MTDs are fundamental elements in the construction and destruction of orogenic belts; indeed they are systematically recorded in different phase of the Wilson cycle and may represent basin-wide stratigraphic markers (Shanmugam, 2000; Camerlenghi & Pini, 2009).

The term "mass-transport deposit" emerged in geological literature in the late 20th century as a seismostratigraphic definition to describe sedimentary deposits formed by submarine mass-wasting events (Weimer, 1989). Before that, previous authors highlighted the significance of mass transport in redistributing deep-sea sediments (e.g. Embley, 1980) and provided foundational insights into sediment gravity flows processes (Middleton & Hampton, 1973; Nardin et al., 1979; Lowe, 1979), which leading to MTDs formation, although they did not specifically use the term "mass-transport deposit".

The increased interest in submarine mass movements during this period led to a better understanding of the depositional processes and the importance of MTDs in the geological record, but they also shew insights on the real complexity of these deposits.

2.1.3 - Mass-Transport Complex (MTC)

While the terms Mass Transport Deposit (MTD) and Mass Transport Complex (MTC, Weimer, 1989) may occasionally have been used interchangeably in geological literature, they have distinct connotations. The "mass-transport complex" (MTC) concept was introduced to characterize large-scale assemblages of MTDs that may represent the cumulative deposits of multiple, often indistinguishable, mass-wasting events (Moscardelli et al., 2006). Their intricate internal

architectures, difficult to disentangle even at the outcrop scale, result from the interplay of various mass-wasting processes and the subsequent reworking of sediments during transport (Shanmugam, 2000).

2.1.4 – Megaturbidite

Bouma (1987) defines a megaturbidite as a thick, extensive, and relatively homogeneous sedimentary deposit formed by a turbidity current. According to this definition, a megaturbidite must:

- be significantly thicker than the surrounding turbiditic deposits.
- exhibit substantial lateral extent across the depositional basin.
- possess a lithological composition that differs, at least partially, from the adjacent sedimentary succession.
- display internal characteristics that indicate deposition from a single event, even if multiple depositional processes were involved.

These attributes make megaturbidites excellent synchronous stratigraphic markers, facilitating correlation and interpretation of sedimentary sequences along the entire basin.

In this thesis, the term will be used with the aforementioned meaning, but it should be take into account that some authors have used “megaturbidites” as a synonym for "’submarine landslides” (Shanmungam, 2020).

2.1.5 – Megabreccia

Megabreccia is a comprehensive term encompassing the outcomes of significant catastrophic events caused by gravitational instability, including both slides and slumps. It involves seafloor sediment that has undergone lithification or partial lithification, which can move in two ways: as large coherent blocks (megablocks) exhibiting brittle behavior, or as debris flows carrying large boulders within a disaggregated matrix with greatly reduced shear strength, displaying plastic behavior. Sometimes, a combination of both movements occurs (Spence & Tucker, 1997). The size of megablocks (olistoliths) can vary from less than one meter to hundreds of meters, and they can be transported up to tens of kilometers towards the basin (Mountjoy et al., 1972).

Megabreccias are distinct from grain flow and turbidity current deposits, which are composed of loose particulate sediment flows (Lowe, 1982). However, megabreccia flows may transform into turbidity currents as sediment breaks apart and incorporates more water during transport and flow evolution (e.g. Fallgatter et al., 2017). They generally show greater variety in lithology and are considerably larger in both volume and lateral extent towards the basin.

2.1.6 – Megabed

In literature, the definition of megabed is not consistent. Bouma (1987) define it as a bed which must reach a critical thickness or, at least, be significantly thicker than other layers. For authors, a megabed is a layer with thickness several orders of magnitude bigger than the surrounding succession (Mutti et al., 1984). Following the criteria outlined by (Catani & Tunis, 2001), in the frame of this work, megabeds s.s. are the MTDs which reach the thickness of 15-20m and present a lower breccia unit with a megaturbidite on top.

2.1.7 - Mass-Wasting Deposit

The term indicates the downslope movement of large amounts of detrital material by gravity (Cheriminosoff, 1997). Mass-wasting processes include debris flow, landslides, and creep (Rahn, 2005).

In their article "The Landslide Problem," Shanmugam and Wang (2015) cite various terms that have, at times, been used interchangeably in the literature on mass transport phenomena, though this usage is neither universal nor without contention. For instance:

- Landslide = slope movement = mass movement = mass transport = mass wasting
- Submarine landslide = megaturbidite = seismo turbidite (Mutti et al. 1984) = homogenite
- Mass-transport complex (MTC) = mass-transport deposit (MTD) = submarine mass failure (SMF)
- Translational landslide = translational slip = block slide = glide = slide

- Rotational landslide = rotational slip = toreva block = slump
- Muddy debris flow = mud flow = cohesive debris flow = slurry flow = mass flow
- Debrite = olistostrome = sedimentary mélange
- Sandy debris flow = granular flow = cohesionless debris flow = density-modified grain flow = cohesionless liquefied sandflow = grain flow = mass flow = high-density turbidity current = hyperconcentrated flow = slurry flow = hybrid flow
- Flow slide = liquefaction slide
- Rock avalanche = debris avalanche = sturzstrom
- Sand fall = cascading dense-water event = sand avalanche = grain flow = mass flow.

It is important to note, however, that many of these so-called equivalences are debated and may not hold in all contexts. Differences often arise from the specific genetic and descriptive frameworks employed.

Among the terms listed above, this thesis will primarily use “mass-transport deposit (MTD).” However, this chapter also examines several other commonly used and important terms in the field.

2.1.8 - Olistostrome and sedimentary mélange

"Olistostrome" and "sedimentary mélange" (mélange [French] = “mixture”) are considered synonyms and refer to the products of ancient underwater mass-transport events in orogenic belts (see, e.g., Ogata et al., 2019).

Mélange is a term that has been introduced by Greenly (1919) as “autoclastic phyllite-and-grit mélange” to define a stratigraphic sequence pertaining to the geology of the Isle of Anglesey (Wales) disrupted by tectonic deformation. Following Greenly’s definition: “The essential characters of an autoclastic mélange may be said to be the general destruction of original junctions, whether igneous or sedimentary, especially of bedding, and the shearing-down of the more tractable material until it functions as a schistose matrix in which the fragments of the more obdurate rocks float as isolated lenticles or phacoids.” (Greenly, 1919, pag. 193). The term mélange has been reintroduced by Hsü (1968) for highly disrupted to block-in-matrix rocks of the Franciscan Complex in California, reaching a worldwide resonance. Although the term has been coined

referring to a tectonic byproduct, it is now recommended to be used as a non-genetic, descriptive term for block-in-matrix units with a mixing of rocks with different age, composition and provenances (Silver and Beutner, 1980). A similar kind of block-in-matrix rocks, but lacking the attribute of mixing of different rocks are the “broken formations” (Hsü, 1968; Raymond, 1984). The fundamental dichotomy between mélanges and broken formation (see, e.g., Festa et al., 2010, 2012 and following papers) seems to be more applicable to tectonic mélanges.

Flores (1955) (qtd. in Abbate et al., 1970) coined the term "olistostrome" to describe sedimentary deposits found within regularly stratified geological sequences, characterized by a mix of different materials in terms of lithology and/or petrography, deposited by a semifluid mass. These formations frequently contain various-sized blocks (known as exotic blocks), ranging from small pebbles to massive boulders, reaching volumes of several cubic kilometers (olistoliths). These blocks are surrounded by a fine-grained matrix (block-in-matrix fabric), reflecting the chaotic nature of the deposit (Ogata et al., 2019). Olistoliths in the original definition of Flores are the largest, out-size blocks (see also “floaters” Festa et al., 2019) included into the sedimentary bodies of olistostromes. The term has over time been extended well beyond the original meaning, comprising single blocks or groups of blocks (olistoliths swarms) dispersed in normal bedded sediments.

However, “sedimentary mélange” represents only a part of the wider definition of “mélange”. Indeed, the internal chaotic block-in-matrix fabric could be the result of different processes, such as (Festa et al., 2010; Silver and Beutner, 1980):

- tectonic disruption (tectonic mélanges),
- mass transport (sedimentary mélanges),
- diapirism and fluid expulsion (diapiric mélanges),

and their interplay.

As stated in Festa et al, 2010 the adjective "sedimentary" in this context encompasses all processes related to slope failure, sediment transport, and deposition, with a particular emphasis on en-masse gravitational movement and deposition of both unconsolidated sediments and rocks, collectively referred to as mass-wasting or mass-transport processes and their resulting bodies. This definition also includes the outcomes of in situ or minimally translated gravity-induced deformation along basin slopes, such as creeping and gravitational spreading, which are classified under "slope tectonics".

Following the above definition, we can define “megabreccia” as a “sedimentary mélange”.

2.1.9 – Seismoturbidite

According to Mutti (1984), seismoturbidites are large, repetitive megaturbidite deposits found in highly tectonically active basins. These deposits make up a significant volume within otherwise "typical" turbidite sequences, composed of smaller-scale, gravity-driven sediment flows, and are indicative of seismic activity.

Key characteristics that suggest a seismoturbidite origin include a substantial volume (approximately 1 km³ or more) and extensive horizontal coverage relative to the basin width, which reflects the influence of lateral confinement on sediment flow.

While not all turbidites qualify as seismoturbidites, the size and geometry are important indicators of their seismic origin.

Additionally, the presence of seismoturbidites highlights areas of active paleoseismicity and ongoing resedimentation processes at basin margins.

2.1.10 - Homogenite

The term "homogenite" has been used in multiple senses.

Rodiguez et al., 2020 described it as the final product of deformation and homogenization of sediments remobilized by a mass flow event, consisting of matrix (the result of complete disaggregation of unlithified to poorly lithified sediments) and, when present, extrabasinal rigid clasts.

Kastens and Cita (1981), Cita et al. (1984) called "homogenites" thick, seismic-transparent units found in deep central-eastern Mediterranean. Each of these beds represents the sedimentary expression of a unique event with a definite stratigraphic position and are interpreted as turbidites (Shanmugam, 2006). That's the definition used in this work. Indeed, combining the descriptions purposes by different authors, the term "homogenite" is here referred to fine-grained turbidite and megaturbidite deposits, up to meters or tens of meters thick (Shinki and Cita, 2008; 2020), with a sandy or sandy-silty base and a muddy upper division (Cita et al. (1996); Reeder et al. (1998);

Mulder et al., 2009), macroscopically homogeneous and lacking apparent sedimentary structures, which occupies as much as two thirds of up to some tens of meters of the entire bed (Shinki and Cita, 2008).

2.1.11 - Tsunamite

The term "tsunamiite" refers to sediments that have been transported and deposited by tsunami events. Initially coined as "tsunamiite" by Yamazaki et al. in 1989 to describe Miocene tsunami-worked boulder sediments in Japan, the spelling was later corrected to "tsunamite" by Shiki and Yamazaki in 2008.

This term is used not only for sediments directly transported by a tsunami but also for those moved by tsunami-induced currents, distinguishing it from other sedimentary deposits like "turbidites," which do not specify the trigger mechanism for sediment transport (Shiki & Yamazaki, 2008).

Tsunamites are characterized by their formation through a threshold mechanism (tsunami event deposits) similar to "tempestites" (storm deposits (Kellig and Mulin, 1975; Aigner, 1980; Allen, 1981)) and "seismites" (deposit deformed by seismic shaking (Moretti et al., 1999, 2010; Marco and Agnon, 2005; Mazumder et al., 2016)). They can include deposits like the Mediterranean homogenite (Kastens and Cita, 1981; Heike, 1984; Shiki and Cita, 2008), which are interpreted to be triggered by tsunamis during their downslope flow and plume up of fine-grained sediments (Shiki & Yamazaki, 2008).

The study of tsunamites represent a complex theme, partly due to the need for a systematic procedure to interpret sedimentary records of tsunamis induced by various triggers such as earthquakes, submarine slides, volcanic eruptions, and meteorite impacts (Shiki et al., 2008).

Unlike deposits such as turbidites, which are classified based on sedimentary features, tsunamites are often identified based on historical evidence of tsunamis, which is not always available for prehistoric events. This reliance on historical evidence rather than sedimentological characteristics makes it difficult to establish definitive criteria for identifying tsunamites in the geological record (Shanmugam, 2006). Additionally, the depositional processes associated with tsunamis involve a complex interplay of various flows and sediment transport mechanisms, which can result in deposits that are difficult to distinguish from those formed by other high-energy events (Cantalamessa & Celma, 2005; Santa Catharina et al., 2022).

2.2 - MTDs Occurrence, Triggers and Mechanisms

2.2.1 - Occurrence

Submarine landslides present the same classification-type of similar subaerial landslides (Varnes, 1978), because many of the processes involved are the same. But their dimension is 2-3 orders of magnitude bigger than the subaerial counterpart (see Crandell et al., 1984; Roberts & Evans, 2013; Bryn et al., 2005; Moore et al., 1989; Dingle, 1977 for some quantitative examples).

Large-scale submarine landslides (> 1 km^3; Urlaub et al., 2013; Pope et al., 2015) are widespread all over the world in every continental margin (Tappin, 2010)(Fig.2.2), also at low-slope gradient (< 2°) and especially where there's large sedimentary input (Urlaub, 2015).

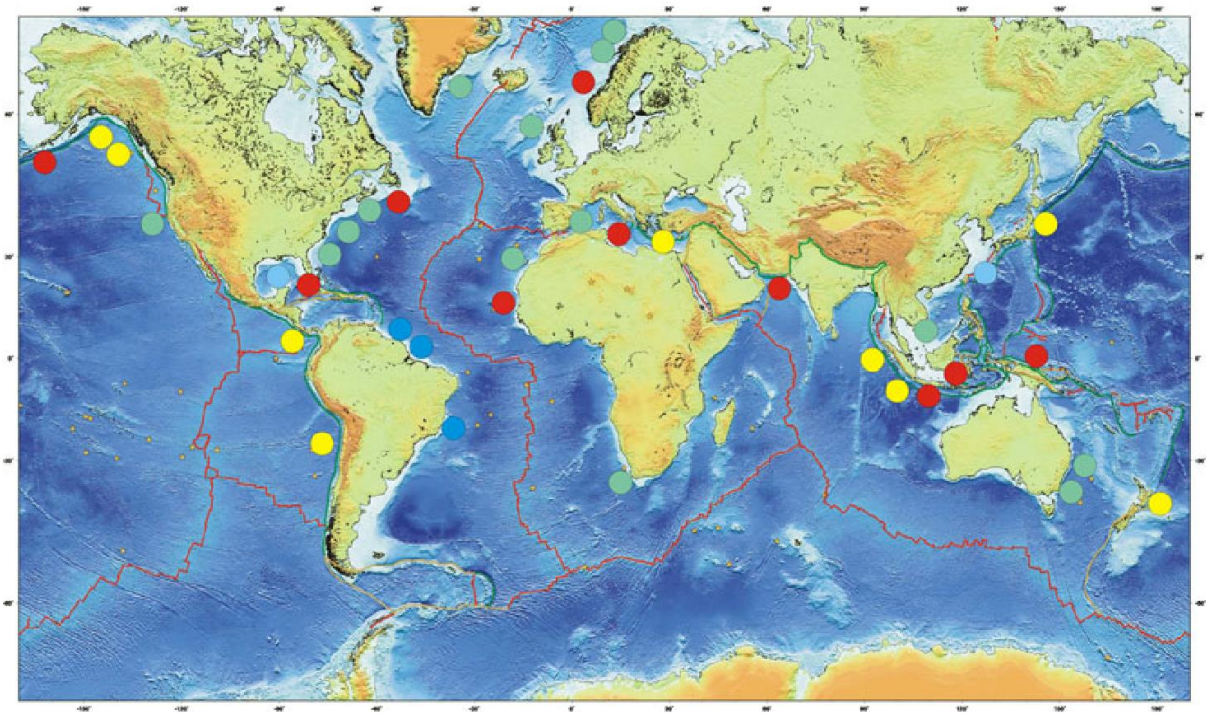

Fig. 2.2 Global distribution of mapped Submarine landslides. Green dots: submarine landslides on continental shelves and fan systems, no identified tsunami. Yellow dots: submarine landslides located along convergent margins, no identified tsunami. Red dots: locations of submarine landslide-sourced tsunamis, or where there may be a landslide contribution. Grey-blue dots, active river systems, no tsunami identified. From Tappin (2010)

Their fossil counterparts have been observed in both active and passive margin settings too (Festa et al., 2010; Ogata et al., 2019).

However in contemporary environments, the majority of mass transport deposits (MTDs) are found in passive margin settings (e.g., Macdonald et al., 1993; Mienert et al., 2003; Camerlenghi & Pini, 2009). In contrast, sedimentary mélanges associated with active margins are predominantly identified within exhumed subduction-accretion complexes. Additionally, modern continental margin MTDs and mass transport complexes (MTCs) tend to be significantly larger than their ancient ("fossil") counterparts (Woodcock, 1979).

This discrepancy, often referred to as a “paradox,” can be partially solved taking into account that these deposits may result from either single depositional events (MTDs) or from multiple, successive events forming composite structures (MTCs) (Heck & Speed, 1987; Macdonald et al., 1993; Lucente & Pini, 2003; Ogata et al., 2012a, 2012b, 2014a; Pini et al., 2012). This reinterpretation aligns the size, distribution, frequency, and runout distances of ancient deposits with those of some modern submarine slide complexes across various tectonic environments (Camerlenghi & Pini, 2009; Festa et al., 2010a; Ogata et al., 2014a; Calvès et al., 2015).

Furthermore multiple factors influence the preservation of MTDs and MTCs in orogenic belts geological record:

- Slide-Flow Transformation During Transfer and Emplacement: The manner in which slide materials transform and are deposited plays a crucial role in their preservation.
- Volume of Failed Material: The amount of material involved in the landslide affects the likelihood of its preservation.
- Type and Magnitude of Overprinting Tectonic Deformation: Subsequent tectonic activities can alter or obscure the original depositional features, impacting preservation (Festa et al., 2016; Ogata et al., 2019)

2.2.2 - Triggers

Submarine landslides occur when the applied shear stresses on underwater slopes surpass the shear strength (τ) of the slope sediments (e.g., Løseth, 1999; Sultan et al., 2004a). These shear stresses can arise from various sources, including gravity, seismic shaking, and wave loading. Understanding the development of submarine landslides requires distinguishing between

preconditioning factors that make slopes susceptible to failure and trigger mechanisms that initiate the actual slope movement.

Preconditioning factors are inherent characteristics of the submarine slope that predispose it to failure. These factors establish the conditions necessary for a landslide but do not directly cause the failure:

- Tectonic Oversteepening: One of the primary preconditioning factors is tectonic oversteepening, where tectonic movements increase the slope angle, thereby enhancing the gravitational forces acting on the sediment (Callot et al., 2008; Gamberi et al., 2011). Oversteepening does not immediately trigger a landslide; instead, it serves as an important precursor by making the slope more susceptible to failure under additional stresses.

- Mechanically Weak Layers: The presence of mechanically weak layers within the slope stratigraphy is another crucial preconditioning factor. These layers, which may consist of soft clays (e.g., Kvalstad et al., 2005; Dan et al., 2007), loose granular silts and sands (e.g., L'Heureux et al., 2012), layers with free gas (Best et al., 2003), high-porosity ash layers (e.g., Kuhlmann et al., 2016), or altered volcanic deposits with high liquefaction potential (Miramontes et al., 2018), inherently possess lower shear strength. The sequencing of these layers with varying physical properties, particularly their permeabilities, influences the localization of failure surfaces. For instance, high-permeability sediments sandwiched between low-permeability layers can inhibit pore fluid escape, leading to overpressure buildup (Dugan & Sheahan, 2012).

- Sediment Properties and Diagenesis: Intrinsic sedimentary characteristics, such as those of contourites—sediments deposited by oceanic bottom currents—can also predispose slopes to instability (Laberg & Camerlenghi, 2008; Verdicchio & Trincardi, 2008; Miramontes et al., 2016). Additionally, processes like sediment compaction and diagenesis (chemical changes post-deposition) can weaken sediment strength over time (Volpi et al., 2003; Davies & Clark, 2006).

Trigger mechanisms are external or internal events that induce the actual failure of a preconditioned slope. These mechanisms typically cause a rapid decrease in shear strength, leading to slope movement:

- Transient Pore Pressure Increases: The most effective trigger mechanism is a transient increase in pore pressure (Δu) within the slope sediments. According to the effective stress principle, $\tau = \mu(\sigma n - \Delta u)$, where σn is the overburden stress and μ is the coefficient of friction (Pestana et al., 2000; Talling et al., 2014). An increase in pore pressure reduces the effective stress, thereby decreasing the shear strength and potentially triggering a landslide. Common processes that elevate pore pressure include:
    - Rapid Sedimentation and High Sedimentation Rates (>mm/yr): Quick deposition of sediments can lead to excess pore fluid generation (Hampton et al., 1996; Sultan et al., 2004b).
    - Tectonic Loading and Earthquakes: Seismic shaking can cyclically load the slope, increasing pore pressure transiently (Urgeles & Camerlenghi, 2013; Hsu et al., 2018).
    - Tidal Variations: Fluctuations in sea level can alter pore pressures within sediments (Løseth, 1999).
    - Mineral Dehydration and Gas Hydrate Dissociation: Thermal and chemical changes can release fluids, increasing pore pressures (Locat & Lee, 2009; Dugan & Sheahan, 2012; Urgeles & Camerlenghi, 2013; Hsu et al., 2018).

- Seismic Triggering and Strengthening: While earthquakes are commonly cited as triggers for submarine landslides (ten Brink et al., 2016), their role is complex. Repeated seismic events can both trigger landslides by increasing pore pressure and strengthen sediments through densification during periods of drainage. This dual effect explains why most modern giant landslides are observed at passive margins rather than active margins: at passive margins, the frequency and intensity of seismic events are generally lower compared to active margins, but the repeated shaking can still lead to the gradual densification and strengthening of the sediments over time (Kvalstad et al., 2005; Masson et al., 2006). This

strengthening effect can make the sediments more resistant to failure, even in the presence of occasional high-magnitude earthquakes.

- In contrast, at active margins, the higher frequency and intensity of seismic events can repeatedly trigger landslides by increasing pore pressure, but the sediments may not have the opportunity to undergo the same degree of densification and strengthening. This can result in a more dynamic and unstable slope environment, where large-scale landslides are less likely to develop and persist over time.
- Gas Hydrate Dissociation and Climate Change: Climate change-induced gas hydrate dissociation is another potential trigger mechanism. Gas hydrates, which are solid compounds of methane and water present in marine sediments within a certain range of pressures and temperatures, are sensitive to changes in both (Brewer et al., 1998). Warming of deepwater environments can cause hydrate dissociation, leading to pore pressure buildup and sediment weakening (Kennett et al., 2003; Grozic, 2010). However, the exact mechanisms and their interplay with slope failure remain poorly understood (Riboulot et al., 2018).

2.2.3 - Mechanisms

(R. H. Dott, Jr. (2) 1963) classified the comprehensive mechanical behavior of subaqueous processes in 4 different types: elastic (rockfall), elastic and plastic (slide and slump), plastic (debris flow), viscous (Newtonian turbidity current). However, these types represent part of a broad continuum of processes and products, which commonly reflects the along-slope flow transformation due to the increase of mass-disaggregation with subsequent variation in sediment concentration and flow dilution (Fig.2.3).

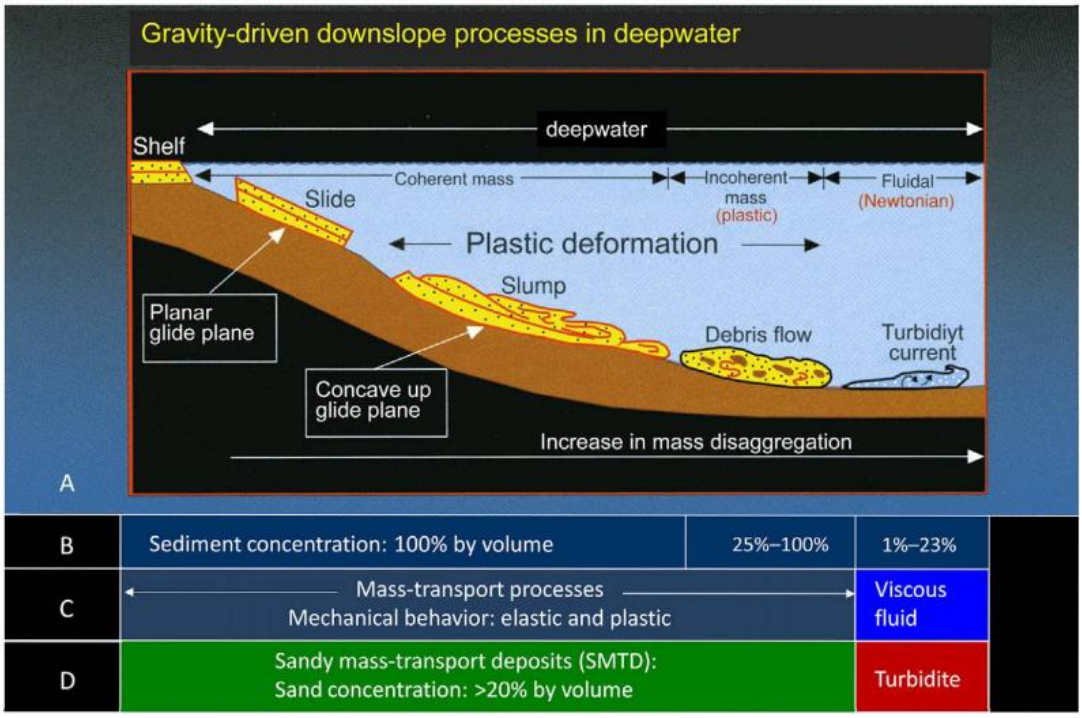

Fig. 2.3 (A) Diagram of four endmembers of gravity-driven downslope processes transporting sediment into deep marine environments: slides, slumps, debris flows, and turbidity currents. Classification based on: (B) sediment concentration (% by volume), (C) mechanical behavior, (D) sand concentration. From Shanmugam (2021).

The core principle of (R. H. Dott, Jr. (2) 1963) classification lies in distinguishing between solid and fluid modes of transport based on sediment concentration. Solid transport mechanisms, which include slides, slumps, and debris flows, typically involve high sediment concentrations ranging from 25% to 100% by volume. These processes are characterized by the movement of solid blocks or aggregates of particles, making them highly efficient for downslope sediment transport (Lucente 2003; R. H. Dott, Jr. (2) 1963). Conversely, turbidity currents involve low sediment concentrations (1% to 23% by volume), where individual particles are suspended by fluid turbulence, resulting in lower flow densities (R. H. Dott, Jr. (2) 1963; Sanders 1963).

About the internal forces acting in subaqueous processes, Middleton and Hampton (1973) identified four main mechanisms of grains support involved: turbulence, upward intergranular flow, grain-to-grain interaction, matrix (mixture of interstitial fluid and fine sediments, (Dasgupta 2003)) strength. The prevalence of one (or some) of these mechanisms over the others was linked to different types of final deposit (Fig.2.4).

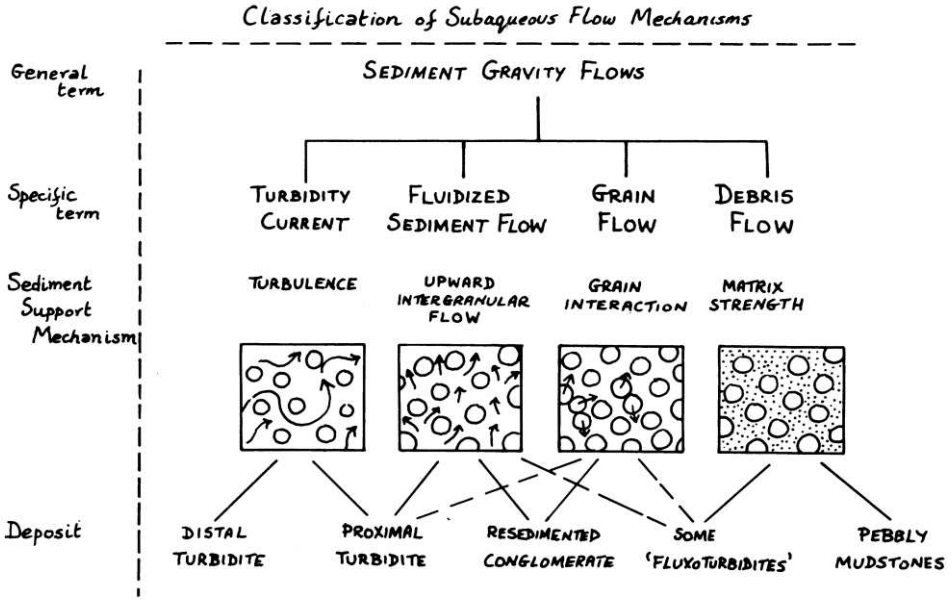

Fig. 2.4 Classification of subaqueous flow mechanisms. From Middleton and Hampton (1973)

Despite that, all of them act in the major MTD-bodies.

2.3 - Submarine landslides and tsunamis

Submarine landslides generate tsunamis primarily through the rapid, vertical displacement of the water column above the failure site rather than simply by pushing water upward. As sediment or rock masses fail and move downslope, they create a sudden depression at the seafloor, which leads to a compensatory flow of surrounding water into the void. This process initiates one or more waves that propagate away from the source region as shallow-water waves, capable of long-range travel with minimal energy loss (McMurtry et al. 2004; Tappin 2017). The scale and energy of these tsunamis depend on factors such as the volume, speed, and geometry of the landslide, as well as the water depth and seafloor slope (Harbitz et al. 2006). In shallower waters, there is less water available to absorb the disturbance, often resulting in larger and more destructive waves impacting nearby coastlines (Ward 2001).

Tsunamis can be triggered both by earthquakes and submarine landslides; however the physical characteristics, mechanism and scale of the two types of waves are different (Harbitz et al. 2006)(Fig.2.5).

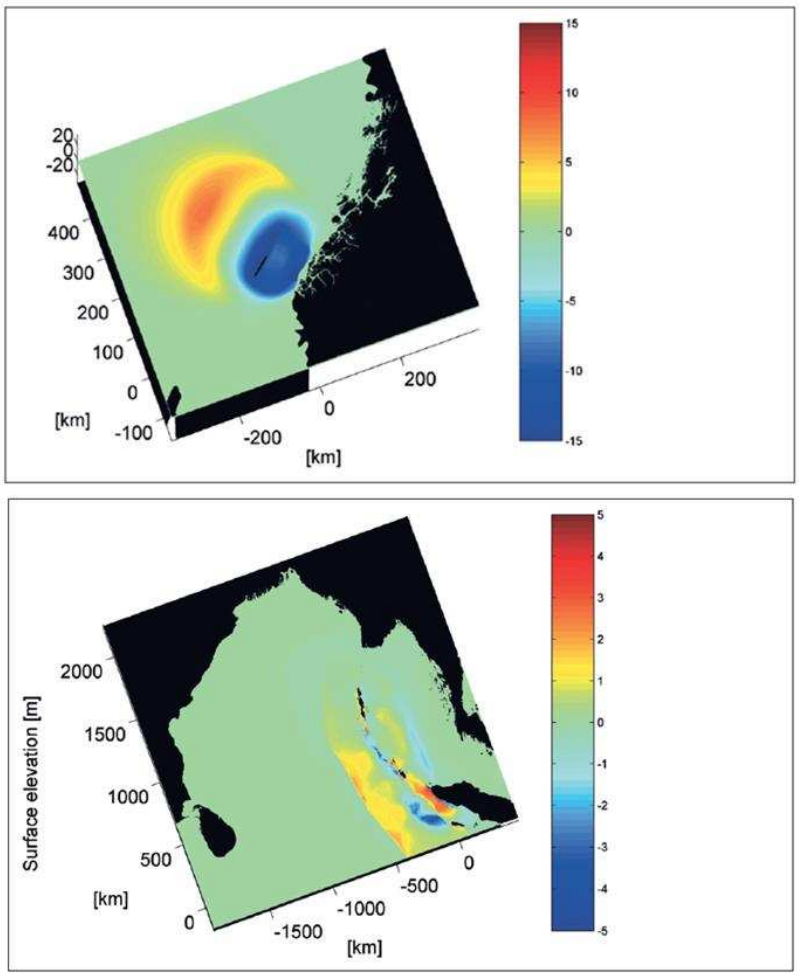

Fig. 2.5 (up) tive of the Storegga slide tsunami, surface elevation after 30 minutes of simulation. The colourbar shows the surface elevation in m. (down) Perspective of the Indian Ocean Tsunami surface elevation after 20 minutes of simulation. The colourbar shows the surface elevation in m. From Harbitz et al. (2006)

Nevertheless, there is a strong connection between landslides and earthquakes, as seismic activity often triggers submarine landslides. When an earthquake shakes underwater slopes, it can destabilize sediments and cause a landslide, which can enhance or modify the tsunami generated by the earthquake itself. This interaction between tectonic activity and slope instability can significantly amplify the effects of a tsunami (Tappin et al. 2014).

Offshore tsunami backwash deposits are formed by the seaward-returning flows following the initial landward surge of a tsunami. After inundating coastal areas, the accumulated water returns to the ocean under the influence of gravity, creating powerful backwash currents. These currents can

erode sediments from inundated land, beaches, and nearshore zones, transporting a mixture of terrestrial and marine materials into the offshore environment (Le Roux and Vargas 2005)(Fig.2.6).

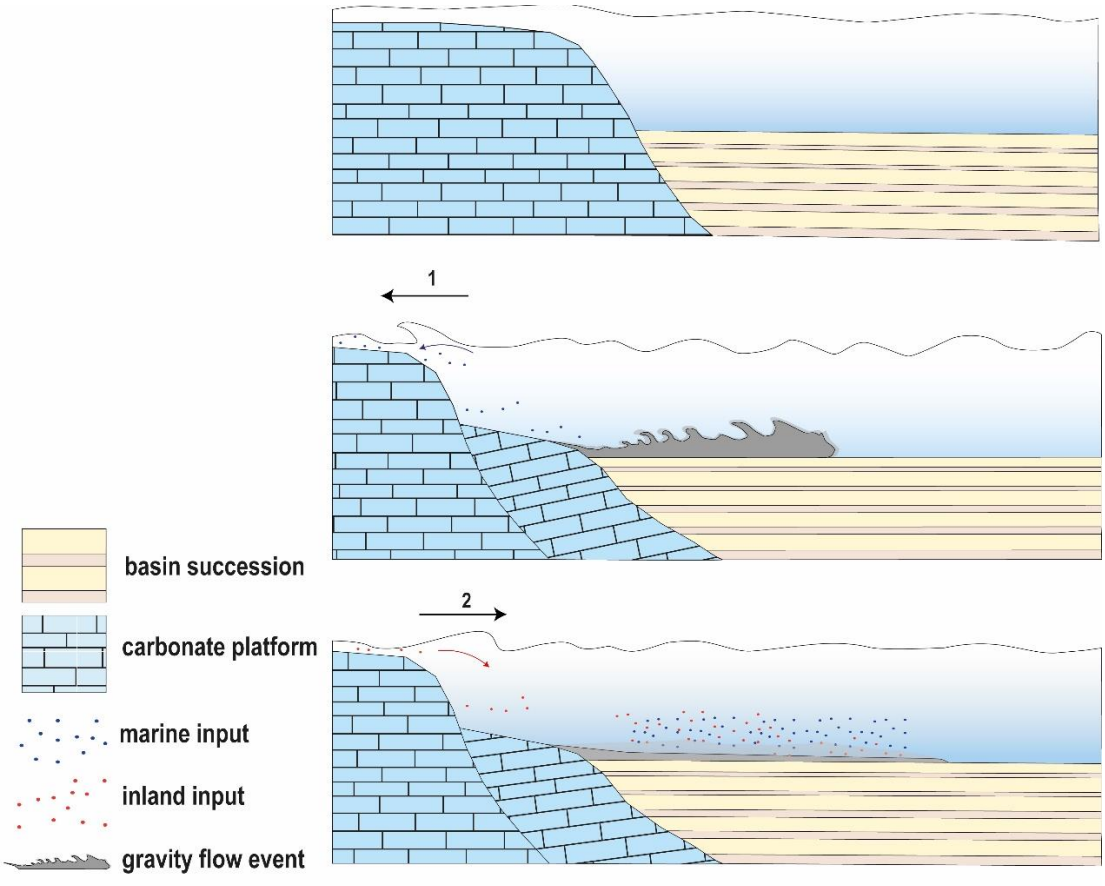

Fig. 2.6 Conceptual model of interaction between an MTD and a tsunami wave. The submarine landslide event, caused by the collapse of a portion of the carbonate platform, trigger a tsunami (1), which propagates onland, ripping up continental material and carrying it into the basin.

As backwash flows move offshore, they can transition into / trigger turbidity currents, especially along the continental shelf and slope. These dense, sediment-laden flows can travel significant distances, depositing sediments toward the basin depocenter (Coleman 1968, 1978). However, so far there is no definite means to identify the tsunamigenic origin of deep-sea turbidites (Chagué-Goff, Szczuciński, and Shinozaki 2017)(Fig.2.7).

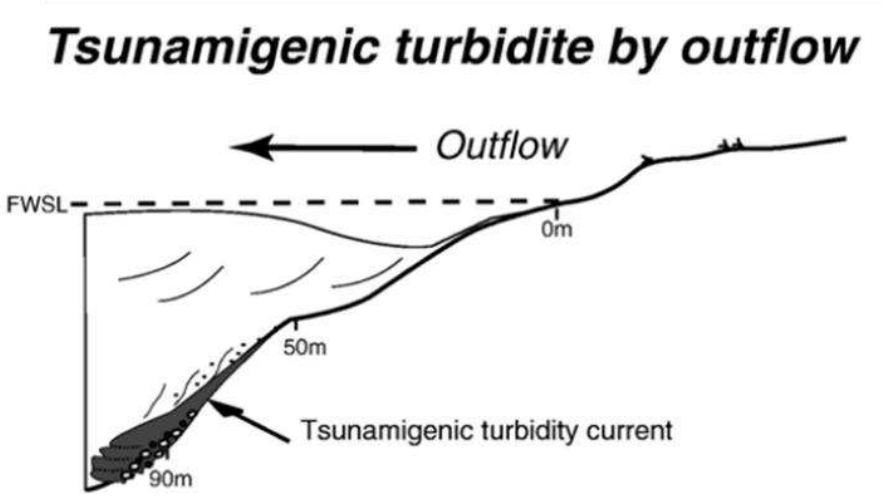

Fig. 2.7 Tsunamigenic turbidity current triggered by the outflow of a tsunami wave. From Nanayama and Shigeno (2006)

The difficulty to relate these deposits to tsunami events is emphasized by (Shiki and Cita 2021), who state that: "There is only one example of a deep-sea tsunamite known in sedimentology, as far as modern tsunamis and their sediments are concerned. That is the "homogenite" of (Blechschmidt et al. 1982; Cita, Camerlenghi, and Rimoldi 1996; Cita et al. 1984; Cita and Aloisi 2000; Kastens and Cita 1981). The layer is characterized by a very thick, gray, visually structureless re-sedimented mud of emipelagic composition, with a normally graded sandy base and a sharp basal contact; it has been interpreted as the sedimentary expression of the tsunami induced by the collapse of the Santorini caldera after the gigantic eruption in the Bronze Age, about 3500 years before present", in 2022 (Polonia et al. 2022) described the deposit known as "Homogenite/Augias turbidite" as tsunami-related, linking it to the 365 CE Crete event. The layer is up to 25 meters thick, covering over 150,000 km² in the Ionian Sea.

2.3.1 - Homogenite characteristics

Cita and Aloisi (2000) defined two types of homogenite based on their characteristics and depositional environments: Type A and Type B.

Type A homogenites are typically found in smaller, perched basins and consist of uniform, thick mud layers without visible sedimentary structures. They are formed by fine particles settling from a suspension cloud generated by the tsunami, with a non-erosional base that reflects minimal disturbance to the seafloor.

Type B homogenites occur in broader, flat seafloor regions. They feature a sandy base transitioning into homogeneous mud and are associated with turbidity currents triggered by tsunamis, transporting material from distant shallow-water areas. These deposits often have an erosional or non-erosional base, depending on the current's energy.

The Homogenite-Augias Turbidite (HAT) described by (Polonia et al. 2022) as "stacked sandy turbidites" at the base, followed by a homogenite layer of fine-grained sediments. The upper part of the HAT deposit, characterized by thin laminated layers, likely formed from seiching caused by water oscillations after the tsunami's passage. (Polonia et al. 2022)

3 - Objectives

The objective of this thesis is to systematically investigate Mass Transport Deposits (MTDs) by thoroughly characterizing their sedimentological, structural, geomechanical, and geochemical properties. Focusing on the Paleogene Julian Basin (between Italy and Slovenia) as a specific case study within a confined basin setting (Ogata et al., 2014c), this research aims to elucidate the mechanisms and dynamics involved in the emplacement of MTDs, as well as to delineate the geometrical configurations of these bodies. Additionally, the study seeks to get new insights on the basinal paleogeography of the Julian Basin to provide context for the environmental and tectonic conditions that influenced MTD formation. By conducting detailed field analyses and comprehensive data interpretation, this work endeavors to enhance the understanding of MTD characteristics and their role in the geological evolution of the basin. The thesis aims to offer insights into the processes governing mass transport phenomena in sedimentary environments, contributing to a better comprehension of sedimentary basin dynamics and the factors driving mass transport events. Ultimately, this work aims to investigate new aspects which could help identifying possible proxies of tsunamites related to the deposition of the MTDs in the fossil record.

4 - Geological Setting

The Julian Basin, or Bacino Giulio in Italian, is a paleogeographic term mostly used by Italian Authors (see, e.g., Venturini and Tunis, 1992; Catani and Tunis, 2001; Lenaz et al., 2000) to define a Late Cretaceous to Eocene deep-sea basin (Cousin, 1981; Pirini et al., 1986; Catani & Tunis, 2001) placed at the northeastern edge of the Friulan-Adriatic-Dinaric (FAD) Carbonate Platform. It has been considered an equivalent of the Slovenian or Tolin Basins as referred in the Slovenian literature (Buser, 1989, 1996; Placer, 1998; Šmuc, 2005; Rožič, 2005; Rožič and Popit, 2006; Miklavič and Rožič, 2008) and in the classic papers of Cousin (1970, 1981). The relationship between these terms is not only semantic, but implies different ages of basin development and different positions of the basin depocenters, as well as different evolution of the sedimentary sequences. The Slovenian Basin is a paleogeographic unit introduced by Cousin (1970) and represents an east-west oriented Jurassic seaway placed between the Julian Carbonate Platform to the north and the FAD Carbonate Platform to the south (Buser, 1989, 1996; Rožič and Šmuc, 2011). The Julian Carbonate Platform drowned during the Early/Middle Jurassic giving rise to a pelagic plateau (Julian High) (Buser, 1989; Šmuc, 2005; Rožič, 2005; Rožič and Šmuc, 2011).

The Slovenian basin originated in the Middle Triassic at the opening of the Neothetys Ocean, evolved as a deeper basin with pelagic and re-sedimented carbonate facies during the opening of the Alpine Tethys in the Early/Middle Jurassic, and became a foreland basin (foredeep) with a turbidite infilling at the stage of Dinaric compressional phases in the Late Cretaceous (Buser, 1989, 1996; Rožič, 2005; Vrabec et al., 2009; Rožič and Šmuc, 2011; Lodowski et al., 2024). Its stratigraphic succession ends at the Maastrichtian with the Upper Flyschiod Formation and the Veliki Formation.

The Tolmin Basin (or Through) represents the western part of the Slovenian Basin sharing the same east-west orientation (Cousin, 1981; Rožič and Reháková, 2024). From the sedimentary facies reconstructed, it is considered as one of the deepest part of the Slovenian basin from Jurassic to Maastrichtian (Cousin, 1981; Šmuc, 2005;).

Starting from the late Campanian, the Julian Basin represents the south/southwestern edge of the Tolmin Basin making transition to the FAD Carbonate Platform through a progressive deepening and drowning of the platform edge and the onset of coarse-grained carbonate resedimentation (megabreccia) (Pirini Radrizzani et al., 1986).

This transformation resulted from lithospheric flexural stages caused by the southwest-directed advance of the migrating front of the Dinaric Thrust Belt, which connects the Dinarides with the Western Carpathians–Alps systems (Csontos and Vörös, 2004). Consequently, the geometry of the depositional setting developed into an elongated foredeep basin, now oriented northwest-southeast (Placer, 1981, 1998; Placer et al., 2010).

The present-day areal expression of the Julian Basin sediment exposures encompasses the Natisone and Iudrio Valleys, the Julian Pre-Alps, and the Tolmin Mountains (Fig.4.1), as part of the Southern Alps/External Dinarides geological framework in northeastern Italy and in western Slovenia (Buser, 1987; Tunis & Venturini, 1992).

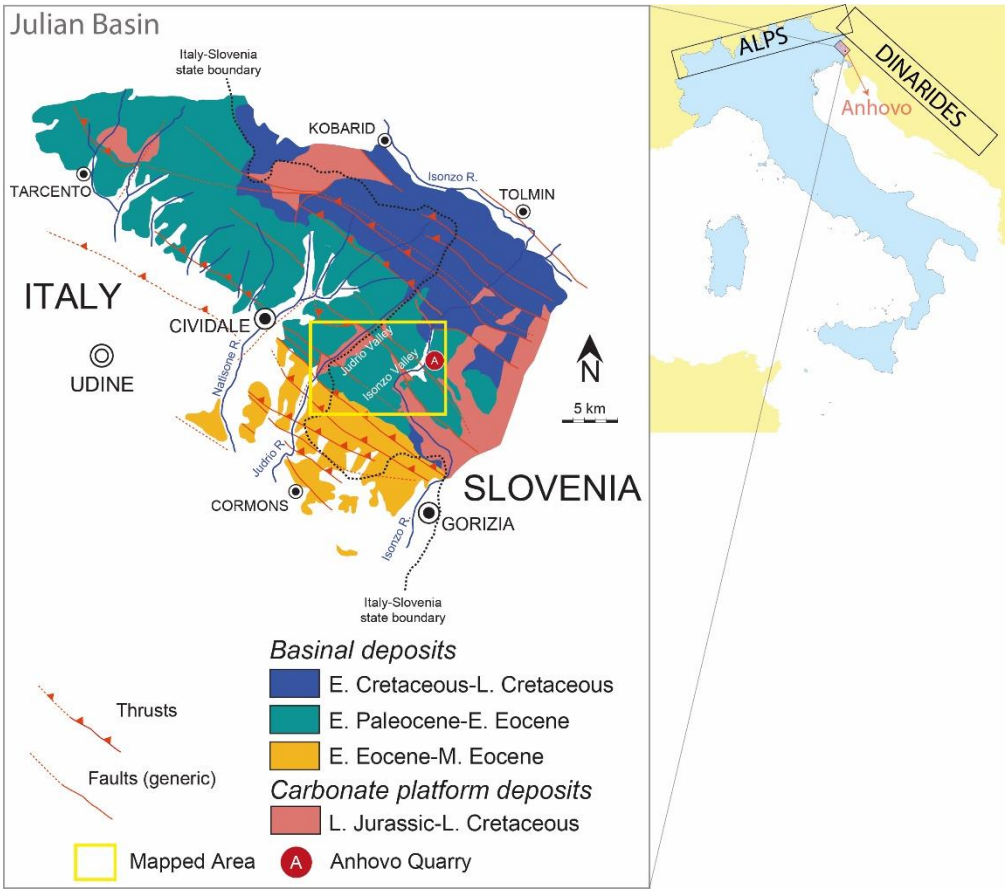

Fig. 4.1 map showing the approximate geographic location of the studied area. The oldest turbiditic deposits outcrop toward the northeast, and proceed southwestward along the Iudrio Valley. Progressively younger strata are encountered in this direction, including Maastrichtian, Paleocene, and Eocene flysch units. The sequence of MTDs of the Julian Basin is contained within the informally named "Grivò Flysch" succession, which ranges from the Late Paleocene to the Early Eocene (see also Fig. 4.2). Modified from Ogata et al. (2014)

This basin was bounded by a shallow-water and partially emergent carbonate platform to the southwest and south, the Dinaric deformational wedge to the northeast, and the nascent Alpine

system to the north (Pirini et al., 1986; Tunis and Pirini Radrizzani, 1987; Tunis and Venturini, 1992; Catani and Tunis, 2001).

The Julian Basin's stratigraphy is marked by a thick succession of flyschoid deposits (Fig.4.2), exceeding 4,000 meters in thickness in some areas (Tunis & Venturini, 1992). These deposits consist of alternating siliciclastic turbidites and carbonate megabreccias and turbidites, reflecting the basin's dynamic depositional environment influenced by both tectonic activity and sea-level fluctuations (Tunis & Venturini, 1992; Catani & Tunis, 2001).

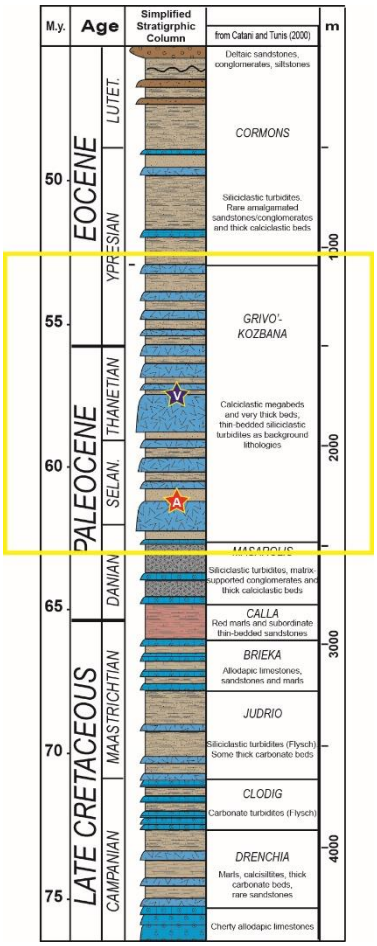

Fig. 4.2 Schematic stratigraphic column of the upper Campanian–Paleogene clastic deposits of the Julian Basin. The mapped area (see yellow square and attached geological map) belongs mainly to the Grivò Flysch succession. At the base of the Grivò Flysch lies the MTD 3 (also known as Mount Ioanaz MTD). Blue Star: stratigraphic position of Vernasso quarry; Red Star: stratigraphic position of Anhovo quarry; grey-brow-reddish: siliciclastic sequence; light blue: calcareous MTDs and limestones. From Ogata et al. (2014).

The terrigenous sedimentary cycle commenced in the Upper Campanian with the deposition of siliciclastic turbidites, initiating a prolonged period of sedimentation that profoundly altered the paleogeography of the eastern South Alpine region (Pirini et al., 1986; Tunis & Venturini, 1992).

Several stratigraphic units have been identified for the Late Campanian to Maastrichtian interval, based on the dominance of siliciclastic versus carbonate sediments (Tunis & Venturini, 1992): Drenchia Unit , Clodig Flysch, Iudrio Flysch, Monte Brieka Flysch.

These units display varying proportions of northern-derived siliciclastic material and carbonate resedimentation from the carbonate platform, indicating shifts in sediment supply and basin dynamics (Tunis & Venturini, 1992).

At the base of the Paleocene lies the Calla Flysch (Pirini et al., 1986; Pavšič, 1985), characterized by reddish pelites alternating with gray sandstones. This unit serves as a significant marker for the Cretaceous-Paleogene boundary (Tunis & Venturini, 1984; Pavšič, 1985). It is followed by the Masarolis Flysch (Middle to Upper Paleocene), predominantly arenaceous and featuring two megabeds, with the second being notably thick (Tunis & Venturini, 1992).

During the Paleocene to Early Eocene epochs, the basin was characterized by complex sedimentation patterns influenced by both carbonate and siliciclastic inputs, as well as significant tectonic activity (Tunis & Venturini, 1992; Ogata et al., 2014).

The Upper Paleocene to Lower Eocene interval is represented by the Grivò Flysch (Tunis & Venturini, 1987), which contains the most significant carbonate megabreccias within the basin (Tunis & Venturini, 1992; Catani & Tunis, 2001). This unit crops out extensively in the southern Julian Pre-Alps and is characterized by large carbonate megabeds interlayered with subordinate siliciclastic turbidites (Tunis & Venturini, 1992; Catani & Tunis, 2001).

These substantial carbonate mass transport deposits (MTDs) are interpreted as the result of catastrophic submarine landslides originating from the collapse of FAD Carbonate Platform margin into the basin (Pirini et al., 1986; Tunis & Venturini, 1992; Ogata et al., 2014c). The collapses were triggered by tectonic forces associated with the advancing Dinaric thrust front, resulting in the deposition of large volumes of carbonate debris into deep-water foredeep settings (Buser, 1987; Placer et al., 2010; Ogata et al., 2014c). The enormous scale of these deposits—with lateral extents over 70 kilometers and in some cases olistoliths (large blocks) several hundred meters long—highlights the magnitude of these events (Tunis & Venturini, 1992; Catani & Tunis, 2001).

Significant MTDs in the basin include the Monte Loanaz Megabed (MB 3), Vernasso Megabed (MB11) Monte Staipa–Topli Uorch Megabed (MB 6), Monte Carnizza Megabed (MB 10), and Porzus Megabed (MB 15) (Tunis & Venturini, 1987; Catani & Tunis, 2001). These megabeds serve as important lithostratigraphic markers due to their basin-wide extent and substantial thicknesses (Tunis & Venturini, 1992; Ogata et al., 2014; Pini & Ponton, 2023).

The turbiditic sequence culminates with the Cormons Flysch (Middle to Upper Ypresian to Lower Lutetian), which includes deltaic deposits indicative of progradation from the north (Venturini & Tunis, 1991; Catani & Tunis, 2001). The upper parts of this unit comprise siltstones, arenaceous beds, and polygenic conglomeratic bodies, reflecting a transition to shallower depositional environments as the basin evolved (Tunis & Venturini, 1992).

From the geodynamic point of view, the evolution of the Julian Basin during the Maastrichtian to Priabonian was complex, involving both extensional and compressional tectonics (Catani & Tunis, 2001). During the Late Senonian to Paleogene, the basin functioned as part of a foreland system migrating southwest from western Slovenia towards eastern Veneto (Doglioni & Bosellini, 1987). Venturini and Tunis (1988) proposed that the flyschoid basins in the western Friuli-Slovenian region evolved through pull-apart mechanisms associated with transtensional to extensional tectonics from the Upper Campanian to the basal Eocene (Venturini & Tunis, 1988; Catani & Tunis, 2001).

In the Ypresian, particularly during the Lower Lutetian, evidence of compressional tectonics emerged, with north-to-south thrusting observed in the Collio region (Venturini & Tunis, 1991; Catani & Tunis, 2001). This tectonic inversion led to the uplift and erosion of northern source areas, contributing to increased siliciclastic sediment input into the basin (Venturini & Tunis, 1991; Tunis & Venturini, 1992).

The tectonic activity, particularly along the carbonate platform margin, is believed to have triggered the massive submarine landslides responsible for the carbonate MTDs (Ogata et al., 2014; Catani & Tunis, 2001). The advancing Dinaric thrust belt induced flexural subsidence in the foredeep basin, creating conditions conducive to slope instability and catastrophic mass-wasting events (Placer et al., 2010; Ogata et al., 2014c). These tectonic forces not only influenced sedimentation patterns but also shaped the basin's morphology and evolution (Catani & Tunis, 2001; Ogata et al., 2014).

Paleocurrent analyses indicate that siliciclastic turbidites were predominantly transported from the northwest towards the southeast, parallel to the basin axis, suggesting a northerly or northwestern source for the terrigenous materials (Venzo & Brambati, 1969; Kuščer et al., 1974; Tunis & Venturini, 1992). Conversely, the carbonate MTDs and turbidites were derived from the disintegration of the FAD Carbonate Platform to the southwest (Pirini et al., 1986; Tunis & Venturini, 1992; Ogata et al., 2014). The composition of the carbonate materials, including olistoliths ranging from the Lower Cretaceous (Hauterivian) to the Lower Eocene, indicates

multiple detachment zones along the platform margin, contributing a variety of ages and lithologies to the megabeds (Tunis & Venturini, 1992; Catani & Tunis, 2001).

Structural analyses conducted in exposures such as the Vernasso and Anhovo quarries provide insights into the transport directions and depositional processes of these MTDs (Ogata et al., 2014c). For instance, in the Vernasso quarry, structural data suggest a transport of the Vernasso Megabed (MB 11) toward the North, consistent with the basin's orientation and tectonic setting (Ogata et al., 2014). Features such as sedimentary injections, ductile shear zones, and fluidized flow structures indicate complex movement mechanisms involving grain-to-grain interactions and fluid overpressure conditions during emplacement (Middleton & Hampton, 1973; Ogata et al., 2012a; Ogata et al., 2014b, 2014c).

The carbonate MTDs within the Grivò Flysch are complex deposits formed through various sedimentary processes, including rockfalls, debris flows, and high-density turbidity currents (Tunis & Venturini, 1992; Catani & Tunis, 2001). The internal structures of these deposits, characterized by varying deformational styles, reflect different submarine flow processes occurring simultaneously (Strachan, 2002; Ogata et al., 2012a).

Their internal organization often follows the facies model proposed by Labaume et al. (1983) and Séguret et al. (1984) and echoed by Tunis and Venturini (1992) and Ogata et al. (2014c) subdividing the MTDs into units (Fig.4.3):

Unit 1 - calcareous breccias embedding oversized carbonate slide blocks (i.e., non-dissociated slide masses)

Unit 2 - calcareous breccias enclosing deformed, bedded siliciclastic-carbonate and marly slide blocks

Unit 3 - massive to crudely laminated, graded calcareous breccias and calcirudites

Unit 4 - graded, laminated fine- to coarse-grained calcareous sandstone and calcarentites

Unit 5 - massive/laminated marlstone (D5).

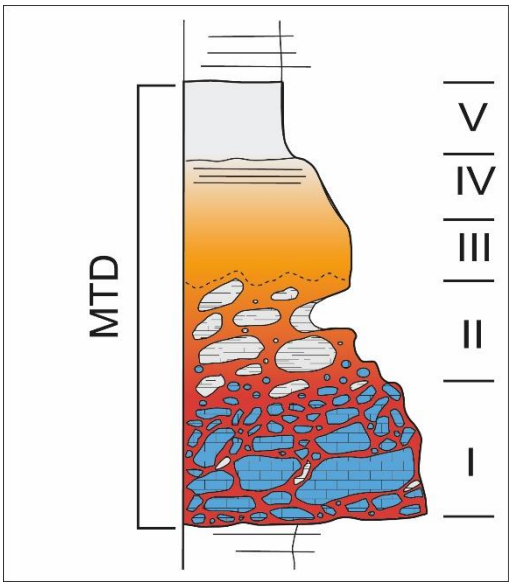

Fig. 4.3 internal units of a Carbonate Mass-Transport Deposit. Modified from Ogata et al. (2014)

Units U1 and U2 are indicative of cohesive debris flows and slump deposits (Tunis & Venturini, 1992); Units U3 to U5 represents high-density turbidity currents and sedimentation from suspension (Tunis & Venturini, 1992; Catani & Tunis, 2001).

Structural features within the MTDs, such as folds, faults, sedimentary injections, and shear zones, suggest complex deformation mechanisms during emplacement (Ogata et al., 2014b, 2014c). These include fluid overpressure, ductile shearing, and grain-flow processes, influenced by both the mechanical behavior of the sliding masses and interstitial fluid dynamics (Middleton & Hampton, 1973; Mutti et al., 2006; Ogata et al., 2012a).

The deposition of these MTDs is attributed to seismic activity associated with tectonic movements along the FAD Carbonate Platform margin and the advancing Dinaric thrust belt (Mutti et al., 1984; Tunis & Venturini, 1992; Catani & Tunis, 2001). Earthquakes likely destabilized the carbonate platform's slope, triggering catastrophic failures and the rapid transport of large volumes of carbonate debris into the basin (Ogata et al., 2014c). The presence of features such as sedimentary injections and fluidized flows supports the hypothesis of overpressure conditions during emplacement, which facilitated the long-distance transport and deposition of the MTDs trough the hydroplaning process (Ogata et al., 2014c).

Structural analyses reveal that the activation of NW–SE-trending Dinaric faults and NE–SW-trending transfer faults along the Friulian Carbonate Platform's slope contributed to mass-transport deposits thickness variations (Tunis & Venturini, 1992; Catani & Tunis, 2001). These paleofaults,

likely inherited from the Cretaceous, acted as morphological steps facilitating the deposition of MTDs parallel to the basin axis (Tunis & Venturini, 1992). The confinement of the basin and the shape of the slope played significant roles in controlling the flow dynamics and sediment distribution of the MTDs (Ogata et al., 2014c).

The advancing Dinaric thrust belt induced flexural subsidence in the foredeep basin, creating accommodation space for thick sedimentary sequences and contributing to slope instability (Placer et al., 2010; Ogata et al., 2014c).

4.1 - Historical Geological Studies

The geological exploration of the Julian Basin and its surrounding areas has a rich history spanning almost a century and a half. Early contributions were made by Pirona (1877) , who advanced geological and paleontological understanding in Friuli. Taramelli (1881) studied the Eocene formations of Friuli, laying foundational work for future research. Dainelli (1915) continued these efforts with detailed paleontological observations focusing on the Tertiary formations of the region.

In the early 20th century, Feruglio (1925) provided comprehensive geological descriptions of the Pre-Alps between the Isonzo and Arzino rivers. He detailed the stratigraphic series of the Natisone area, distinguishing between lower complexes characterized by extensive conglomerate axes (pseudocretaceous conglomerates) interbedded with arenaceous layers, and an upper complex primarily composed of arenaceous-marly alternations and occasional nummulitic breccias. His meticulous field observations, including sections like the M. Tomba–M. Lauer–M. Cladis valley, laid a crucial foundation for subsequent studies.

Advancements in geological mapping occurred when drilling by Agip in the Bernadia structure provided new data. Martinis (1966) analyzed these results, confirming the existence of the Bernadia ellipsoid previously studied by Taramelli (1881) , Tellini (1891) , and Marinelli (1902) . Martinis identified repetitions in the stratigraphic succession due to intense tectonization, causing the fold to behave as an overthrust and leading to complex structural relationships.

Venzo and Brambati (1969) classified the flysch formations of eastern Friuli into three types: Flysch of Cormons, Flysch of Stregna, and Flysch of Pulfero. Brambati (1970) conducted grain-size statistical analyses on sandstones, utilizing the turbidite facies criteria of Mutti and Ricci Lucchi (1975) . Fontolan and Tunis (1989) studied coarse calciclastic sequences in apron-basin margin environments in the "Flysch del Matajur," contributing to the understanding of sedimentary processes in the region.

Biostratigraphic and sedimentological research expanded with studies by Cousin (1981) , who revised earlier profiles, and Pavšič (1985) , who investigated calcareous nannoplankton in flysch sequences near Breginj, Slovenia. Pavšič identified the "red flysch" (Calla Flysch) as a marker for the Cretaceous-Paleogene boundary, supporting the findings of Tunis and Venturini (1984) .

Additionally, Buser and Pavšič (1978) discussed the shifting of Upper Cretaceous and Paleogene flysch basins in western Slovenia, providing insights into regional tectonics and basin development.

A significant stratigraphic revision was conducted by Pirini Radrizzani et al. (1986) , who identified informal units of Maastrichtian, Paleocene, and Eocene ages in the Natisone Valleys and analyzed the biostratigraphy and paleogeography of the southwestern area of the M. Mia–M. Matajur anticline. Sartorio et al. (1987) contributed new insights into the geological and paleogeographic interpretation of the Julian Pre-Alps through the study of the Span well, enhancing the understanding of subsurface geology.

Ponton (1986) developed a tectonic model for the area south of Monteaperta. Tunis and Venturini (1987, 1988, 1992) provided comprehensive geological-structural schemes for the southern Julian Pre-Alps, proposing a Dinaric-trending transpressive system resulting from inherited Jurassic-Cretaceous transtensional phases and Paleogene transpressive phases. They refined the structural arrangement of the Bernadia area, highlighting the role of subvertical Dinaric faults in the tectonic evolution. Catani and Tunis (2001) further analyzed the sedimentological characteristics of the Paleogene carbonate megabeds in the Julian Basin, emphasizing the interplay of tectonics and sedimentation in the evolution of megabed and turbidite sequences.

In Slovenia, studies by Skaberne (1987), included in the proceedings of the International Symposium on the Evolution of the the Karstic (FAD) Carbonate Platform, focused on the geology of the Anhovo area, enhancing the understanding of sedimentation processes and stratigraphy in the western part of the basin.

Recent studies have continued to advance knowledge of the region. Ogata et al. (2014a,b,c, 2016, 2019) extensively investigated the internal anatomy, kinematic indicators, and emplacement mechanisms of the carbonate mass transport deposits (MTDs) in the Friuli Basin. Their detailed structural analyses revealed complex deformation processes involving fluid overpressure, ductile shearing, and grain-flow mechanisms during emplacement, providing valuable analogs for modern submarine landslides in carbonate-dominated margins.

In 2023, Pini and Ponton published a geological map of the Grivò Flysch megabeds, mapping the main MTDs initially indicated by Feruglio, from the Bernadia to the Iudrio Valley. This work significantly enhanced the understanding of the spatial distribution and structural relationships of these megabeds within the basin.

4.2 Lithotypes and uses of the raw material from the principal quarry Sites

The lithologies composing the MTDs of the Grivò Flysch hold significant economic importance, as demonstrated by various extraction activities in the region. In particular, on the Italian side, active quarries in the Julian Prealps extract "Pietra Piasentina," the commercial name for the calcirudites and calcarenites found in Units U3 and U4 of the MTDs (Fig.4.4). This stone was first used by the Romans in Cividale del Friuli since its foundation between 56–50 B.C. (Visintini, 1980) and is now predominantly sold as an ornamental stone.

Fig. 4.4 "Pietra Piasentina"calcarenite of Megabed n.3 (Mount Ioanaz Megabed) with clay chips holes. The lines are saw marks.

"Piasentina Stone" is defined as calcirudites and calcarenites characterized by grey background color verging on brown, the presence of white veins (spar calcite) and darker shades (oxidation of constituent minerals, particularly terrigenous elements), with no apparent sedimentary structures (Bertagnin & Frangipane, 2007). The stone is classified based on grain size into three types: fine-grained (calcarenite with grains of an average diameter equal to or less than 1 mm), medium-grained (with grains between granule to small pebbles), and coarse-grained (calcirudite with grains between fine to medium pebbles), although this classification is not rigorous and the ranges between types are not precisely set (Bertagnin & Frangipane, 2007). Currently, Piasentina Stone is

quarried in a geographically limited area in the province of Udine, within the municipalities of Torreano, Faedis, San Pietro al Natisone, and San Leonardo.

The remaining internal units of the major MTDs of the Grivò Flysch, as well as parts of the turbiditic succession between MTDs, are extracted in larger quarries for the production of Portland cement. These deposits represent ideal components for imparting distinctive properties to cement.

The main quarry fronts examined can be divided into three groups based on their geographical location and the part of the stratigraphic succession they extract:

1. Anhovo Area: The Anhovo quarry is located in Slovenia, in the Soča River valley near the town of Kanal. This quarry is currently the closest to the carbonate platform margin, situated to the south in the Banjšice Plateau. It features the largest quarry face among all sites, and the entire extraction activity is aimed at cement production. Within the quarry, several thick MTDs are visible, named in Slovenian (from oldest to youngest): Rodež, Podbrdo, Perunk, Lastivnica, and Deskle. The considerable thicknesses of these individual MTDs may be due to the quarry's proximity to the source area.

2. Vernasso Area (Fig.4.5): The Vernasso quarry is located near Cividale del Friuli, specifically between it and the locality of San Pietro al Natisone. Currently inactive, this quarry also extracted material for cement production. The quarry face is extensive and shows a succession that starts from Unit U2 of MB 11 (Vernasso Megabed) up to MB 15 (Porzus Megabed).

3. Clastra Area: Situated near the village of Clastra, east of San Pietro al Natisone, this area includes several smaller quarries belonging to the Consorzio della Pietra Piasentina, used to extract Piasentina Stone from Unit 4 of MB 3 (Monte Ioanaz Megabed). This group also includes the Tarpezzo quarry, located opposite the Clastra group on the southern slope of the facing hill.

Additionally, other quarries belonging to the Consorzio della Pietra Piasentina are located on the Italian side of the Julian Prealps, also within the Grivò Flysch.

Fig. 4.5 3D virtual outcrop model of the Vernasso Quarry with the exposed MTDs

5 - Methodology

5.1 - Field survey and Remote Sensing

Within the framework of this thesis project, an extensive field survey was carried out to correlate the main mass-transport deposits in the area between the Iudrio Valley and the Isonzo Valley. The investigated region is bounded by the towns of Kanal (Slovenia) and Prepotto (Italy) to the east and west, respectively, and by Vrhovlje pri Kožbani (Slovenia) to the south, with the Iudrio River forming the northern boundary. Covering approximately 85 km², the area is densely vegetated and offers scarce extensive geological exposures, compounded by significant tectonic overprinting. These factors presented considerable challenges for traditional geological mapping and necessitated innovative approaches to data acquisition and analysis, including the usage of advanced remote sensing procedure in a GIS environment.

Field data were primarily collected using an iPad Pro tablet equipped with the applications Fieldmove by Petex and QField. These tools facilitated efficient data recording, mapping, and integration with other geospatial datasets. To address the limitations imposed by dense vegetation and limited outcrop exposure, field observations were supplemented with high-resolution Digital Terrain Models (DTMs) derived from LiDAR acquisitions.

DTMs were sourced from the official service of the Friuli-Venezia Giulia region and downloaded via the “Eagle FVG” (FVG stands for Friuli Venezia Giulia) portal, at the URL (https://eaglefvg.regione.fvg.it/eagle/main.aspx?configuration=guest). The datasets included a DTM produced by the Civil Protection Agency with a 1-meter resolution in the RDN2008/TM33 reference system, and regular grid altimetric models with a 0.5-meter resolution, obtained from LiDAR point clouds collected between 2017 and 2020. For additional details, refer to the dataset "Nuvole punti rilievo LIDAR RAFVG 2017-2020".

For the Slovenian portion of the study area, 1-meter resolution DTMs were obtained from the Slovenian Environment Agency portal, at the URL (https://gis.arso.gov.si/evode/profile.aspx?id=atlas_voda_Lidar@Arso&culture=en-US&AspxAutoDetectCookieSupport=1). Higher-resolution 0.5-meter DTMs were provided with the assistance of Prof. Žiga Kokalj of the Institute of Anthropological and Spatial Studies (Slovenia), derived from processing Digital Surface Models (DSMs) acquired in Slovenia.

I've processed the DTMs using various Geographic Information System (GIS) software suites, including the open-source QGIS Long Term Release 3.16 (LTR) and subsequent versions, Global Mapper versions 24 and 25, and ArcGIS versions 10.8.2 and Pro 3. The 3D visualization capabilities of these software packages gave a new perspective in the investigation of terrain features and interpreting geological structures. A fundamental tool in the analysis was the Relief Visualization Toolbox (RVT), developed by the team of Žiga Kokalj, PhD, Klemen Zakšek, PhD, Peter Pehani, Klemen Čotar, and Maja Somrak at the Institute of Anthropological and Spatial Studies (Slovenia) (https://www.zrc-sazu.si/en/rvt). The RVT was designed to assist scientists in visualizing raster elevation model datasets, focusing on techniques effective for identifying small-scale features. The default settings assume the use of high-resolution digital elevation models derived from airborne laser scanning missions (LiDAR).

While initially intended for specific applications, the techniques implemented in RVT are versatile and have been applied in various fields. The sky-view factor (SVF), for example, can be efficiently used in studies where digital elevation model visualizations and automatic feature extraction are essential, such as geography, geomorphology, cartography, hydrology, glaciology, forestry, and disaster management (Kokalj and Somrak, 2019; Kokalj & Hesse, 2017). Methods implemented in RVT include hillshading, hillshading from multiple directions, principal component analysis (PCA) of hillshading, slope gradient, simple local relief model, sky-view factor, anisotropic sky-view factor, positive and negative openness, sky illumination, and local dominance. Various data blending modes were also utilized to enhance visualization outcomes. RVT supports the conversion of elevation raster file data into formats such as GeoTIFF, ASCII gridded XYZ, Erdas Imagine, and ENVI. Mosaicking multiple files, such as tiled LiDAR elevation models, is effective when data are consistent in projection, resolution, and pixel dimensions.

The sky-view factor was particularly instrumental in visualizing and identifying characteristic morphologies of individual MTDs. Traditional visualization methods relying on direct illumination often obscure subtle features due to shadows and varying lighting angles. The SVF method, based on diffuse illumination, overcomes these limitations by representing the portion of the visible sky obscured by terrain features. Assuming isotropic diffuse illumination, areas with a larger visible sky portion appear brighter, enhancing subtle topographic variations. Applying SVF for visualization offers advantages over other techniques by revealing relief features without sharp edges while preserving general topography. It not only presents information differently but also extracts new attributes that can be further processed (Zakšek et al., 2011).

The Google Earth Engine platform was also explored, leveraging its multi-petabyte catalog of satellite imagery and geospatial datasets combined with planetary-scale analysis capabilities. The aim was to identify potential features of interest using high-resolution satellite data. However, the Sentinel imagery available lacked the necessary detail for this study's objectives.

5.2 - Virtual Outcrop Exploration

To examine the internal anatomy of the mass-transport deposits in greater detail, drone surveys of the main quarry faces in the Vernasso and Clastra areas were conducted in collaboration with Dr. Corradetti of the University of Trieste. The drones and cameras used included the DJI Air 2S, DJI Mini 2, and DJI Spark, along with ground cameras such as the Nikon D5100 and the iPad 11 Pro 2nd Generation. For the Vernasso quarry, over 2,500 images were collected and processed into a single 3D model using Agisoft Metashape software, yielding detailed representations of the outcrops. In addition to creating 3D models, image pre-processing techniques were tested using RawTherapee software. Efforts focused on eliminating shadows to enhance model resolution and converting images into false-color representations with exaggerated saturation to facilitate the identification of features within the models.

5.3 - Sedimentological, geochemical and mineralogical studies

The sampling strategy centered on collecting sediment from the uppermost portion of the main Mass Transport Deposits (MTDs), extending from the top of interval U5 down several meters. This approach aimed to characterize the MTD’s composition and identify sedimentological or geochemical signals indicative of tsunami deposits. Fieldwork employed both traditional sampling techniques and portable drills; however, while drills could produce immediate powder samples suitable for p-XRF analysis, concerns over tool portability, potential sample contamination from the metal bit, and thermal alteration ultimately led to favoring traditional, non-drill methods. The few drill-collected samples were retained for subsequent tests on possible integrity issues. The underlying hypothesis suggested that a tsunami’s backwash might have deposited finer sediments and terrestrial organic matter beneath U5, mixing with its settling sediments and creating a distinct compositional layer that could be traced even far from the landslide’s source area. The underlying hypothesis indicated that if an MTD triggered a tsunami, the main backwash deposit might be located below U5 closer to the submarine landslide's source area. Finer-grained sediments and continental organic matter representing tsunami backwash could have mixed with settling sediments

comprising U5, creating a compositionally distinct layer detectable even far from the source. A particularly interesting transect was the Lastivnica MTD near the Anhovo quarry, which exhibited peculiar sedimentological features compared to other observed MTDs. Within unit U5, hybrid thin-bedded turbidites were identified. Samples from U5 units of other main mass transports at the Anhovo quarry were also analyzed to establish baseline compositions.

Samples were pulverized using an agate mortar and the Planetary Ball Mill XQM-2A. The powders were analyzed using portable X-ray fluorescence (p-XRF) at the University of Trieste, employing an Olympus Vanta C Series with an Ag anode X-ray tube (VCA) and silicon drift detector (Fig.5.1). The instrument detects elements from magnesium (Mg) to uranium (U) with excitation sources ranging from 8 to 50 keV. Two factory calibration methods were used: the "Soil" method for trace element concentrations and the "Geochem" method for higher concentrations of major elements (Barago et al., 2022). Both methods were employed without moving the analyzer between measurements to optimize data quality (Ross et al., 2014; Lemière, 2018). Data exceeding 1 wt.% were taken from the Geochem method, while values below 1 wt.% were from the Soil method. Each method used three beams set to 20 seconds, totaling one minute per analysis, replicated three times per sample spot.

Fig. 5.1 Olympus Vanta C Series

Powdered samples were also analyzed using X-ray powder diffraction (XRD) to determine their mineralogical composition. A STOE D500 powder diffractometer with Cu Kα radiation (λ=1.5418Å) and Bragg-Brentano geometry (Siemens, Germany) was utilized for this purpose. The instrument is equipped with Soller slits and a series of interchangeable slits with different angular

apertures. The radiation is monochromatized by a secondary flat graphite crystal. The scanning angle ranged from 2 to 90° of 2θ, steps were of 0.005° of 2θ, and the counting time was of 6 s/step. The current used was 20 mA and the voltage 40 kV. The "Match!" software version 3.14 and the reference patterns calculated from the COD (Crystallography Open Database) database were used for phase identification.

The TOC content was initially measured using a Perkin-Elmer 2400 CHNS/O Elemental Analyzer at the University of Trieste. Carbonates were dissolved using 1 M HCl in silver capsules, and samples were analyzed in duplicate. Combustion in pure oxygen reduced samples to elemental gases like CO_2. To verify accuracy, samples were also analyzed at the Department of GeoEnergy and Storage of the Geological Survey of Denmark and Greenland (GEUS).

Lastivnica samples underwent further analysis using ICP-MS at Bureau Veritas laboratories in Poland to determine detailed chemical compositions. The instrumentation parameters included lithium borate fusion coupled with ICP-ES/MS analysis, providing accurate total elemental content determination for both major and trace elements.

Lastivnica samples were also acidified with HCl-10% to remove the carbonate component; then sieved using 50-micron and 20-micron mesh sieves and processed with the ISODYNAMIC Separator Franz (Fig.5.2) to separate heavy magnetic minerals from the fine fraction. These minerals, part of the siliciclastic fraction, provide insights into material provenance. The ISODYNAMIC Separator Franz uses an electromagnet with a specially contoured air gap to separate paramagnetic particles (Frantz User Manual).

Fig. 5.2 Franz isodynamic separator

Separated fractions were analyzed using a ZEISS GEMINI 300 FEG SEM at the Interdepartmental Center of Advanced Microscopy "Carlo and Dirce Callerio" (CIMA) at the University of Trieste. The SEM was equipped with a Metallizer S150A Sputter Coater for sample conductivity and an EDX system with a PENTAFET PLUS Si(Li) detector, along with SE and BSE imaging capabilities.

Thin sections of Lastivnica samples were prepared at the University of Trieste's petrography laboratory. Observations and photographs were taken using an optical microscope at 2.5× magnification. Hundreds of images for each section were stitched together to create high-resolution composites for detailed analysis. Due to internal structures observed in thin sections and apparently high TOC content, an image analysis workflow was tested using Fiji/ImageJ software and Python via Anaconda and Jupyter Notebook. This approach aimed to provide insights about TOC content in the thin sections.

6- Geological Mapping

6.1 – Field Geological Mapping

During the field survey, I recognized several distinct facies corresponding to the sub-units of the mass-transport deposits: mainly carbonate breccias of U1, more siliciclastic-rich breccias of U2, calcirudites of U3, calcarenites of U4, and marls of U5. Additionally, I mapped the flysch succession enclosing these MTDs, as well as carbonate turbidites interbedded within the stratigraphic sequence. The presence of high vegetated area, together with limited exposure of some outcrops complicated the identification of certain lithologies (i.e. making it difficult to determine whether isolated calcarenite blocks represented olistoliths entrained within a larger breccia unit, or whether they were in situ occurrences of U4). For these reasons, I supplemented field observations with remote sensing techniques, using them to verify and integrate the on-site geological data. Other criteria were also considered for correlation, such as the presence of black, gray, and reddish chert grains, ranging from sub-angular to sub-rounded, especially within the calcirudite of U3 and the calcarenite of U4. However, these chert grains appeared too infrequently to serve as reliable stratigraphic markers and their presence needs to be studied in detail.

6.2 - DEM/DTM Analysis

Alongside the fieldwork, a detailed study was conducted on the morphological expressions of the Mass Transport Deposits (MTDs) in the region. These MTDs exhibit distinctive geomorphological features due to the differential erosion of their internal lithological units and their interactions with the enclosing flysch formations.

The megaturbidite units, specifically internal units U3 to U5, and most notably the calcarenitic unit U4, are less susceptible to erosion compared to the siliciclastic surrounding lithologies. This increased resistance is largely attributable to their calcite-rich composition, which also predisposes them to karstification processes, with the formation of dolines, sinkholes and caves (Cucchi & Finocchiaro, 2017; Ponton, 2019)(Fig. 6.1). This reduced erodibility is confirmed by weathering-resistance tests performed by quarry companies of the Pietra Piasentina Consortium (Liuzzi, 1994).

On the other hand, the development of karst features is influenced by the entity of the surface exposure of the carbonate bodies and by the thickness of siliciclastic cover, both of which may

affect weathering processes. In locations where the cover is limited, sinkholes can form due to the collapse of subterranean caves within the underlying carbonate units (Cucchi & Finocchiaro, 2017).

Fig. 6.1 Collapse of a cave into the Unit 4 of MTD n.3 (Mt. Ioanaz MTD in Clastra Area). In yellow the calcarenitic lithology.

Differential erosion processes and development of karstic features are some of the main morphological features which help to identify the Mass-Transport Deposits (MTDs) using Remote Sensing DEM analysis.

The complete list of morphological features of the Grivò Flysch succession, useful to identify and map the MTDs, can be summarized as follows (Fig.6.2):

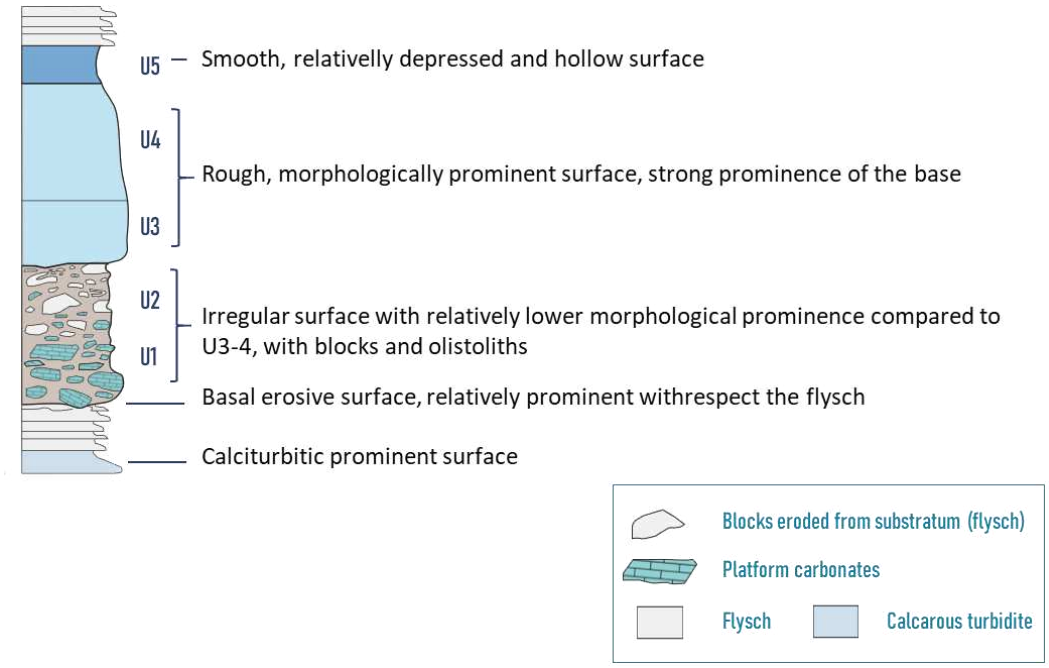

Fig. 6.2 Main MTDs morphological features. Modified from Pini & Ponton, 2023.

By utilizing the Relief Visualization Toolbox (RVT) (Zakšek et al., 2011; Kokalj and Somrak, 2019) and integrating the methodology developed by Pini and Ponton (2023) for constructing the map of the Julian Basin MTDs, additional Digital Elevation Model (DEM) elaborations were developed beyond traditional techniques (such as hillshade, slope, multidirectional hillshade, curvature analysis) to accentuate the characteristic morphologies of Mass Transport Deposits (MTDs).

Among the processing conducted, some integrated methodologies were particularly effective and will be described hereafter (Fig. 6.3).

6.2.1 - Sky-View Factor (SVF):

SVF is a parameter that quantifies the proportion of the sky visible from a specific point on the terrain. It generates a raster output with values ranging from 0 (indicating that almost no sky is visible) to 1 (signifying that nearly the entire hemisphere above the pixel is visible) (Kokalj and Hesse, 2017).

This method was predominantly utilized due to its straightforward visualization and its ability to immediately highlight the morphological characteristics of the terrain.

SVF effectively reveals subtle topographic variations by illustrating how open or enclosed a location is, thereby making it particularly useful for identifying features like depressions, ridges, differential erosion surfaces and other landforms associated with MTDs.

6.2.2 - Advanced Blending Techniques:

The RVT tool allows for sophisticated blending of multiple raster layers to enhance specific terrain features. A particularly successful combination involved layering the following datasets:

- RGB Hillshading: Generated from three azimuth directions - Red at 315°, Green at 15°, and Blue at 75°
- Slope: Values from 0° to 65°, applied with 80% opacity using the 'luminosity' blending mode.
- Positive Openness: Values between 65 and 95, applied with 50% opacity using the 'overlay' blending mode
- Sky-View Factor with values ranging from 0.55 to 1.0, applied with 30% opacity using the 'multiply' blending mode

This composite blending approach, as suggested by Kokalj and Hesse (2017), enhanced the general surface trends and made lithologies composed of pure limestone more discernible. It also accentuated certain olistoliths embedded within the basal units of the MTDs.

6.2.3 - Visualization for Archaeological Topography (VAT)

VAT combines hillshading (or hillshading from three directions), slope, positive openness and sky-view factor with predetermined calculation and blending settings for ‘normal’ (complex) and very flat terrain (Kokalj and Somrak, 2019). These processing helped to identify smaller topographic features and surface variations.

6.2.4 - Integration with Red Relief Image Map (RRIM):

By blending the slope layer without vertical exaggeration (z factor = 1), the SVF layer using the “multiply” blending mode and Red Relief Image Map (RRIM) (developed using the procedure of Chiba et al., 2008) with the “overlay” blending mode, was obtained an alternative visualization that subtly accentuates less prominent morphological features.

This method was useful in emphasizing limestone lithologies and highlighting minor topographic variations. The RRIM overlay enhances the perception of depth and relief, making it easier to identify and analyze features that might otherwise be overlooked.

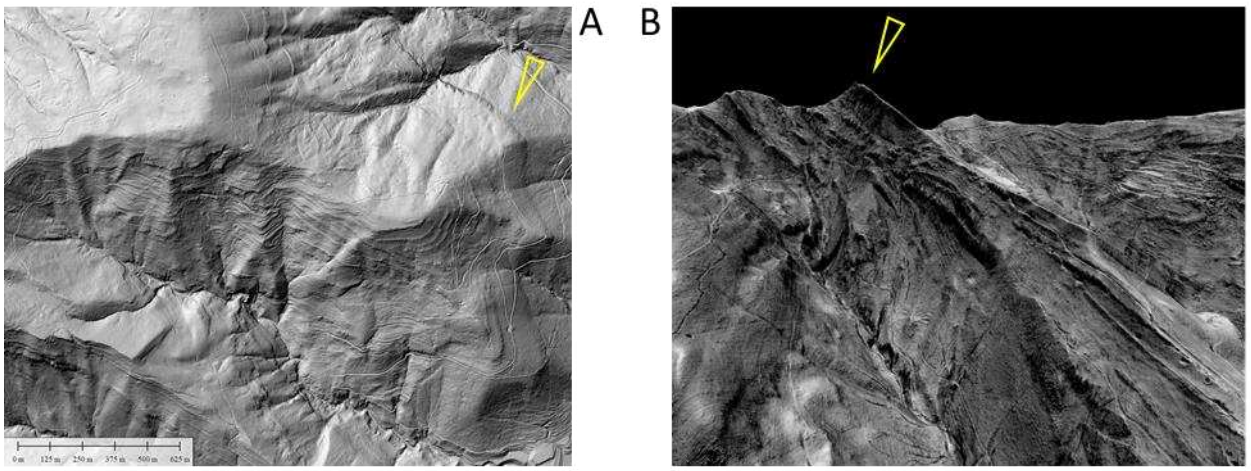

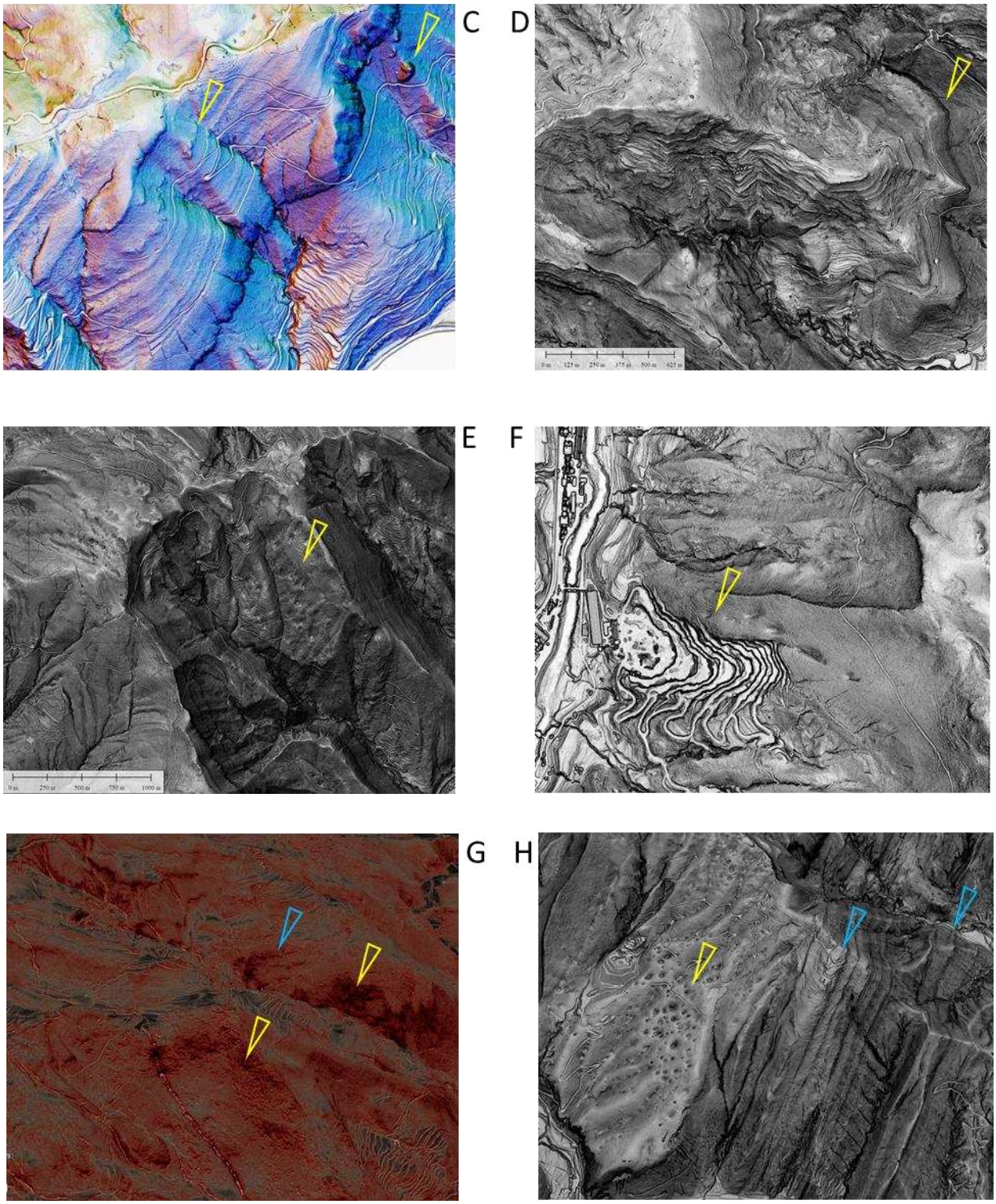

Figure 6.3 (A) Hillshade in 3 directions: contact U1-2/U3-4 of an MTD; (B) 3D visualization of SVF with vertical exageration: the yellow pointer indicates a calcarenitic crest; (C) Blend (3 directions hillshade RGB - positive openess - slope - SVF): pointer indicates olistoliths in Unit 1-2 of the MTDs; (D) sky-view factor (SVF) visualization of the contact U1-2/U3-4 of an MTD; (E) Visualization for Archaeological Topography (VAT) of karst features in Unit 4 of an MTD; (F) SVF with emphasis on possible eroded marl/flyschoids olistoliths in MTD-U2; (G) Integration with Red Relief Image Map (RRIM): yellow pointers indicates limestone surfaces, blue pointer shows minor topographic variations; (H) SVF: yellow pointer indicates karst features on U4 of an MTD, blue pointers show U4 crests in subvertical MTDs.

7- Results

7.1 – Geological Map

The geological map developed during this research illustrates the correlated Mass Transport Deposits (MTDs) across the Julian Basin in the area between Iudrio and Isonzo (Soča). The map provides a visual synthesis of the findings that will be discussed and can be accessed at the following link: [https://figshare.com/s/57ea5f990e10f17cdfc5].

One of the primary results obtained, discussed in the following chapter, is the correlation between the MTDs observed in the Anhovo quarry (Slovenia) and those identified on the Italian side (see Table 7.1 below). This correlation was established using the geological map developed by Pini and Ponton (2023) as the baseline for the Italian side.

Slovenian Name	Italian Name
Deskle	MTD 3
Lastivnica	MTD 2bis
Perunk	MTD 2
Podbrdo	MTD 1bis
Rodez	MTD 1

Tab.7.1 correlation of the Anhovo quarry MTDs (Slovenian Name column) and the Italian MTDs numbers (Italian Name column). See also Fig. 81.

7.2 - Mineralogical and Geochemical Results

The Anhovo quarry in western Slovenia offers exceptional exposure of significant Paleogene carbonate mass transport deposits (MTDs) within the Grivò Flysch of the Julian Basin, notably the Rodež, Podbrdo, Perunk1, Perunk2 and Lastivnica units (Ogata et al., 2014).

The Rodež Unit, one of the most substantial MTDs in the quarry, reaches thicknesses up to 300–400 meters and features chaotic carbonate megabreccias containing large olistoliths derived from the FAD Carbonate Platform (Ogata et al., 2014). Above it lies Podbrdo MTD, Perunk Units (Perunk 1 and Perunk 2), Lastivnica and Deskle (Fig.7.1).

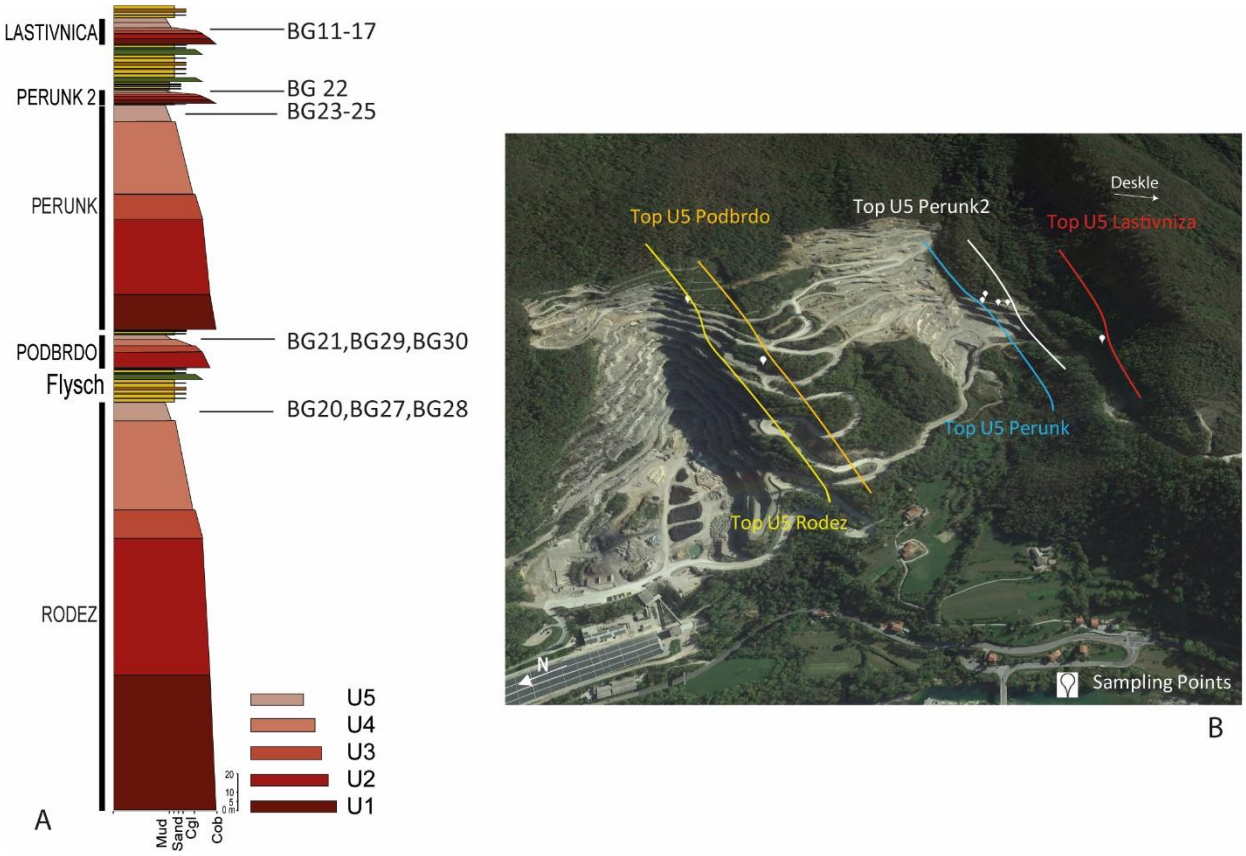

Fig. 7.1 (A) Stratigraphic succession of the MTDs in the Anhovo quarry with collected samples numbers. (B) Overview of the top of each MTD with corresponding sampling locations. See Fig.7.2 for the zoom on Lastivnica Section sampled at Lastivnica top U5 (samples BG11-17).

Within the marls of Unit U5 in the Lastivnica succession, a series of hybrid thin-bedded turbidites (Lastivnica-HT) approximately 1.65 meters thick has been identified. Embedded within the massive pelitic-grained lithology, this series consists of 13 graded layers, each a few centimeters thick, with grain sizes ranging from sandy-silty to pelitic (Fig.7.2-7.3). Some layers exhibit plane-parallel lamination at their bases. Due to the unusual nature of this structure, the transect containing these marls was sampled to characterize both the marls and the embedded deposits. Additional samples were collected from the roof marls of the underlying MTDs sequence.

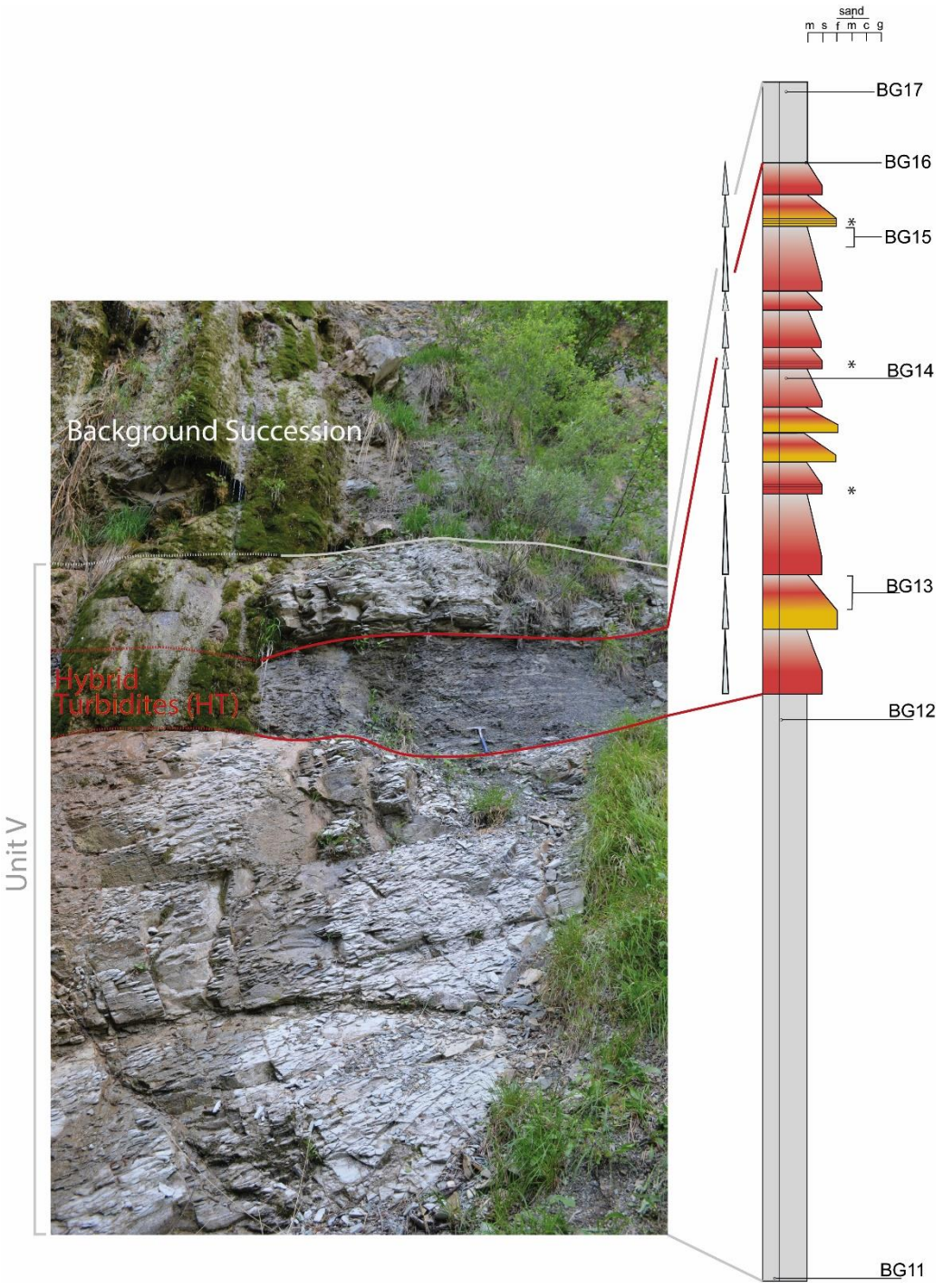

Fig. 7.2 image of hybrid-TBT embedded into Lastivnica Unit 5 (left). Stratigraphic log with sample positions (right). Symbol (*) indicates parallel lamination horizons

Fig.7.3 Zoom of lamination in fine sand of hybrid-TBT sequence embedded Lastivnica U5

The obtained powder samples from the stratigraphic sections were analyzed using portable X-ray fluorescence (p-XRF) spectrometry. Prior to analysis, the instrument was calibrated using certified reference materials (CRMs) to ensure the accuracy and reliability of the elemental data.

The geochemical analysis of the entire Ahnovo Quarry MTDs sequence revealed a progressive increase in siliciclastic major elements, including silicon (Si), iron (Fe), potassium (K), aluminum (Al), and titanium (Ti), as observed stratigraphically from the oldest to the youngest mass transport deposits (MTDs). This upward trend is accompanied by a concomitant decrease in calcium (Ca) content. The increasing concentration of siliciclastic elements suggests a gradual shift in sedimentary input, possibly reflecting changes in provenance.

The most significant enrichment of these siliciclastic elements was detected within the hybrid turbidites (Lastivnica-HT) embedded in the Lastivnica unit.

The analysis of the elemental concentrations demonstrated an inverse correlation between Ca and Si contents, with a coefficient of determination (R^2) of 97%, which underscores the compositional transition within the stratigraphic succession, with gradual enrichment of siliciclastic elements (Fig.7.4).

In addition to the major elements, trace elements associated with heavy minerals were also determined. Notably, zirconium (Zr) exhibited a positive correlation with Si, suggesting its association with siliciclastic material. The main host for Zr is zircon ($ZrSiO_4$), which is considered as a member of the ZTR group (zircon-tourmaline-rutile), the ultrastable heavy minerals resistant to weathering and commonly found in siliciclastic sediments.

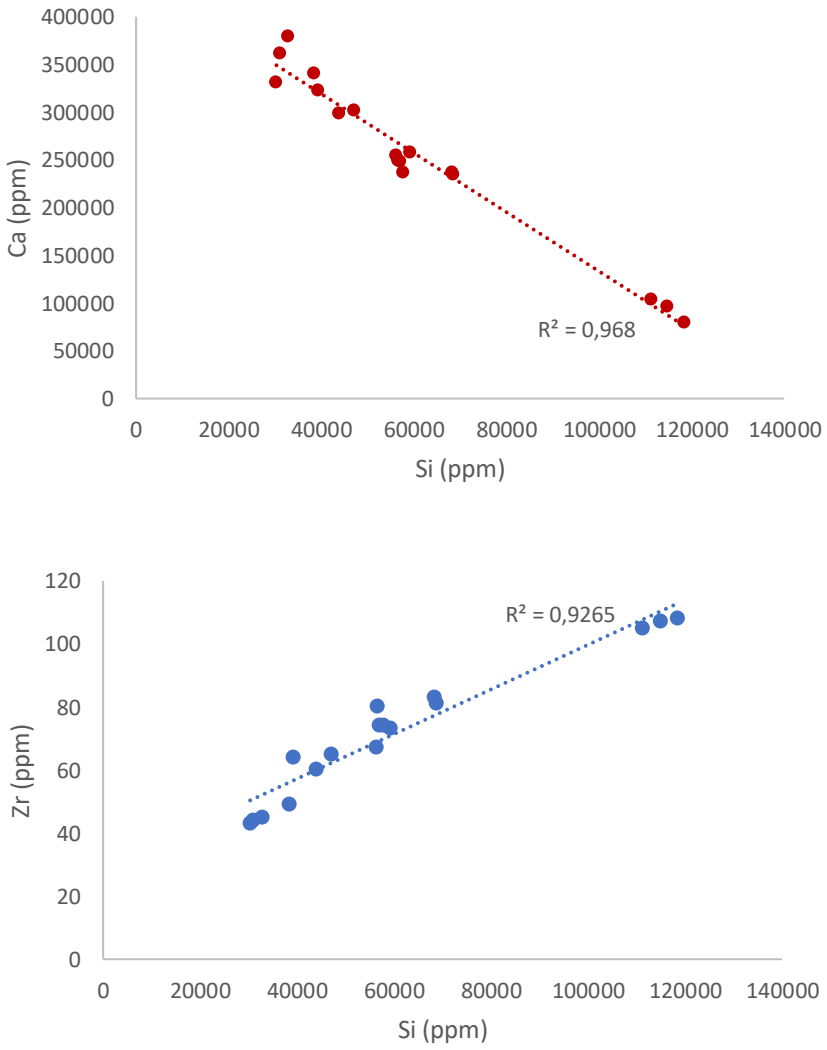

Fig. 7.4 Correlations of the entire MTDs sequence between p-XRF calues of Si/Ca (red) and Si/Zr (blue), expressed in ppm.

Subsequent analyses were conducted using powder X-ray diffraction (XRD) on the same samples to validate and extend the findings from the p-XRF studies.

The XRD analyses provided detailed mineralogical insights, revealing a progressive stratigraphic increase in siliciclastic mineral phases from the marls associated with the older mass transport deposits (MTDs) to those of the younger MTDs. This upward trend was accompanied by a

corresponding decrease in calcite content, indicating a shift in the dominant mineralogical composition of the sediments (Fig.7.5).

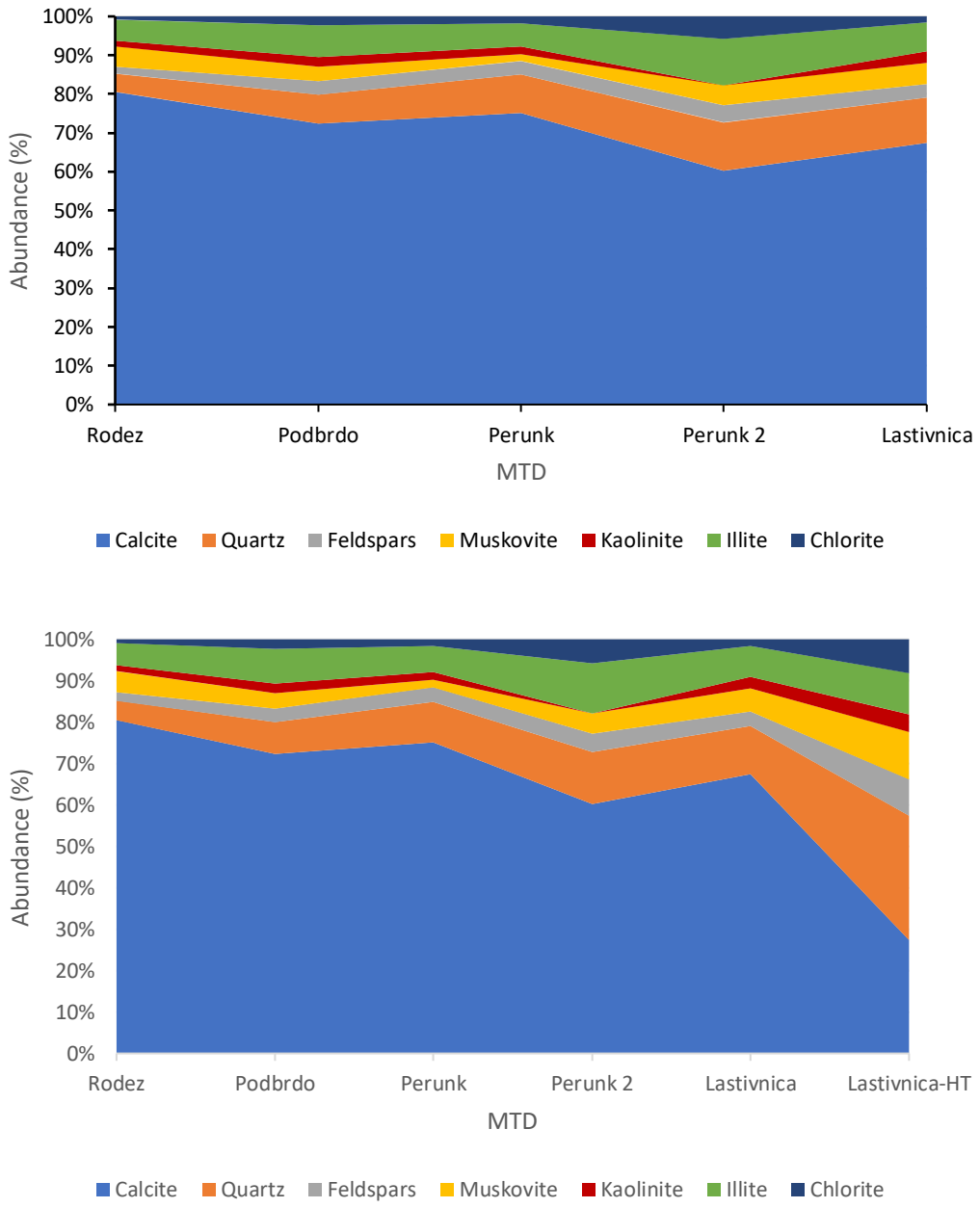

Fig. 7.5 Average minerals abundances of the Anhovo MTDs sequence (up). Same data, but with the addiction of the Lastivnica thin-bedded-turbidites (Lastivnica-TBT) for comparison. Values were measured with powder-XRD.

Various clay minerals were identified throughout the entire stratigraphic sequence, including illite, smectite, and kaolinite, each present in varying proportions.

The XRD data confirmed also the enrichment of siliciclastic minerals within the hybrid thin-bedded-turbidites (TBT), embedded in the Lastivnica unit, compared to the background marls (Fig. 7.5 lower graph).

To overcome portable X-ray fluorescence (pXRF) spectroscopy sensitivity limitations due to its higher method detection limits (MDLs) compared to inductively coupled plasma mass spectrometry (ICP-MS) (Schmidt, Autenrieth, and Nagisetty 2024), we also analyzed the Lastivnica samples, our primary focus, using ICP-MS.

The analyses confirmed a tendency of pXRF to overestimate concentrations of certain elements (Barago et al. 2022), e.g. nickel (Ni) and barium (Ba), when compared with ICP-MS values (Fig.7.6).

Analyses of the Lastivnica samples demonstrated a strong correlation between CaO and loss on ignition (LOI). LOI is a parameter determined by heating the samples at 1100°C in a muffle furnace overnight, causing the loss of all volatile components. This parameter correlates with calcium content because minerals rich in calcite exhibit higher LOI values (due to the high percentage of volatile release during the heating) indicating that the measured calcium is derived mainly from calcium carbonate ($CaCO_3$). Indeed, a 99% correlation between CaO and LOI was observed (Fig.7.7-A). Although plagioclase feldspars also contain calcium, their presence would not significantly affect LOI since they do not release volatiles upon heating. Therefore, the strong correlation between CaO and LOI confirms the predominance of calcite over Ca-plagioclase in these samples.

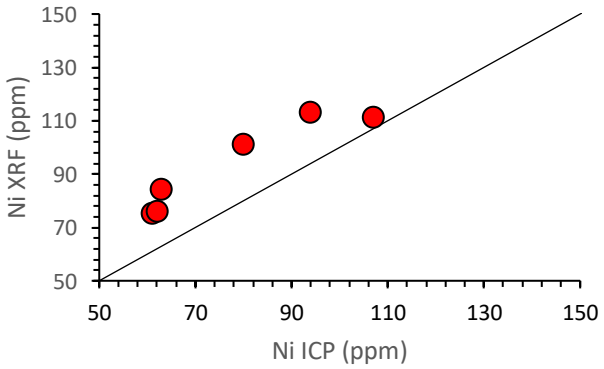

Figure 7.6 Ni concentration (in ppm) measured with pXRF and ICP-MS. Values lie above the trend-line because pXRF slightly overeatimates the concentration of the element compared to ICP-MS

The analyses also indicated a decrease in strontium (Sr) concentrations within the hybrid turbidite samples (Lastivnica-HT) compared to the overlying and underlying marls of Lastivnica Unit U5. Strontium is chemically similar (vicariant) to calcium and often substitutes into the calcite lattice. However, the correlation between Sr and calcite was only 87%, suggesting that strontium is also incorporated into other minerals, possibly micas (Fig.7.7-B).

Further ICP-MS data demonstrated that zirconium (Zr) is closely associated with silica (SiO_2), exhibiting a 99% correlation (Fig.7.7-C). This relationship indicates the possible presence of zircon ($ZrSiO_4$) within the samples. Additionally, potassium (K) and aluminum (Al) showed a 99% correlation, implying their joint occurrence in aluminosilicate minerals such as micas and feldspars (Fig.7.7-D).

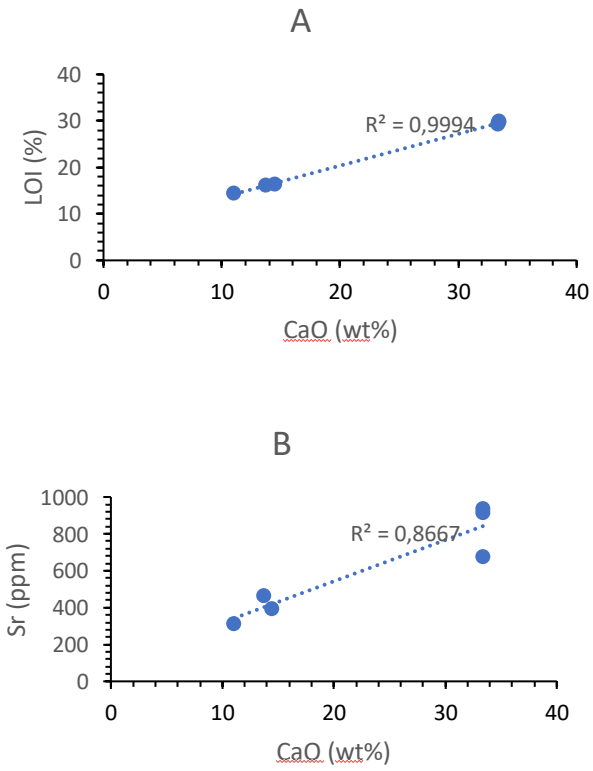

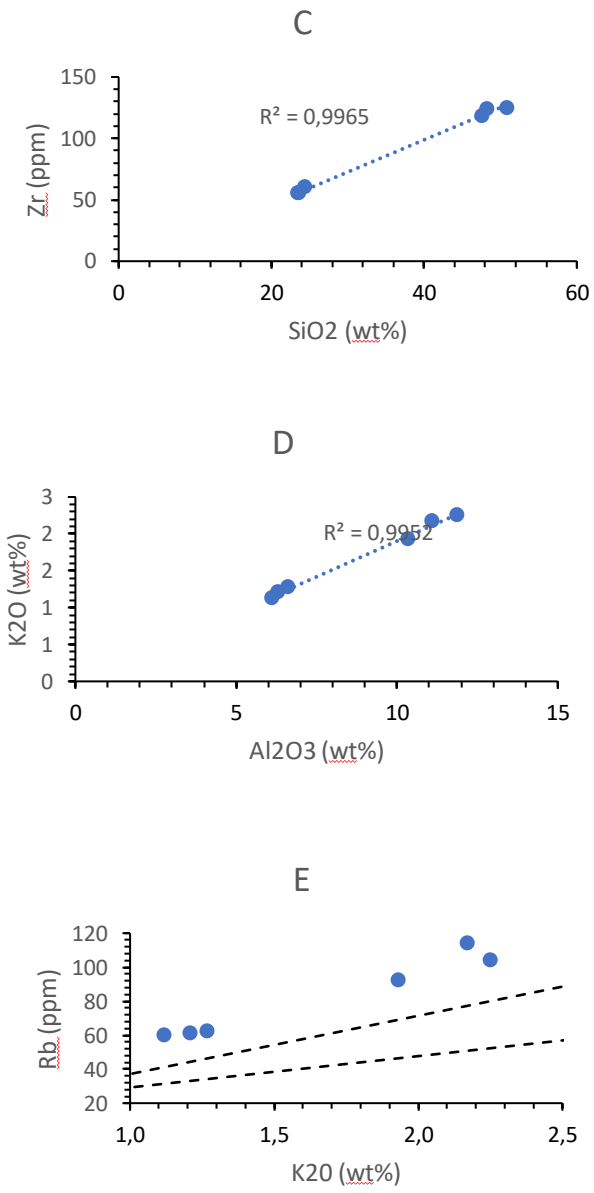

Fig. 7.7 (A) correlation between CaO and LOI in Lastivnica samples; (B) Correlation between CaO and Sr; (C) correlation between SiO_2 and Zr; (D) correlation between Al_2O_3 and K_2O; (E) correlation between K_2O and Rb; trend lines are taken from Zhang et al. (2014); upper line is mica-trend, lower line is feldspar-trend.

To distinguish whether this correlation pertains to mica or feldspar, we referenced the study by Zhang et al. (2014), which outlines distinct trends for these minerals based on the distribution coefficients of rubidium (Fig.7.7-E). Our data align with the mica trend, which is consistent with the fine-grained nature of the samples, mica being more prevalent than feldspar in such sediments. Supporting this, a correlation of 92% was found between potassium content and the sum of clay minerals and muscovite identified in our XRD powder diffractograms.

To gain further insights into the potential sources of the materials involved, Lastivnica samples were acidified with 10% hydrochloric acid (HCl) to remove carbonates, then sieved using 50-micron and 20-micron mesh screens. Subsequently, heavy minerals were separated from each size fraction into ultramagnetic, magnetic, and non-magnetic categories using a Franz Isodynamic Separator. The magnetic and ultramagnetic fractions of samples BG12, BG13, BG15, and BG17 were selected, carbon-coated, and analyzed using Scanning Electron Microscopy (SEM).

For most samples, the 50-micron fractions were used; however, for sample BG17, the uppermost marl sample at the bench top, the 50-micron fraction was insufficient; so the 20-micron fraction was utilized instead. Various mineral phases were identified across all analyzed samples, including micas (primarily muscovite), clay minerals, quartz, and titanium oxides.

Notably, certain source-indicator minerals were detected: magnetite was found in sample BG12, which corresponds to the basal marls; chromite crystals were present in samples BG13 and BG15; and tourmaline was identified in sample BG17. These findings provide valuable information about the provenance of the materials, which is presumably associated to a Dinaric input (Fig.7.8).

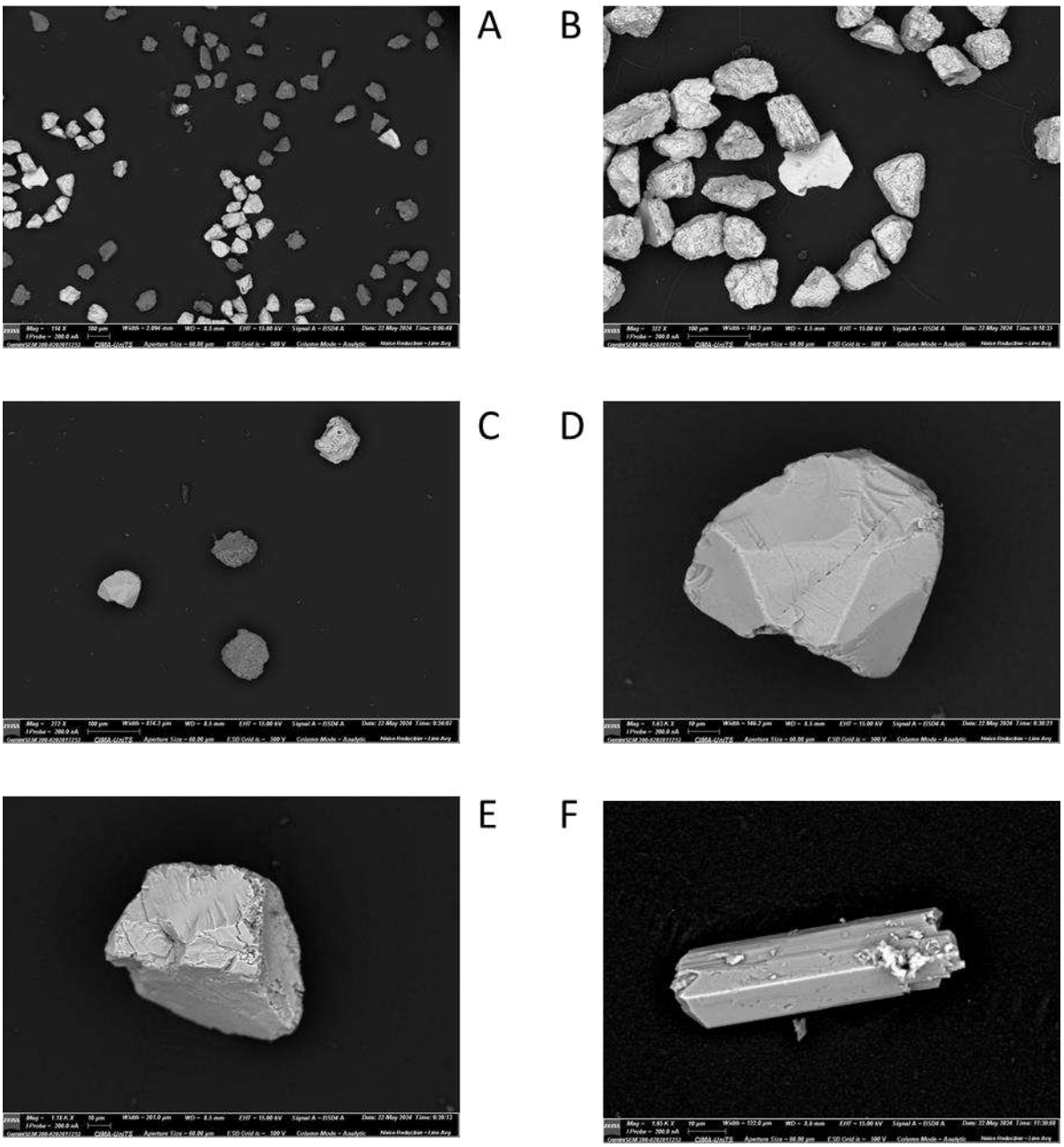

Fig. 7.8 (A) overview of sample BG12 with magnetite; (B) zoom on magnetite fragment in BG12; (C) overview of sample BG13 with Cr-spinel; (D) zoom on Cr-spinel fragment in BG13; (E) Cr-spinel fragment in BG13; (F) Tourmaline fragment in BG17. Scale symbol size in the images is 10µm.

7.3 - TOC Analysis

Samples collected from Anhovo were analyzed to determine their Total Organic Carbon (TOC) content, focusing on characterizing the organic matter within the upper sections of the bench formations. By quantifying TOC, we aimed to determine whether the sediments contained notable

amounts of terrigenous (land-derived) organic material, thus providing insights into a possible continental input triggered by a tsunami.

TOC analyses were conducted at both the Trieste laboratories and the GEUS laboratories in Denmark to ensure measurement reliability. The limits of detection (LOD) for TOC analysis with CHN analyzers vary according to the model and specific methodology used, ranging in the literature between 0.02% and 0.1% (Ribes et al., 2003; Vinturella et al., 2004).

At the Trieste laboratories, powders from all the marls of the U5 units of the Anhovo succession were analyzed, whereas in Denmark, analyses were performed on a set of powders created exclusively from the Lastivnica and Lastivnica-HT samples (Fig.7.9). A comparison between the same samples (from BG11 to BG17) in both sets revealed slight variability, which falls within the instrumental error margin.

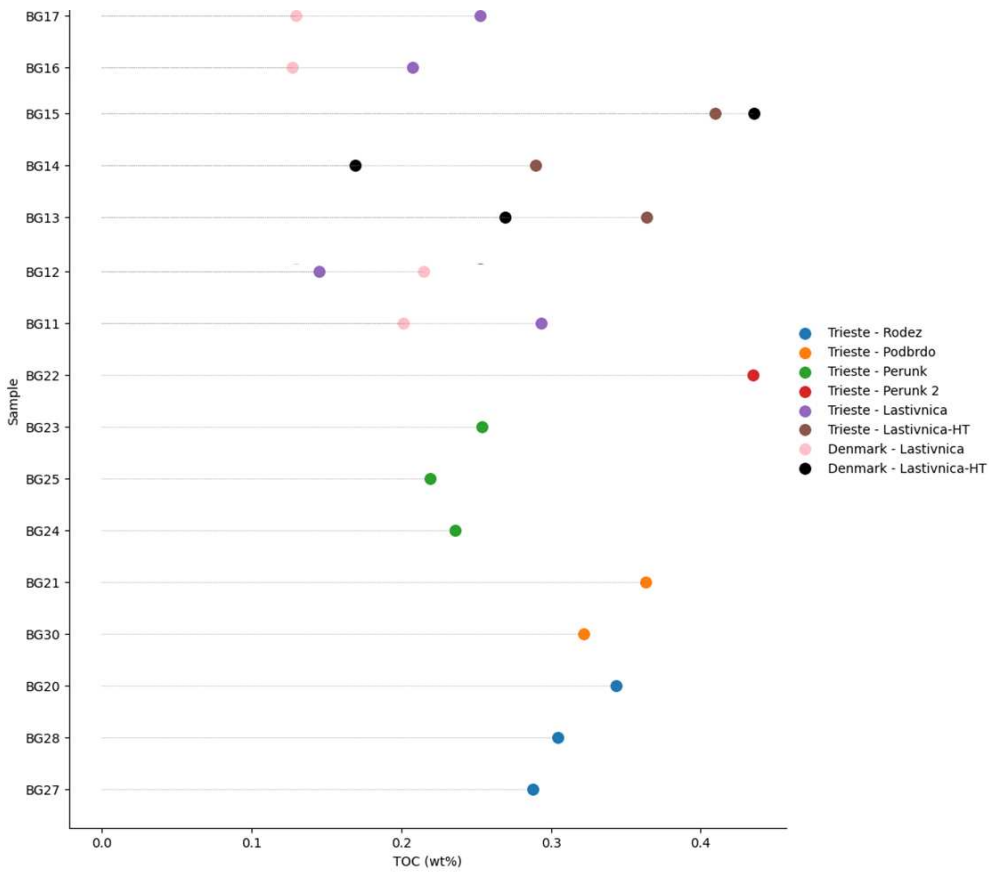

Fig. 7.9 The plot displays TOC analysis values, with samples arranged in stratigraphic order along the Y-axis.

In the Trieste dataset, the Lastivnica samples exhibited TOC values ranging from 0.145% to 0.293%, with a mean of 0.224%, while the Lastivnica-HT samples showed a higher mean TOC of

0.354%, ranging from 0.290% to 0.410%. In the Denmark dataset, the Lastivnica samples demonstrated a lower mean TOC of 0.168%, with values from 0.127% to 0.215%. The Lastivnica-HT samples in Denmark displayed higher TOC variability, with a mean of 0.291% and values ranging from 0.169% to 0.436%, similar to the higher mean observed in Trieste.

The analysis shown a varied but relatively low organic carbon content across the samples. C/N ratio is a possible indicator of the origin of organic matter. Omura et al. (2006) states that C/N ratio greater than 15 is often associated with terrigenous organic matter, while ratios between 3 and 10 are indicative of marine organic matter. The Corg/Ntot ratio averages around 8.4, with values ranging from about 4.7 to 13.5, into the marine organic matter limits (Fig.7.10).

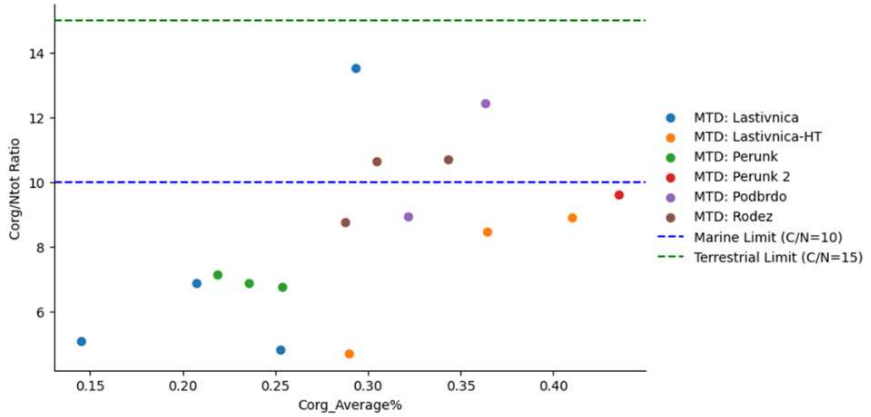

Fig. 7.10 Corg vs C/N plot. Marine and terrestrial limit are taken from Omura et al. (2006).

Lastivnica and Lativnica-HT (BG11-17) show variable temperature of maximum pyrolysis (Tmax) values, in a range from 428°C to 605°C, indicating possible different levels of thermal maturity (Abarghani et al., 2020) (Fig.7.11). The average Hydrogen Index (HI) of these samples is 63.5, a low value indicative of limited hydrocarbon potential in the organic matter present, consistent with the low TOC (Passey et al., 2010).

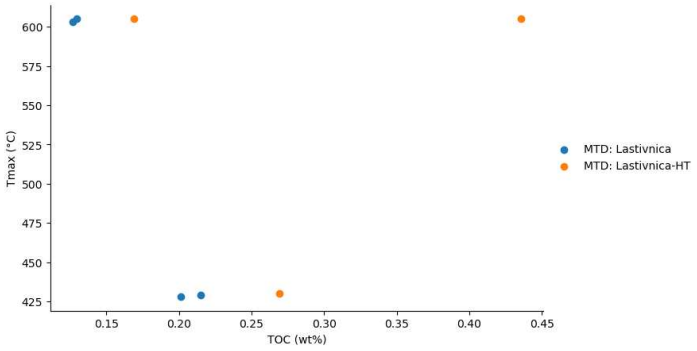

Fig. 7.11 TOC / Tmax in BG11-BG17 GEUS analysis

7.4 - Thin-sections and experimental procedures

As part of the study of the Lastivnica marl deposits, thin sections were prepared to investigate the microstructures within the samples. These thin sections revealed the presence of traction structures within the hybrid-TBT and in the marls above and below, which appear massive to the naked eye (Fig.7.12).

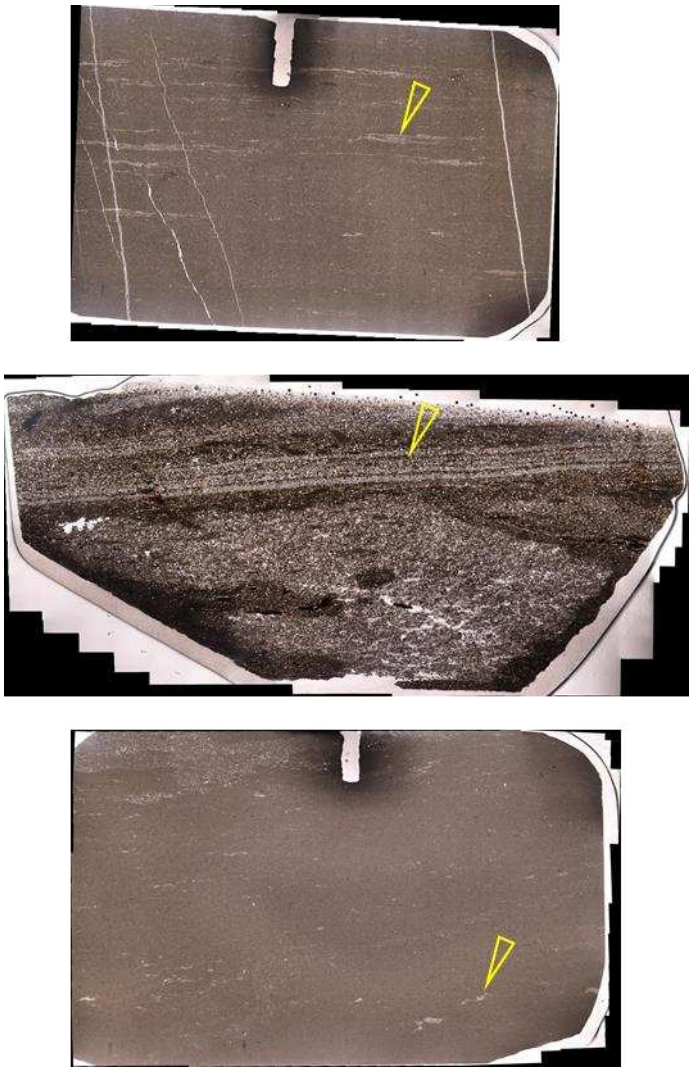

Fig. 7.12 some examples of laminar structures in BG11 (marlstone, llower thin-section), BG13 (hybrid-TBT, medium thin-section), BG17 (marlstone, upper thin-section)

Experimental image analysis techniques were applied to some marl thin sections to automatically map both organic matter and internal clast orientations. Although these preliminary results were

promising, they require further refinement and optimization. Since organic matter appears black in thin sections, the analysis involved converting thin section mosaics into binary images by manually setting a threshold for visualization. After applying a noise filter, the shapes were simplified into ellipses, circles, and squares. Squares were discarded because they were likely residual pixels or opaque minerals, which also appear black in the images. The orientations of the ellipses were then calculated to assess whether they exhibited a preferred orientation (Fig.7.13). The results were coherent with the visual observations.

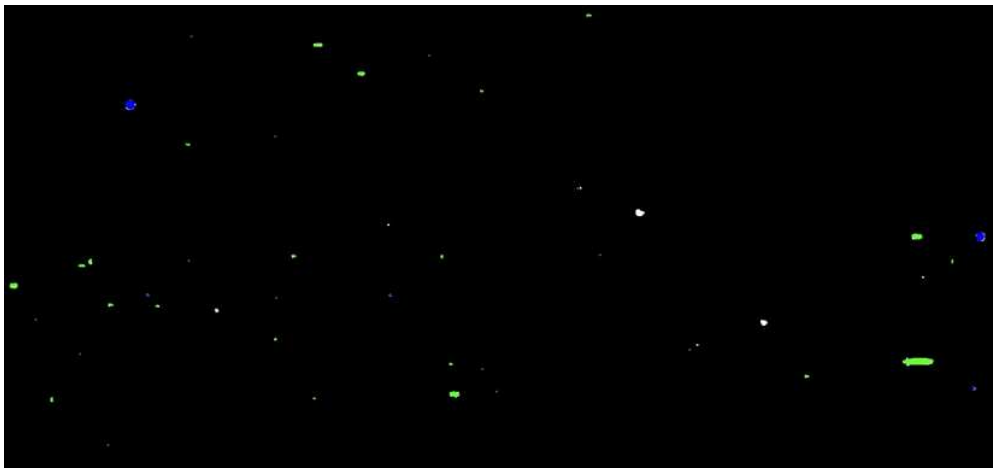

Figure 7.13 Example of shape associations: zoom on BG11 thin-section after binary conversion. Green: ellipses-associated shapes, blue: circles-associated shapes, white: unselected square-associated shapes. Below: rose diagram with ellipse orientations. Note that thin section is oriented normal to the bedding.

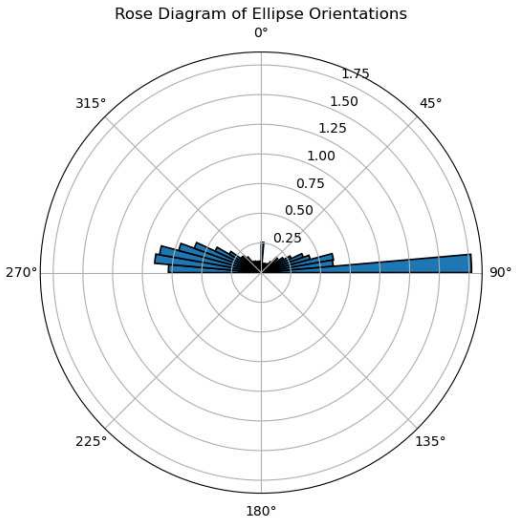

To analyze lineations, a Python script was developed to determine the orientation of linear structures within the thin section mosaics. This script processed the images to detect edges and major alignments, calculated the angles of these lines, and generated orientation data (Fig.7.14).

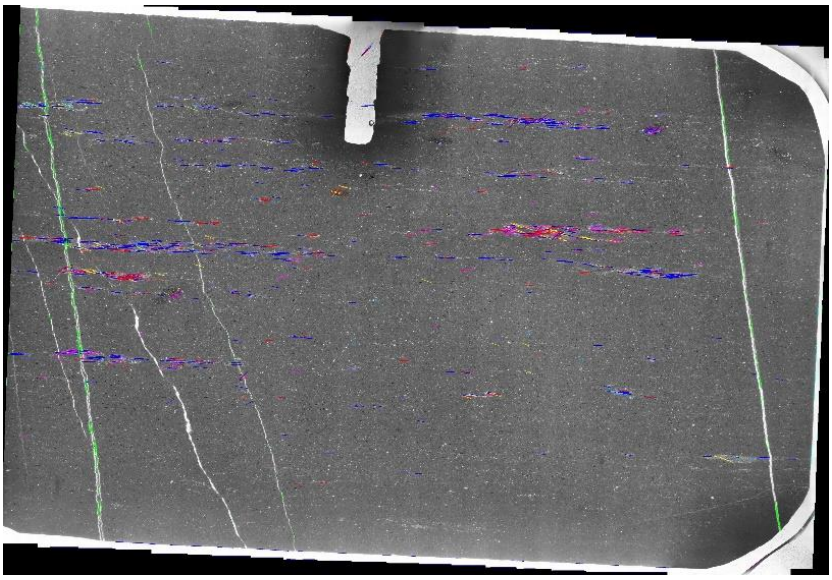

Fig. 7.14 Example of thin-section lineations detection on sample BG17

8- Discussions

8.1 - MTDs Correlation

The geological map resulting from our correlation of the Mass Transport Deposits (MTDs) in the Julian Basin was developed by tracing the main MTDs of the Grivò Flysch beyond the Italian border, correlating the principal Italian MTDs with the well-documented MTDs of the Anhovo quarry in Slovenia. This interpretation incorporates field data, remote sensing analyses, and existing bibliographic and cartographic resources. The correlation between the regions between the Iudrio and Isonzo rivers and the Anhovo quarry has highlighted particular situations that merit discussion (see Fig.8.1-8.2).

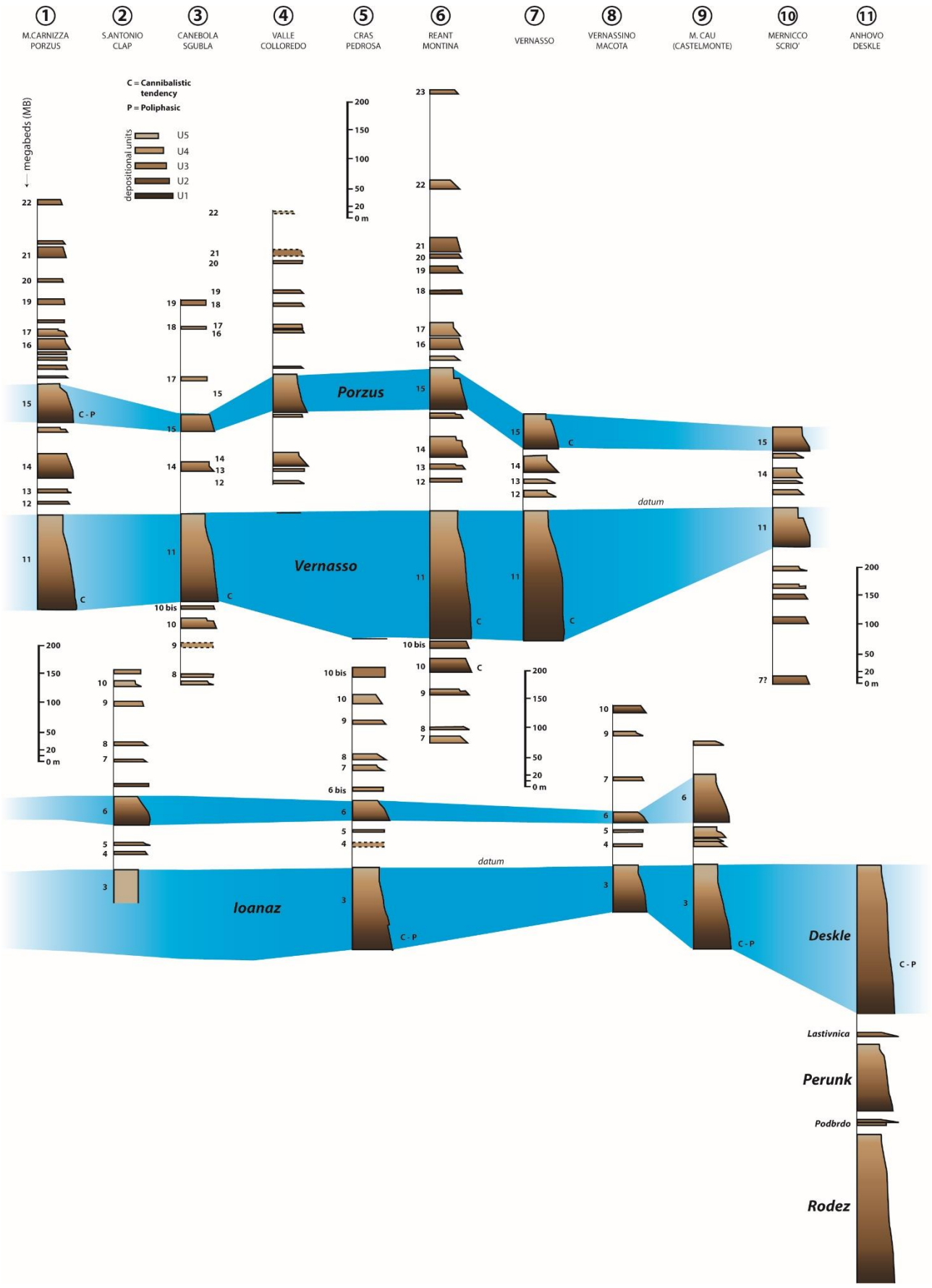

Fig.8.1 Correlation of megabeds in the Julian Basin (datum in the schematic stratigraphic logs = top of MB11, thickness maintained). Locations of sections are in Fig.8.2. Redrawn and modified from Tunis and Venturini (1992). The five depositional units are defined from Tunis and Venturini (1992). Modified from Ogata et al., 2014

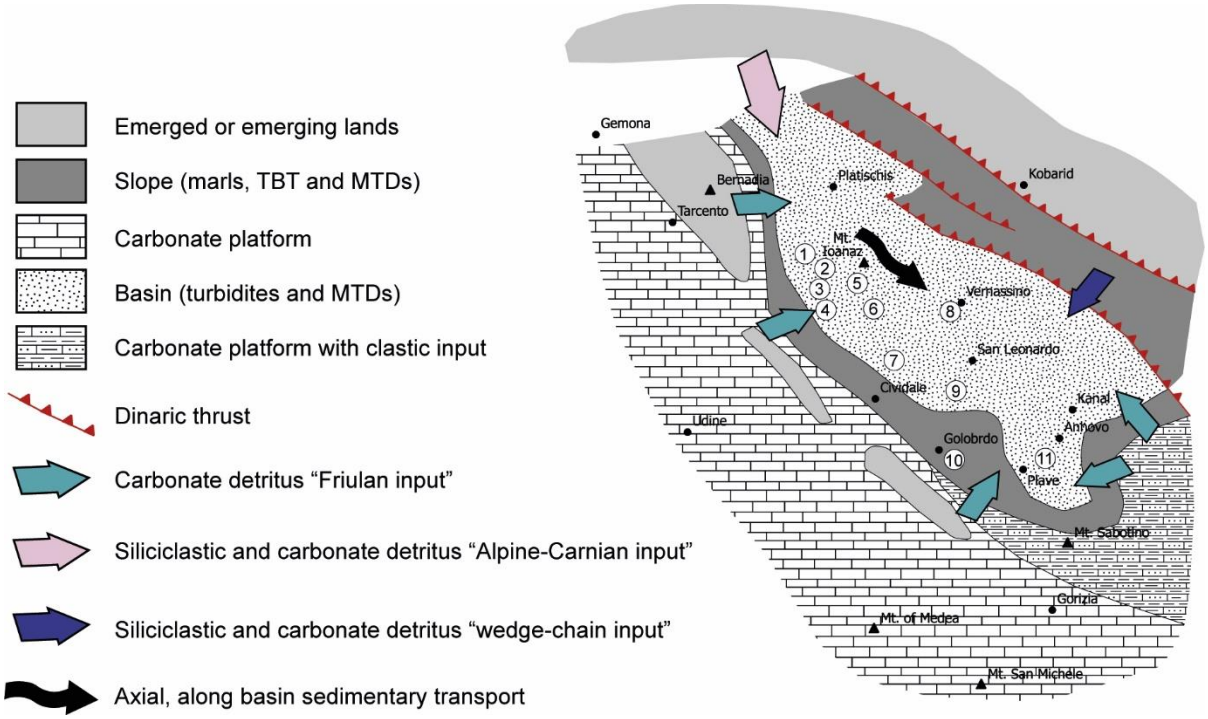

Fig. 8.2 Paleogeographic map of the Friuli Basin at the early Ypresian (Ilerdian), from Pirini et al. (1986), redrawn and modified. The map is based on the present-day position of the stratigraphic sections and outcrops, with no retro-deformation of tectonic structures (i.e. not a palinspastic reconstruction). From Ogata et al., 2014

The largest MTDs were a primary focus of the correlation efforts, specifically MTDs 3 (Mt. Ioanaz), 11 (Vernasso), and 15 (Porzus). Beginning from Kozbana (see attached geological map), the western area with apparently less tectonic overprint, MTDs were traced moving eastward using Digital Elevation Model (DEM) analyses and field control points. MTD 15 is located above the village of Kozbana, while MTD 11 corresponds to Mt. Korada.

Of particular interest was the correlation of MTD 3. According to Catani and Tunis (2001), MTD 3 crops out in the Iudrio area, reaching thicknesses of the lower breccia unit (U1-U2) of about 80 meters and a total thickness of over 150 meters.

As noted by Tunis and Venturini (1992), MTD 3 is a composite bed that internally shows two repetitions of the flow in their Cras-Pedrosa section, repeating the U2 over the U3 and the U3 over the U4. I recognize a surface in the Clastra extraction area (Fig.8.3), where, in various quarry faces, Unit U2 with some large substratum clasts is in direct contact with the underlying Unit U4.

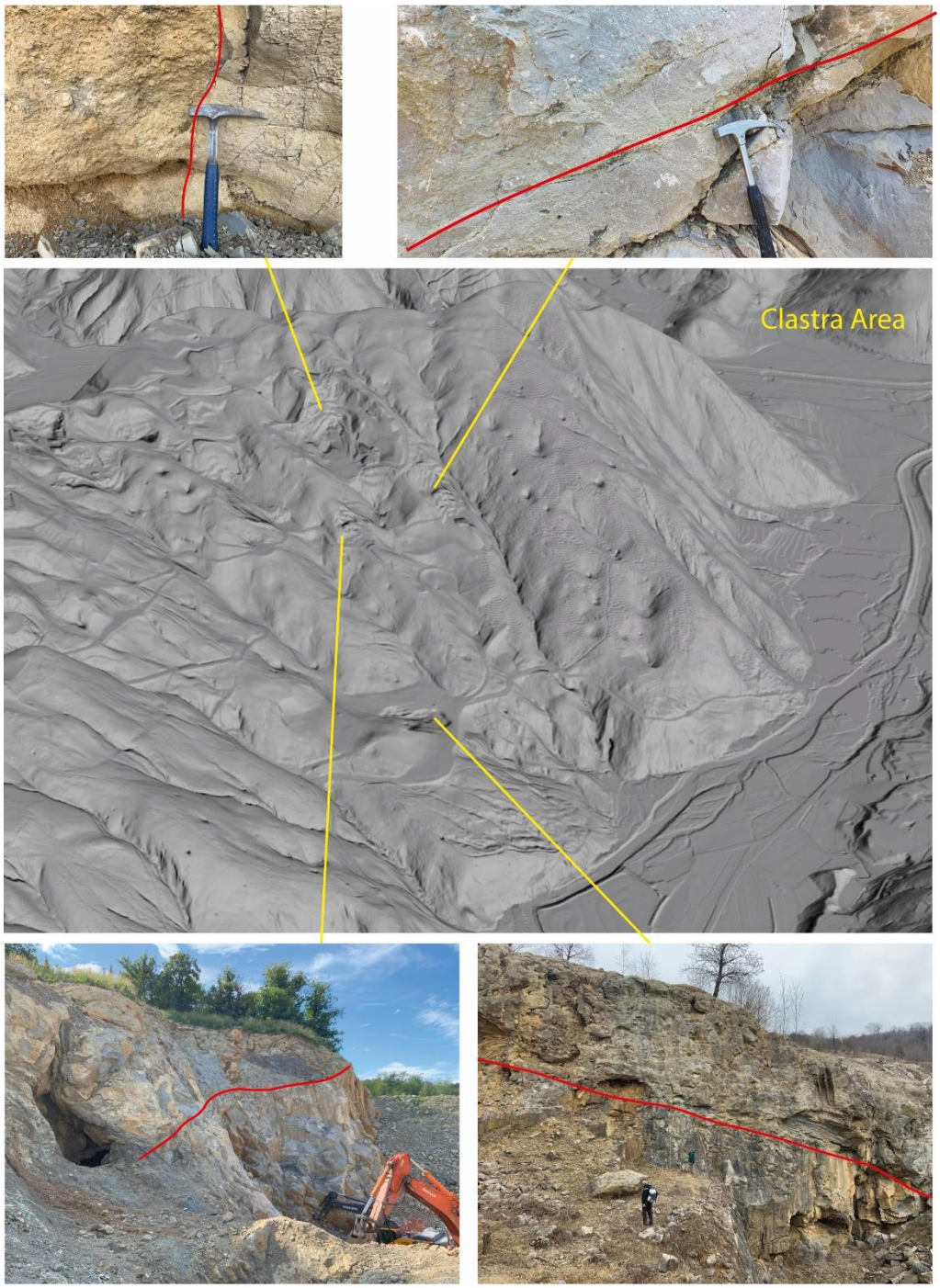

Fig. 8.3 flow repetition surface in Clastra Area

Skaberne (1987) identifies within the Anhovo succession an MTD that exhibits strong cannibalistic tendencies (i.e., it erodes into, reworks, and incorporates material from previously deposited strata, including earlier MTDs) above the Deskle MTD, partially eroding it and containing several sizable olistoliths. This MTD has also been identified on the map, and the correlation suggests that it could be the main candidate to correlate with MTD 3, together with the Deskle MTD that should be the lower interval of the poli-phased megabed (sensu Tunis and

Venturini, 1992). The megabed above Deskle shows significant cannibalistic behavior, with very large olistoliths and possibly large platform blocks that could have been dislodged by the megabed itself.

According to the literature, the Julian Basin was bounded by a shallow-water and partially emergent carbonate platform to the southwest and south, the Dinaric deformational wedge to the northeast, and the emerging Alpine system to the north (Pirini et al., 1986; Tunis and Pirini Radrizzani, 1987). These data must be interpreted considering the paleotransport directions identified by various authors.

Following from the structural analysis carried on by Ogata et al. (2014) in the Vernasso quarry the MTD 15 and 11 display a paleo-transport direction NE-ward and, therefore, a southwestern provenance has been suggested, in accordance with the insights derived from the compositional and provenance analysis of the internal components as detailed by Tunis and Venturini (1992) and Catani and Tunis (2001).

The Deskle underlying succession (from Rodež to Lastivnica MTDs) shows very thick bodies within the Anhovo quarry, which, according to Ogata et al. (2014), have a provenance from the N-NE and thus a S-SW transport direction, at least for the main ones (Rodež, Perunk and Perunk2), although with a considerable spread of azimuths. Based on the main compositions and inferred provenances, Skaberne (1987) suggests a source area located to the southeast and east for these carbonate MTDs. This discrepancy is likely due to the coeval and similar nature of the sedimentary deposits rimming the southeastern part of the basin, the very proximal depositional environment, and the structurally confined setting.

According to Tunis and Venturini (1992), on the NW–SE-directed, elongated, and narrow shape of this inner foredeep basin, Grivò Flysch MTDs could have spread out, coming either from the "passive" (southwestern) or "active" (northeastern) margin. From the above-cited data, the Anhovo quarry MTDs (Rodež, Perunk and Perunk 2) seem to originate from the northern–northeastern sectors.

To the N-NE and E, carbonate platform limestones are observed and mapped (Buser, 1974; Wagen, 1898), suggesting proximity to the basin margin (Ogata et al., 2014; Skaberne, 1987), and it is plausible that these bodies significantly reduce their thickness moving westward. As demonstrated by Pini and Ponton (2023), moving westward, beds like MTD 2 thin considerably from a hundred meters to ten meters of thickness Assuming the correlation between MTD 3 and the supra-Deskle and Deskle MTD, Perunk unit can tentatively be correlated to MTD 2, being the thick megabed below. MTD 2 bis can be correlated to Lastivnica or to Perunk 2. The stratigraphically

lower succession consists of MTDs with significant local thickness, like Podbrdo and, above all, Rodež, which might be correlated with smaller MTDs like MTD 1 bis and MTD 1 of Pini and Ponton (2023).

An additional complicating factor is a detachment surface located near the locality of Lig (see attached geological map), close to the summit of Mt. Kuk, which seems to significantly displace and cause erosion of the succession between MTD 2 and the underlying ones, making correlation more difficult, as well as overturning the beds themselves.

The established correlation leads to make the important yet problematic assumption that the Rodez Unit may correspond to MTD1. This poses a challenge because, at Anhovo, the Rodez reaches thicknesses of several hundred meters (Ogata et al., 2014), whereas according to the literature (Pini and Ponton, 2023; Feruglio, 1925) MTD1 in the region of the Italian Julian Prealps does not exhibit significant thicknesses. This assumption will undoubtedly require further investigation in future studies by expanding the study area.

8.2 - Marlstone Thickness

Certain observations have been noted about the significant amount of material constituting Unit U5, which is considerable and apparently homogeneous. However, upon thin-section examination, structures due to traction currents have been observed. In agreement with Pirini et al. (1986), this fact may suggest phenomena of suspension of an enormous amount of fine material due to the MTD emplacement (e.g., the thickness of marls and calcilutites in MTD 3 can reach 60 meters in certain sections), which was ponded, possibly multiple times, due to the confinement of the basin and deposited in deeper areas. The traction structures may be related to this movement.

Another phenomenon that should be considered is flocculation, i.e., the role of organic matter as a nucleus for floc formation. This process could significantly affect the deposition rate of U5, potentially making it more rapid than expected, and give new insights on the genesis of deposits contained within U5 (e.g., the thin-bedded turbidites found in the Lastivnica marls).

8.3 - Tsunamigenic Potential

Regarding tsunamigenic potential, no definitive evidence has been found. It is supposed that, given the volumes of material involved (tens of km³; Tunis and Venturini, 1992), the confined nature of the basin, and the magnitude of the possible trigger, it is plausible that the larger bodies generated tsunamis. However, no particular proxies have been found at the top of these beds that directly indicate the presence of tsunami deposits. Indeed, the mineral-petrographic results do not show significant variations compared to the sources studied in the enclosing flysch succession, and the organic matter content appears low and mainly related to marine organic matter. The presence of hybrid turbidites within the marl horizon has been observed in other outcrops of the basin, but not with the thickness seen in Lastivnica, and can be associated with various types of triggers (e.g. co-seismic turbidites associated to a subsequent seismic shock).

Another possible hypothesis is that the marls at the top of the MTDs could potentially represent a Type-B homogenite of Cita et al. (1996). However, the absence of a basal erosive surface at the interface between marls and calcarenites, as well as the presence of traction structures within the marls, allows us to discard this hypothesis.

8.4 - Emplacement Dynamics

Ogata et al. (2014) adopted Mutti's bipartite flow model to explain the emplacement dynamics of these bodies (Fig.8.4). In interpreting field observations and 3D outcrop models, we chose to compare this model with that of Li et al. (2024). Both Ogata et al. (2014) and Li et al. (2024) investigate the emplacement processes of carbonate-rich MTDs in deep-water environments, yet they propose different conceptual models based on their observations and interpretations. Despite focusing on different geological settings - the Paleogene Friuli Basin in Italy and Slovenia for Ogata et al., and the Triassic deep-water system of the West Qinling Orogenic Belt in Central China for Li et al. - both studies delve into the complexities of gravity-driven sedimentary processes involving carbonates.

Ogata et al. (2014) propose that the MTDs in the Friuli Basin were generated by a bipartite coherent and cohesive flow. This flow consisted of a lower debris-blocky flow or avalanche, carrying outsized carbonate and siliciclastic slide blocks (olistoliths), overlain by an upper diluted debris or grain flow. When considering the additional high- to low-density turbulent parts, the parent flow can be described as tripartite. The lower slide division itself exhibits a bipartite nature, featuring a basal, thinner matrix-dominated portion and an upper, thicker block-dominated portion, each characterized by different types of background sedimentary matrix, here understood as the finer-grained sediment that surrounds and supports larger clasts, which varies in composition from predominantly calcareous to more siliciclastic. The mechanism of suspension and transport for these deposits involves a combination of matrix overpressure, dispersive pressure from grain-to-grain interactions, and buoyant forces acting on less dense elements such as vuggy or potentially gas-charged carbonates and loosely packed substrate rip-up blocks. The overpressured matrix allows for the suspension of large olistoliths within the flow. As the flow moves downslope, it becomes highly erosive when encountering slope gradient breaks or paleo-topographic highs, leading to the entrainment of additional sediments from the seafloor and underlying sedimentary sequences. The emplacement of the lower portion of the slide mass occurs through differential movements of internal components, with shearing and flowing of the overpressured matrix facilitating the passive deformation and accommodation of the plastic olistoliths and underlying sediments.

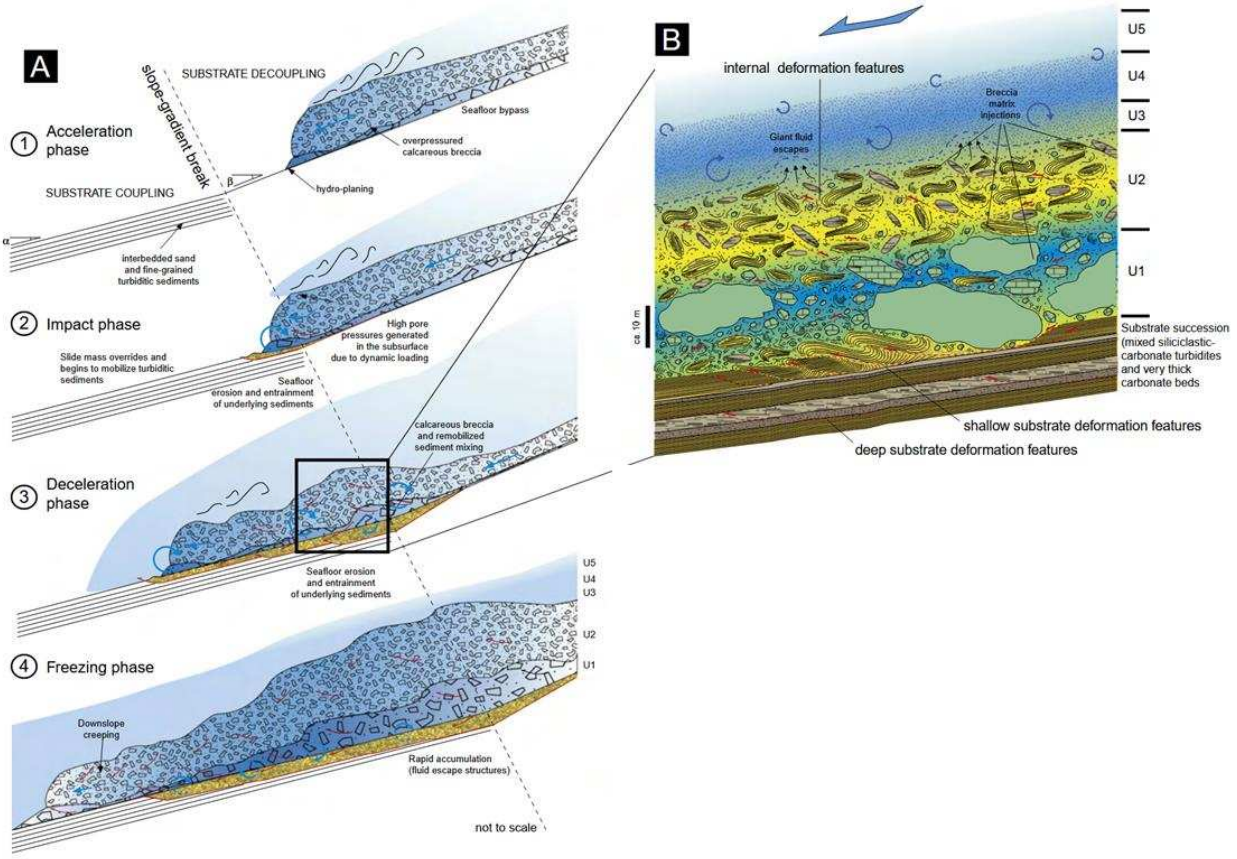

Fig. 8.4 (A) conceptual model illustrating the different stages of the slide mass—from acceleration to deposition—with a focus on substrate erosion and bypass related to dynamic loading. (B) hypothetical close-up illustration showing how mass transport leads to seafloor erosion, as well as the internal deformation features in both shallow and deep substrate layers. From Ogata et al. (2014)

In contrast, Li et al. (2024) interpret the carbonate-rich megabeds in the West Qinling Orogenic Belt as deposits from mixed carbonate-siliciclastic gravity flows involving more than one flow type (Fig.8.5). Each megabed represents a single depositional event with gradational boundaries between divisions. The basal clast-supported division (Division I) is rich in large clasts such as cobbles and boulders, overlain by a matrix-supported division (Division II), and capped by a division indicative of turbidity current deposition (Division III). The superposition of Division II on Division I suggests that the initial deposition involved the accumulation of large clasts at the front of a debris flow, which were then overrun by the main body of the flow. Alternatively, it could represent cobbles and boulders that settled out from an overriding flow unable to support them due to rheological limitations, leading to a jammed basal layer. Li et al. propose that Division II represents plug flow behavior, where the flow's yield stress has been exceeded, resulting in instantaneous freezing. Division III records a transformation from debris flow to turbidity current, occurring through mechanisms such as admixing water into the flow body, stripping sediment from the flow's upper surface, or hydraulic jumps, which lead to flow dilution and turbulence. This transformation

reflects a rheological evolution from non-Newtonian to Newtonian behavior as the flow becomes less concentrated and more turbulent.

The critical difference between the two models lies in the mechanisms proposed for the transport and deposition of large clasts, including olistoliths. Ogata et al. emphasize the role of fluid overpressure within a cohesive flow in suspending and transporting outsized blocks. The overpressured matrix provides buoyant support, and dispersion pressure contributes to maintaining the suspension of particles. This combination allows large olistoliths to be incorporated into the flow and transported over significant distances. The flow's erosive capacity is enhanced when it encounters slope breaks or topographic obstacles, leading to additional entrainment of sediments and contributing to the flow's ability to move large blocks. Li et al., on the other hand, suggest that while the debris flow initially supports large clasts, rheological changes within the flow limit its capacity to maintain clast support. As the flow evolves, the yield stress is exceeded, causing the large clasts to settle and accumulate at the base, forming a jammed layer (Division I). The overlying flow (Division II) moves as a plug over this jammed layer, and the subsequent transformation into a turbidity current (Division III) marks a shift in the flow's ability to transport coarse material. In this model, the transport of large clasts is limited to the early stages of the flow, and their deposition results from rheological constraints rather than sustained support within an overpressured matrix.

Two types of observations made on the MTDs of the Julian Basin could be considered in this discussion. The first is the apparent absence of a true gradation or observable trend at the outcrop scale within the U2 breccia unit. As observed in U2 of MTD 11 exposed at the Vernasso quarry, the distribution of rip-up blocks of the substrate and marly olistoliths does not seem graded, and some of them, even of considerable size, are visible up to the interface with Unit U3 (Fig.8.6-8.7). This observation could favor the model proposed by Li et al. (2024). Moreover, the distribution of flysch rip-up olistoliths within U2 seems to contradict the model of Ogata et al. (2014), as they should have been distributed by the flow above U1, forming U2; yet Unit U2 does not present particular gradations referable to an internal distribution process.

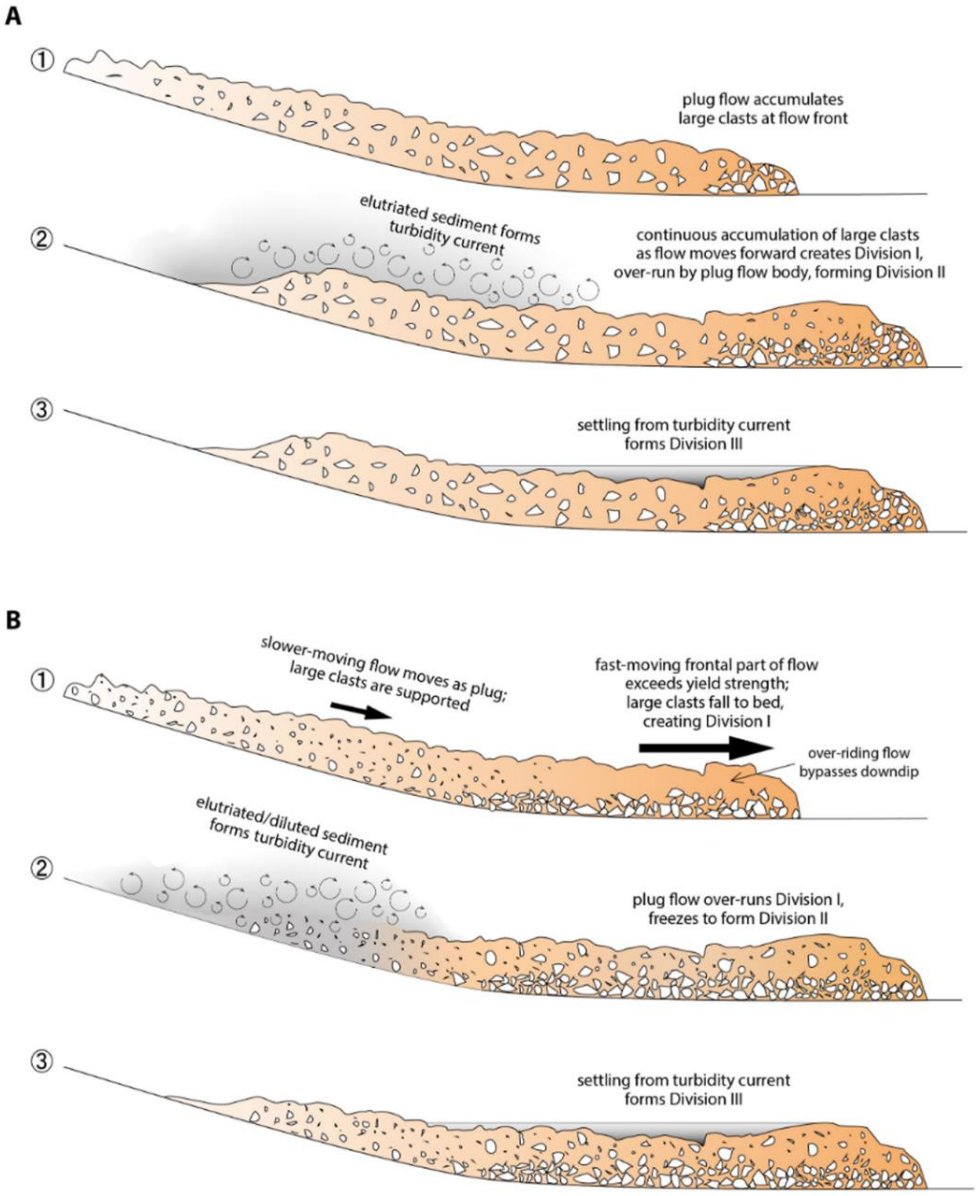

Fig. 8.5 two depositional mechanisms and processes for MTDs, with the key difference being the formation of Divisions I and II. (A) Frontal Accumulation Model: In stage 1, a plug flow collects large clasts at its leading edge, forming a continuous layer (Division I) as it progresses. By stage 2, the flow then freezes, creating Divisions I and II. Simultaneously, finer sediments are elutriated from the plug flow, transforming into a turbidity current (also in stage 2), which later settles to form Division III in stage 3. (B) Longitudinal Segregation Model: Initially, the flow separates into a slower-moving plug flow and a faster-moving frontal flow. During stage 1, the faster frontal flow forms Division I by accumulating large clasts at the base due to jamming from an over riding shearing and bypassing flow. In stage 2, the slower plug flow overtakes Division I to form Division II, with a portion of it transitioning into a turbidity current. Finally, in stage 3, the trailing turbidity current deposits material that becomes Division III. From Li et al., 2024.

However, within the Vernasso quarry, MTD 15 seems to show, at the interface between the substrate and U1, a flysch olistolith eroded from the background succession (Fig.8.8). This observation supports the model proposed by Ogata et al. (2014). If the olistolith were eroded from the substrate by the part of the flow that subsequently becomes a higher unit, it would not be at the base of the deposit. Observing an olistolith at the base of the deposit suggests two possibilities: one

is that it was within the flow and suddenly settled, which could happen with large, heavy, fully lithified olistoliths in a relatively weak matrix; the other is that the part of the flow that eroded material from the substrate remained at the bottom until it ceased moving. If a higher unit overtakes, the substrate-derived olistolith should be higher in the deposit. This is consistent with our observations, as we have marlstone and flysch olistoliths close to the top of the breccia unit, and there is no vertical sorting within the deposit. This likely indicates an interaction of multiple processes.

Figure 8.6 drone image of the Vernasso quarry. Focus on the MTD11.

In explaining the emplacement dynamics of the MTDs of the Julian Basin, perhaps a combination of processes expressed by both models can be considered.

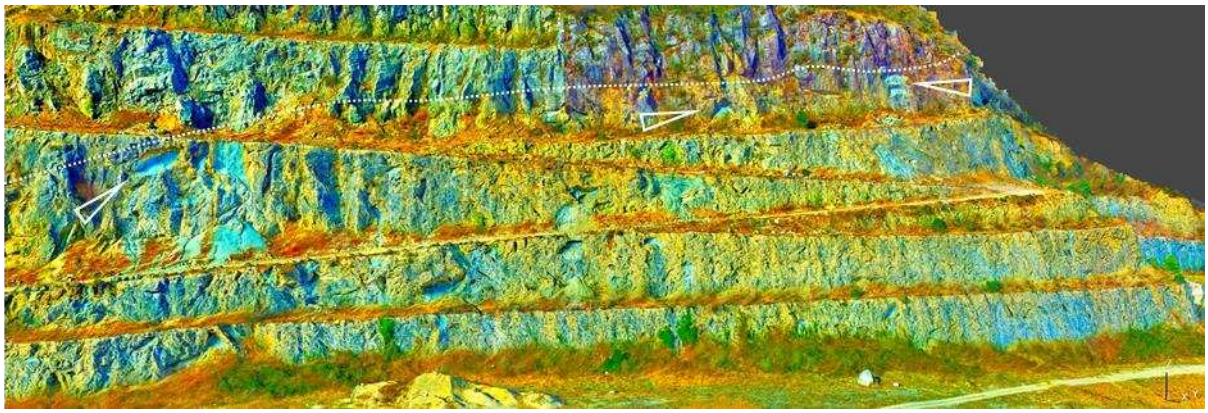

Fig. 8.7 false-color 3D virtual outcrop model of U2 of MTD11 in Vernasso Quarry. Marl olistoliths are in light-blue (see white pointers). Dotted line is the limit between U2-U3

The emplacement of a Division I that has, at its front, a "bulldozer" behavior, incorporating rip-up olistoliths of the substrate, to then be covered by Division II and finally by the overlying megaturbidite, reflects aspects of both models. Alternatively, it might be that each model better explains the behavior of individual MTDs; thus, the model of Ogata et al. (2014) could better explain the emplacement dynamics of MTD 15, while that of Li et al. (2024) might be suitable for MTD 11. The different behavior may be due to the amount of material involved in the MTD emplacement and the local basin shape.

Fig. 8.8 flysch olistolith (yellow) at the base of MTD15 (purple) in Vernasso Quarry

9- Conclusions

A multi-approach study of the Julian Basin MTDs has been applied to provide some new insights into the geology of the Paleogene rocks in the area crossing the border between Italy and Slovenia. The study integrated field surveys, remote sensing techniques, sedimentological analyses, and geochemical investigations to enhance the understanding of the Carbonate Mass Transport Deposits (MTDs) in the Grivò Flysch formation.

Through detailed field mapping and remote sensing analyses, utilizing tools such as the Relief Visualization Toolbox (RVT) and sky-view factor (SVF), this study achieved a correlation of the principal MTD units across the Italian-Slovenian border. The enhanced morphological characterization facilitated the identification and tracing of key units, including MTD 3 (Monte Ioanaz), MTD 11 (Vernasso), and MTD 15 (Porzus). Despite the challenges associated with establishing these correlations, the geological map derived from detailed field surveys and DEM analyses marks a significant step in clarifying the stratigraphy of the Julian Basin. Notably, the pronounced variation in bed thickness, also observed on the Italian side (e.g., MTD 2; see Pini and Ponton, 2023), offers critical insight into basin dynamics. Thus, based on paleocurrent data and object dimensions (Pirini et al., 1986; Tunis and Pirini Radrizzani, 1987; Ogata et al., 2014), it can be inferred that the MTDs succession in Anhovo may represents the expression of a basin margin setting.

This correlation therefore appears both reasonable and feasible, although there is naturally room for further discussion of specific details and interpretations, as well as the incorporation of additional data from adjacent areas.

Mineralogical and geochemical analyses of samples from the Anhovo quarry MTDs sequence revealed a progressive increase in siliciclastic elements stratigraphically upward, accompanied by a decrease in calcium content. This trend suggests a gradual shift in sedimentary input and provenance. The identification of heavy minerals like zircon, magnetite, chromite, and tourmaline provided some insights into the material sources, coherent with a possible Dinaric input, and sedimentary processes involved in the formation of these deposits.

Total Organic Carbon (TOC) analyses indicated a relatively low organic carbon content across the samples, with values consistent with marine organic matter. The presence of hybrid thin-bedded turbidites within the marls of the Lastivnica unit, displaying traction structures, suggests complex

sedimentation patterns potentially influenced by tectonic, seismic activities and related consequences (e.g. tsunami).

Thin-section analyses and experimental image processing techniques uncovered traction structures within the hybrid turbidites and marls, which are not apparent at the macroscopic scale. These findings highlight the internal architectures of the MTDs uppermost unit and its depositional mechanisms, potentially related to sediment pounding.

While the study provides new data about the Julian Basin's geology, certain limitations must be acknowledged:

Data Coverage: The dense vegetation and limited outcrop exposure in the study area constrained the availability of field data in some areas.

Tsunamigenic Evidence: The study did not find definitive sedimentological or geochemical proxies indicative of tsunami deposits associated with the MTDs. The potential tsunamigenic impact of these mass-wasting events remains a reasonable possibility, but at the moment speculative without direct evidence.

9.1 – Future research

Building on the findings and acknowledging the limitations, the following recommendations are proposed for future research:

Extending the mapping area to reach the platform margin and revisiting correlation uncertainties, particularly by overcoming the challenges posed by the area's complexity, could integrate, confirm, or refine the existing geological mapping, possibly in collaboration with Slovenian geologists.

Employing high-resolution biostratigraphic analyses would improve the temporal resolution and correlation between different Mass Transport Deposit (MTD) units, thereby enhancing the chronological framework; samples have already been collected, and a potential collaboration with the National Research Center - Marine Science Institute (CNR-ISMAR) has been established to facilitate this work.

Continuing detailed studies of Units U1 and U2 is essential to obtain new data regarding the distribution and fragmentation of blocks within the MTDs. This research would contribute to existing emplacement models and improve understanding of the internal architecture of these deposits. Additionally, a thorough biostratigraphic analysis of the calcareous olistoliths in different MTDs could elucidate their provenance and depositional history.

An in-depth study of the calcarenite units, particularly those within MTD3, is recommended. Horizons rich in organic matter have been cited in previous works (e.g., Liuzzi, 1994) and observed by quarry workers; sampling and analyzing these horizons could reveal significant information about the depositional environment and organic content.

Studying heavy mineral phases and quantifying them along various basin transects could provide insights into the paleotransport directions of the MTDs, as higher concentrations of heavy minerals may be deposited closer to source areas. These mineralogical studies could also characterize the source of the siliciclastic material in detail. This research is feasible thanks to an internal collaboration with the Department of Mathematics, Informatics, and Geoscience at the University of Trieste.

Moreover, new insights into the emplacement dynamics of the MTDs and the characteristics of the "Pietra Piasentina" (U3-U4 calcirudites and calcarenites) may positively impact local quarry extraction activities, with which we already maintain good relationships and have opportunities to regularly visit quarry sites.

To better understand the relationship between hybrid turbidites and the marls of Unit U5, particularly in the Lastivnica case, it is important to quantify the role of organic matter and flocculation in marl deposition rates. Conducting analog experiments on unconsolidated sediments with compositions and total organic carbon (TOC) contents similar to the lithified rocks could simulate depositional processes and improve interpretations of sedimentation dynamics. To this end, a collaboration with the Section of Environmental Fluid Mechanics of the University of Delft has been established, and the necessary resources to conduct such experiments are available.

References

Abarghani, A., Gentzis, T., Liu, B., Khatibi, S., Bubach, B., & Ostadhassan, M. (2020). Preliminary investigation of the effects of thermal maturity on redox-sensitive trace metal concentration in the bakken source rock, north dakota, usa. ACS Omega, 5(13), 7135-7148. https://doi.org/10.1021/acsomega.9b03467

Abbate, E., Bortolotti, V., & Passerini, P. (1970). Olistostromes and Olistoliths. Sedimentary Geology, 4(3–4), 521–557. https://doi.org/10.1016/0037-0738(70)90022-9

Accaino, F., Busetti, M., Böhm, G., Baradello, L., Affatato, A., Dal Cin, M., & Nieto, D. (2019). Geophysical investigation of the Isonzo Plain (NE Italy): Imaging of the Dinaric-Alpine chain convergence zone. Italian Journal of Geosciences, 138(2), 202–215. https://doi.org/10.3301/IJG.2019.01

Aigner, T. (1980). *Storm deposits as a tool in facies analysis*. Abstracts: International Association of Sedimentologists 1st European Meeting, 44

Allen, P. A. (1981). Wave-generated structures in the Devonian lacustrine sediments of southeast Shetland and ancient wave conditions. *Sedimentology* 28, 369–379. https://doi:10.1111/j.1365-3091.1981.tb01686.x

Alves, T. M. (2015). Submarine slide blocks and associated soft-sediment deformation in deep-water basins: A review. Marine and Petroleum Geology, 67, 262–285. https://doi.org/10.1016/j.marpetgeo.2015.05.010

Alves, T.M., Cardona, S., & Rodrigues, M.C.N.L. (2022). Mass transport processes, injectites and styles of sediment remobilization, in: Deepwater Sedimentary Systems. Elsevier, pp. 361–406. https://doi.org/10.1016/B978-0-323-91918-0.00013-X

Alves, T.M., & Cartwright, J.A. (2010). The effect of mass-transport deposits on the younger slope morphology, offshore Brazil. Marine and Petroleum Geology 27, 2027–2036. https://doi.org/10.1016/j.marpetgeo.2010.05.006

Alves, T. M., Kurtev, K., Moore, G. F., & Strasser, M. (2014). Assessing the internal character, reservoir potential, and seal competence of mass-transport deposits using seismic texture: A

geophysical and petrophysical approach. AAPG Bulletin, 98(4), 793–824. https://doi.org/10.1306/09121313117

Bahk, J.-J., Kang, N.K., Yi, B.-Y., Lee, S.-H., Jeong, S.-W., Urgeles, R., & Yoo, D.-G. (2017). Sedimentary characteristics and processes of submarine mass-transport deposits in the Ulleung Basin and their relations to seismic and sediment physical properties. Marine Geology 393, 124–140. https://doi.org/10.1016/j.margeo.2017.05.010

Barago, N., Pavoni, E., Floreani, F., Crosera, M., Adami, G., Lenaz, D., Larese Filon, F., & Covelli, S. (2022). Portable X-Ray Fluorescence (pXRF) as a Tool for Environmental Characterisation and Management of Mining Wastes: Benefits and Limits. Applied Sciences 12(23): 12189. https://doi:10.3390/app122312189

Benedetti, A., Papazzoni, C. A., Bosellini, F., Giusberti, L., & Fornaciari, E. (2024). High-diversity larger foraminiferal assemblages calibrated with calcareous nannoplankton biozones in the aftermath of EECO (Collio, Friuli-Venezia Giulia, Northeastern Italy). Palaeoworld, 33(2), 492–503. https://doi.org/10.1016/j.palwor.2023.01.013

Bhaumik, A.K., Kumar, S., Chaudhuri, S., Mohanty, S., Mukherjee, M.K., Sain, K., Gupta, A.K., & Kumar, P. (2024). Accumulation of gas hydrates in mass transport deposits at Krishna-Godavari Basin, Bay of Bengal: Foraminiferal, sedimentologic, and seismic evidence. AAPG Bulletin, 108(9), 1687–1703. https://doi.org/10.1306/03222423052.

Bertagnin, M., & Frangipane, A. (2007). Pietra Piasentina - Tradizione e Modernità.

Best, A. I., C. R. I. Clayton, O. Longva, and M. Szuman. 2003. 'The Role of Free Gas in the Activation of Submarine Slides in Finneidfjord'. In Submarine Mass Movements and Their Consequences: 1st International Symposium, eds. Jacques Locat, Jürgen Mienert, and Luc Boisvert. Dordrecht: Springer Netherlands, 491–98. doi:10.1007/978-94-010-0093-2_54.

Blechschmidt, G, Maria Bianca Cita, Roberto Mazzei, & Gianfranco Salvatorini. (1982). Stratigraphy of the Western Mediterranean and Southern Calabrian Ridges, Eastern Mediterranean. Marine Micropaleontology 7(2): 101–32.

Bouma, A. H. (1987). Megaturbidite: An Acceptable Term? Geo-Marine Letters, 7(2), 63–67. https://doi.org/10.1007/BF02237985

Bryn, Petter, Kjell Berg, Carl F. Forsberg, Anders Solheim, and Tore J. Kvalstad. 2005. 'Explaining the Storegga Slide'. Marine and Petroleum Geology 22(1–2): 11–19. doi:10.1016/j.marpetgeo.2004.12.003.

Bull, S., Cartwright, J., & Huuse, M. (2009). A review of kinematic indicators from mass-transport complexes using 3D seismic data. Marine and Petroleum Geology, 26(7), 1132–1151. https://doi.org/10.1016/j.marpetgeo.2008.09.011

Buser, S. (1974). Geological Map of SFRJ 1 :100000 Sheet TOLMIN. Geologija, 17(1), 493–496. Retrieved from https://www.geologija-revija.si/index.php/geologija/article/view/332

Buser, S. (1989): Development of the Dinaric and Julian carbonate platforms and the intermediate Slovenian basin (NWYugoslavia). In: Carulli, GB., Cucchi, F., Radrizzani, CP. (eds.): Evolution of the Karstic carbonate platform: relation with other periadriatic carbonate platforms. Memorie della Società Geologica Italiana, 40, 313-320.

Buser, S. (1996): Geology of Western Slovenia and its paleographic evolution. In: Drobne, K. et al. (ed.): The role of impact processes in the geological and biological evolution of planet Earth. International workshop, September 27 – October 2, 1996, Postojna/Slovenia, pp. 111–123.

Buser, S., Kolar-Jurkovšek, T., & Jurkovšek, B. (2008). The Slovenian Basin during the Triassic in the Light of Conodont Data, Bollettino della Società Geologica Italiana 127(2), 257-263

Buser, S., & Pavšič, J. (1978). Pomikanje zgornjekrednega in paleogenskega flisnega bazena v zahodni Sloveniji. In 9. Kongres geologa Jugoslavije (pp. 74–81). Sarajevo.

Bryn, P., Berg, K., Forsberg, C.F., Solheim, A., & Kvalstad, T. (2005). Explaining

the Storegga slide. Marine and Petroleum Geology, 22(1–2), 11–19. https://doi:10.1016/j.marpetgeo.2004.12.003.

Camerlenghi, A., & Pini, G. A. (2009). Mud Volcanoes, Olistostromes and Argille Scagliose in the Mediterranean Region. Sedimentology, 56(1), 319–365. https://doi.org/10.1111/j.1365-3091.2008.01016.x

Cantalamessa, G., & Di Celma, C. (2005). Sedimentary features of tsunami backwash deposits in a shallow marine Miocene setting, Mejillones Peninsula, northern Chile. Sedimentary Geology 178, 259–273. https://doi.org/10.1016/j.sedgeo.2005.05.007

Cardona, S., Wood, L. J., Day-Stirrat, R. J., & Moscardelli, L. (2016). Fabric development and pore-throat reduction in a mass-transport deposit in the Jubilee Gas Field, eastern Gulf of Mexico: Consequences for the sealing capacity of MTDs. Submarine Mass Movements and Their Consequences, 27–37. https://doi.org/10.1007/978-3-319-20979-1_3

Callot, P., Sempere, T., Odonne, F., & Robert, E. (2008). Giant submarine collapse of a carbonate platform at the Turonian–Coniacian transition: The Ayabacas Formation, southern Peru. Basin Research 20, 333–357. https://doi.org/10.1111/j.1365-2117.2008.00358.x

Carter, L., Gavey, R., Talling, P., & Liu, J. (2014). Insights into submarine geohazards from breaks in subsea telecommunication cables. Oceanography, 27(2), 58–67. https://doi.org/10.5670/oceanog.2014.40

Catani, G., & Tunis, G. (2001). Caratteristiche sedimentologiche dei megabanchi carbonatici paleogenici del Bacino Giulio (Valli del Natisone, Friuli orientale). In: Evolution of the Southern Margin of the Julian Basin with Emphasis on the Megabeds and Turbidites Sequence of the Southern Julian Prealps (NE Italy). Geologia Croatica, 54(2), 127-150.

Chiba, T., Kaneta, S., & Suzuki, Y. (2008). Red Relief Image Map: New Visualization Method for Three Dimensional Data. The international archives of the photogrammetry, remote sensing and spatial information sciences 37(B2): 1071–76.

Cita, M.., Camerlenghi, A., & Rimoldi, B.. (1996). Deep-Sea Tsunami Deposits in the Eastern Mediterranean: New Evidence and Depositional Models. Sedimentary Geology 104(1–4): 155–73. https://doi.org/10.1016/0037-0738(95)00126-3

Coleman, J. M., Prior, D. B., & Garrison, L. E. (1978). Submarine Landslides in the Mississippi River Delta. OTC, OTC-3170.

Colizza, E., Costa, R., Cucchi, F., & Pugliese, N. (Eds.). (1987). International Symposium on the Evolution of the Karstic Carbonate Platform. Udine: Università di Trieste.

Cousin, M. (1970) Esquisse geologique cles confins italo-yougoslaves: leur place dans les Dinarides et \es Alpes meridionales. - Bulletin de la Societe geologique de France 7, 1034-1047.

Cousin, M. (1981): Les repports Alpes – Dinarides. Les confins de l' Italie et dela Yougoslavie. Sociètè Gèologique du Nord.; Publi. 5, Vol. 2 – Annexe, 521 p., Villenueve.

Csontos, L., Vörös, A., 2004. Mesozoic plate tectonic reconstruction of the Carpathian region. Palaeogeography, Palaeoclimatology, Palaeoecology 210, 1–56. https://doi.org/10.1016/j.palaeo.2004.02.033

Cucchi, F., & Finocchiaro, F. (2017). Karst Landforms in Friuli Venezia Giulia: From Alpine to Coastal Karst. In Landscapes and Landforms of Italy, World Geomorphological Landscapes, eds. Mauro Soldati and Mauro Marchetti. Cham: Springer International Publishing, 147–56. doi:10.1007/978-3-319-26194-2_12.

Dainelli, G. (1915). Il Terziario del Friuli. Firenze: Tipografia Ricci.

Dasgupta, P. (2003). Sediment Gravity Flow—the Conceptual Problems. Earth-Science Reviews 62(3–4): 265–81. https://doi.org/10.1016/S0012-8252(02)00160-5

Dolenec, T., Pavšič, J., & Lojen, S. (2000). The Paleocene-Eocene boundary in a flysch sequence from Goriška Brda (Western Slovenia): Oxygen and carbon stable isotope variations. Geologija, 43(1), 37–42. https://doi.org/10.5474/geologija.2000.002

Eckel, E. B. (1958). Introduction to Landslides and Engineering Practice. Highway Research Board Special Report. https://www.semanticscholar.org/paper/INTRODUCTION-TO-LANDSLIDES-AND-ENGINEERING-PRACTICE Eckel/66275db7606122b974e27ddc3a099f52a032013a

Embley, R. W. (1980). The Role of Mass Transport in the Distribution and Character of Deep-Ocean Sediments with Special Reference to the North Atlantic. Marine Geology, 38(1–3), 23–50. https://doi.org/10.1016/0025-3227(80)90050-X

Fallgatter, C., Kneller, B., Paim, P. S. G., & Milana, J. P. (2017). Transformation, Partitioning and Flow–Deposit Interactions during the Run-out of Megaflows. Sedimentology, 64(2), 359–387. https://doi.org/10.1111/sed.12307

Feruglio, F. (1925). La geologia delle Prealpi Giulie fra l'Isonzo e l'Arzino. Bollettino della Società Geologica Italiana, 44, 1–113.

Fontolan, G., & Tunis, G. (1989). Sequenze calciclastiche grossolane in ambiente di apron - margine di bacino ("Flysch del Matajur", Friuli orientale). Memorie della Società Geologica Italiana, 40, 117–126.

Festa, A., Dilek, Y., Pini, G.A., Codegone, G., & Ogata, K. (2012). Mechanisms and processes of stratal disruption and mixing in the development of mélanges and broken formations: Redefining and classifying mélanges. Tectonophysics, 568–569, 7–24. https://doi.org/10.1016/j.tecto.2012.05.021

Festa, A., Ogata, K., Pini, G. A., Dilek, Y., & Alonso, J. L. (2016). Origin and Significance of Olistostromes in the Evolution of Orogenic Belts: A Global Synthesis. Gondwana Research, 39, 180–203. https://doi.org/10.1016/j.gr.2016.08.002

Festa, A., Pini, G.A., Ogata, K., & Dilek, Y. (2019). Diagnostic features and field-criteria in recognition of tectonic, sedimentary and diapiric mélanges in orogenic belts and exhumed

subduction-accretion complexes. Gondwana Research, 74, 7–30. https://doi.org/10.1016/j.gr.2019.01.003

Gamberi, F., Rovere, M., & Marani, M. (2011). Mass-transport complex evolution in a tectonically active margin (Gioia Basin, Southeastern Tyrrhenian Sea). Marine Geology 279, 98–110. https://doi.org/10.1016/j.margeo.2010.10.015

Gan, Y., Almeida, F., Rossi, V., Steel, R., & Olariu, C. (2022). Sediment transfer from shelf to deepwater slope: How does it happen? Journal of Sedimentary Research, 92(6), 570–590. https://doi.org/10.2110/jsr.2021.013

Greenly, E. (1919). The Geology of Anglesey. Memoirs of The Geological Survey, England & Wales, 1-494.

Hampton, M., Lee, H., & Locat, J. (1996). Submarine Landslides. Reviews of Geophysics, 34 (1), 33-59. https://doi.org/10.1029/95RG03287

Harbitz, C. B., Løvholt, F., & Bungum, H. (2014). Submarine Landslide Tsunamis: How Extreme and How Likely? Natural Hazards, 72(3), 1341–1374. https://doi.org/10.1007/s11069-013-0681-3

Heezen, B. C., & Ewing, W. M. (1952). Turbidity currents and submarine slumps, and the 1929 Grand Banks earthquake. American Journal of Science, 250(12), 849–873. https://doi.org/10.2475/ajs.250.12.849

Hieke, W. A. Thick Holocene homogenite from the Ionian abyssal plain (Eastern Mediterranean). *Mar. Geol.* **55**, 63–78 (1984).

Hsü, K.J. (1968). Principles of Mélanges and Their Bearing on the Franciscan-Knoxville Paradox. Geological Society of America Bulletin, 79, 1063-1074. https://doi.org/10.1130/0016-7606(1968)79[1063:POMATB]2.0.CO;2

Huhn, K., Arroyo, M., Cattaneo, A., Clare, M. A., Gràcia, E., Harbitz, C. B., Krastel, S., Kopf, A., Løvholt, F., Rovere, M., Strasser, M., Talling, P.J., & Urgeles, R. (2019). Modern submarine landslide complexes: A short review. In: Ogata, K., Festa, A., Pini, G.A. (eds.), Submarine Landslides: Subaqueous Mass Transport Deposits from Outcrops to Seismic Profiles, Geophysical Monograph 247, American Geophysical Union and John Wiley & Sons, Inc., 181–200. https://doi.org/10.1002/9781119500513.ch12

Kanamatsu, T., Kawamura, K., Strasser, M., Novak, B., & Kitamura, Y. (2014). Flow dynamics of Nankai Trough submarine landslide inferred from internal deformation using magnetic fabric. Geochemistry, Geophysics, Geosystems, 15, 4079–4092. https://doi.org/10.1002/2014GC005409

Kastens, K. A. & Cita, M. B. Tsunami-induced sediment transport in the abyssal Mediterranean Sea. *Geol. Soc. Am. Bull. Part* **I**(92), 845–857 (1981).

Kawamura, K., Laberg, J.S., & Kanamatsu, T. (2014). Potential tsunamigenic submarine landslides in active margins. Marine Geology, 356, 44–49. https://doi.org/10.1016/j.margeo.2014.03.007

Kelling, G., & Mullin, P. R. (1975). Graded limestones and limestone-quartzite couplets: Possible storm-deposits from the Moroccan carboniferous. *Sediment. Geol.* 13, 161–190. https://doi:10.1016/0037-0738(75)90019-6

Kneller, B., Dykstra, M., Fairweather, L., & Milana, J.P. (2016). Mass-transport and slope accommodation: Implications for turbidite sandstone reservoirs. AAPG Bulletin, 100, 213–235. https://doi.org/10.1306/09011514210

Kokalj, Ž., Somrak, M. (2019). Why Not a Single Image? Combining Visualizations to Facilitate Fieldwork and On-Screen Mapping. Remote Sensing, 11(7), 747.

Kokalj, Žiga, Hesse, R. (2017). Airborne Laser Scanning Raster Data Visualization: A Guide to Good Practice. Ljubljana: Založba ZRC.

Kvalstad, Tore J., Lars Andresen, Carl F. Forsberg, Kjell Berg, Petter Bryn, and Magnus Wangen. 2005. 'The Storegga Slide: Evaluation of Triggering Sources and Slide Mechanics'. Ormen Lange - an integrated study for the safe development of a deep-water gas field within the Storegga Slide Complex, NE Atlantic continental margin 22(1): 245–56. doi:10.1016/j.marpetgeo.2004.10.019.

Lee, H.J. (2005). Undersea landslides: extent and significance in the Pacific Ocean, an update. Natural Hazards Earth System Sci. 5, 877–892. https://doi.org/10.5194/nhess-5-877-2005

Liu, J., Gupta, S., Rutqvist, J., Ma, Y., Wang, S., Wan, K., Fan, C., & Yan, W. (2024). Can Glacial Sea-Level Drop-Induced Gas Hydrate Dissociation Cause Submarine Landslides? Geophysical Research Letters, 51, e2023GL106772. https://doi.org/10.1029/2023GL106772

Liuzzi, F. (1994). L'apertura, la coltivazione ed il recupero ambientale di cave di materiali lapidei nella zona del "Cividalese" (Friuli Orientale). Master Thesis, University of Trieste.

Lastras, G., Canals, M., & Urgeles, R. (2003). Lessons from Sea-Floor and Subsea-Floor Imagery of the Big'95 Debris Flow Scar and Deposit, in: Locat, J., Mienert, J., Boisvert, L. (Eds.), Submarine Mass Movements and Their Consequences, Advances in Natural and Technological Hazards Research. Springer Netherlands, Dordrecht, pp. 425–431. https://doi.org/10.1007/978-94-010-0093-2_47

Lemière, B. (2018). A review of pXRF (field portable X-ray fluorescence) applications for applied geochemistry. Journal of Geochemical Exploration, 188, 350–363. https://doi.org/10.1016/j.gexplo.2018.02.006

Li, Pan, Ben Kneller, and Victoria Valdez Buso. 2024. 'Carbonate-rich Megabeds within a Triassic Siliciclastic Deep-water System, West Qinling Orogenic Belt, Central China: Character, Processes and Implications'. The Depositional Record: dep2.301. doi:10.1002/dep2.301.

Lodowski, D.G., Grabowski, J., Rožič, B., Žvab-Rožič, P., Reháková, D., Slapnik, L., Iwańczuk, J., Chmielewski, & A., Teodorski, A.(2024). The Jurassic–Cretaceous Transition in the Slovenian Basin (Alpine Atlantic): Further Evidence for Palaeoenvironmental Record in Pelagic Sediments. Geochemistry, Geophysics, Geosystems, 25, e2024GC011728. https://doi.org/10.1029/2024GC011728

Marco, S., & Agnon, A. (2005). High-resolution stratigraphy reveals repeated earthquake faulting in the Masada Fault Zone, Dead Sea Transform. Tectonophysics, 408, 101–112. https://doi.org/10.1016/j.tecto.2005.05.036

Marinelli, O. (1902). Studi geologici sulle Prealpi Giulie. Bollettino della Società Geologica Italiana, 21, 11–58.

Martinis, B. (1966). Risultati di sondaggi profondi nel Friuli orientale. Memorie della Società Geologica Italiana, 5, 1–27.

Maslin, M., Mikkelsen, N., Vilela, C., & Haq, B. (1998). Sea-level –and gas-hydrate–controlled catastrophic sediment failures of the Amazon Fan. Geology, 26, 1107. https://doi.org/10.1130/0091-7613(1998)026<1107:SLAGHC>2.3.CO;2

Masson, D.G., Harbitz, C.B., Wynn, R.B., Pedersen, G., & Løvholt, F. (2006). Submarine landslides: processes, triggers and hazard prediction. Phil. Trans. R. Soc. A. 364, 2009–2039. https://doi.org/10.1098/rsta.2006.1810

Mazumder, R., Van Loon, A.J. (Tom), Malviya, V.P., Arima, M., & Ogawa, Y. (2016). Soft-sediment deformation structures in the Mio-Pliocene Misaki Formation within alternating deep-sea

clays and volcanic ashes (Miura Peninsula, Japan). Sedimentary Geology, 344, 323–335. https://doi.org/10.1016/j.sedgeo.2016.02.010

Meilijson, A. (2023). Long-term carbon sequestration in the Eocene of the Levant Basin through transport of organic carbon from nearshore to deep marine environments. Chemical Geology, 642, 121800. https://doi.org/10.1016/j.chemgeo.2023.121800

Miklavič, B., Rožič, B., 2008. The onset of Maastrichtian basinal sedimentation on Mt. Matajur, NW Slovenia. RMZ – Materials and Geoenvironment, (2), 199-214.

Moretti, M., Alfaro, P., Caselles, O., & Canas, J.A. (1999). Modelling seismites with a digital shaking table. Tectonophysics, 304, 369–383. https://doi.org/10.1016/S0040-1951(98)00289-3

Moretti, M., & Ronchi, A., 2011. Liquefaction features interpreted as seismites in the Pleistocene fluvio-lacustrine deposits of the Neuquén Basin (Northern Patagonia). Sedimentary Geology, 235, 200–209. https://doi.org/10.1016/j.sedgeo.2010.09.014

Mulder, T., & Alexander, J. (2001). The physical character of subaqueous sediment density flows and their deposits. Sedimentology, 48(2), 269–299. https://doi.org/10.1046/j.1365-3091.2001.00360.x

Mulder, T., & Cochonat, P. (1996). Classification of Offshore Mass Movements. Journal of Sedimentary Research, 66 (1): 43–57. https://doi.org/10.1306/D42682AC-2B26-11D7-8648000102C1865D

Nardin, T., Hein, F., Gorsline, D., & Edwards, B. (1979). A review of mass movement processes, sediment and acoustic characteristics, and contrasts in slope and base-of-slope systems versus canyon- fan- basin floor systems. Spec. Publ. Soc. Economic Paleontologists Mineralogists, 27, 61-7

Nanayama, Futoshi, and Kiyoyuki Shigeno. 2006. 'Inflow and Outflow Facies from the 1993 Tsunami in Southwest Hokkaido'. Sedimentary Geology 187(3–4): 139–58. doi:10.1016/j.sedgeo.2005.12.024.3.

Ogata, K., Festa, A., Pini, G., & Alonso J.L. (2019). Submarine Landslide Deposits in Orogenic Belts: Olistostromes and Sedimentary Mélanges. In: Ogata, K., Festa, A., Pini, G.A. (eds.), Submarine Landslides: Subaqueous Mass Transport Deposits from Outcrops to Seismic Profiles, Geophysical Monograph 247, American Geophysical Union and John Wiley & Sons, Inc., 181–200. https://doi.org/10.1002/9781119500513.ch1

Ogata, K., Festa, A., Pini, G. A., Pogačnik, Ž., & Lucente, C. C. (2016). Meso-scale kinematic indicators in exhumed mass transport deposits: Definitions and implications. In Submarine Mass Movements and Their Consequences. Springer, 461–468. https://doi.org/10.1007/978-3-319-20979-1_46

Ogata, K., Mountjoy, J., Pini, G.A., Festa, A., & Tinterri, R. (2014a). Shear zone liquefaction in mass transport deposit emplacement: A multi-scale integration of seismic reflection and outcrop data. Marine Geology, 356, 50-64. http://dx.doi.org/10.1016/j.margeo.2014.05.001

Ogata, K., Pini, G., Festa, A., Pogačnik, Ž., Tunis, G., Mountjoy, J., Senger, K., Strasser (2014b). High-Resolution Studies of Mass Transport Deposits: Outcrop Perspective for Understanding Modern Submarine Slope Failure and Associated Natural Hazards. In: Lollino, G., Manconi, A., Locat, J., Huang, Y., Canals Artigas, M. (eds.), Engineering Geology for Society and Territory, Volume 4. https://doi.org/10.1007/978-3-319-08660-6

Ogata, K., Pini, G. A., Tunis, G., & Festa, A. (2014c). The carbonate mass transport deposits of the Paleogene Friuli Basin (Italy/Slovenia): Internal anatomy and inferred genetic processes. Marine Geology, 356, 88–110. https://doi.org/10.1016/j.margeo.2014.06.014

Passey, Q. R., Bohacs, K. M., Esch, W. L., Klimentidis, R., & Sinha, S. (2010). From oil-prone source rock to gas-producing shale reservoir – geologic and petrophysical characterization of unconventional shale-gas reservoirs. Proceedings of International Oil and Gas Conference and Exhibition in China. https://doi.org/10.2523/131350-ms

Pavšič, J. (1985). Biostratigraphy of the Tolmin flysch (NW Yugoslavia) based on calcareous nannoplankton. Geologija, 28(1), 123–142.

Pini, G. A., & Ponton, M. (2023). Carta geologica dei megabanchi del Bacino Giulio – Geological map of the Julian Basin megabeds. Geological Survey of Friuli Venezia Giulia Region. http://dx.doi.org/10.13140/RG.2.2.18193.61287/1

Piper, D. J. W., Cochonat, P., & Morrison, M. L. (1999). The sequence of events around the epicentre of the 1929 Grand Banks earthquake: Initiation of debris flows and turbidity current inferred from sidescan sonar. Sedimentology, 46(1), 79–97. https://doi.org/10.1046/j.1365-3091.1999.00204.x

Piper, D. J. W., Pirmez, C., Manley, P. L., Long, D., Flood, R. D., Normark, W. R., & Showers, W. (1997). Mass-transport deposits of the Amazon Fan. Proceedings of the Ocean Drilling Program, Scientific Results, 155, 109–146.

Pirini Radrizzani, C., Tunis, G., & Venturini, S. (1986): Biostratigrafia e paleogeografia dell'area sud-occidentale dell' anticlinale M. Mia – M. Matajur (Prealpi Giulie). Rivista Italiana di Paleontologia e Stratigrafia, 92 (3), 327-382.

Placer, L., 1981. Geološka zgradba jugozahodne Slovenije = Geologic structure of southwestern Slovenia. Geologija 24 (1), 27–60.

Placer, L., 1998. Contribution to macrotectonic subdivision of the border region between Southern Alps and External Dinarides = Prispevek k makrotektonski rajonizaciji mejnega ozemlja med Južnimi Alpami in Zunanjimi Dinaridi. Geologija 41, 223–255.

Placer, L., Vrabec, M., Celarc, B., 2010. The bases for understanding of the NW Dinarides and Istria Peninsula tectonics = Osnove razumevanja tektonske zgradbe NW Dinaridov in polotoka Istre. Geologija 53 (1), 55–86.

Pleničar, M., Jurkovšek, B., & Buser, S. (2001). Redeposited rudists in Paleocene flysch near Anhovo (Slovenia). Geologija, 44(1), 115–136. https://doi.org/10.5474/geologija.2001.009

Ponton, M. (1986). Modello tettonico dell'area a sud dell'abitato di Monteaperta. Gortania, 7, 41–54.

Pirini Radrizzani, C., Tunis, G., & Venturini, S. (1986). Biostratigrafia e paleogeografia dell'area sud-occidentale dell'anticlinale M. Mia - M. Matajur (Prealpi Giulie). Rivista Italiana di Paleontologia e Stratigrafia, 92(3), 291–324. https://doi.org/10.54103/2039-4942/13279

Ponton, M. (1985). Morfogenesi di una cavità in flysch carbonatico (Grotta Pod Lanisce, Fr. 573 - Friuli orientale). Gortania, Atti Museo Friulano di Storia Naturale, 6, 59-82.

Raymond, L.A. (1984). Classification of mélanges: in Raymond, L.A., (Ed.) Mélanges: Their Nature, Origin, and Significance: Geological Society of America Special Paper, 198, 7-20. https://doi.org/10.1130/SPE198-p7

Ross, P.-S., Bourke, A., Fresia, B. (2014). Improving lithological discrimination in exploration drill-cores using portable X-ray fluorescence measurements: (1) Testing three Olympus Innov-X analysers on unprepared cores. Geochemistry: Exploration, Environment, Analysis, 14, 171–185. https://doi.org/10.1144/geochem2012-163

Rožič, B., Šmuc, A., 2011. Gravity flow deposits in the Toarcian Perbla Formation (Slovenian Basin, NW Slovenia). Rivista Italiana di Paleontologia e Stratigrafia 117, 283–294.

Rožič, B. (2005): Albian - Cenomanian resedimented limestone in the Lower flyschoid formation of the Mt. Mrzli Vrh Area (Tolmin region, NW Slovenia). Geologija, 48 (2), 193-210.

Rožič, B., Popit, T. (2006): Resedimented Limestones in Middle and Upper Jurassic Succession of the Slovenian Basin. Geologija, 49, 219-234.

Rožič, B., Reháková, D., 2024. Sedimentology and biostratigraphy of the Biancone Limestone Formation of the Tolmin Basin (Southern Alps, NW Slovenia). Cretaceous Research 163, 105958. https://doi.org/10.1016/j.cretres.2024.105958

Santa Catharina, A., Kneller, B.C., Marques, J.C. et al. Timing and causes of forest fire at the K–Pg boundary. Sci Rep 12, 13006 (2022). https://doi.org/10.1038/s41598-022-17292-y

Satake, K. (2012). Tsunamis generated by submarine landslides. Submarine Mass Movements and Their Consequences, 475–484. https://doi.org/10.1007/978-94-007-2162-3_42

Sartorio, D., Tunis, G., & Venturini, S. (1987). Nuovi contributi per l'interpretazione geologica e paleogeografica delle Prealpi Giulie (Friuli orientale): Il pozzo Span. Memorie della Società Geologica Italiana, 38, 73–85.

Schmidt, K., Autenrieth, D., & Nagisetty, R. (2024). A Comparison of Field Portable X-Ray Fluorescence (FP XRF) and Inductively Coupled Plasma Mass Spectrometry (ICP-MS) for Analysis of Metals in the Soil and Ambient Air. Research Square Preprint, 1-19. https://doi:10.21203/rs.3.rs-3849271/v1

Shanmugam, G. (2006). The Tsunamite Problem. Journal of Sedimentary Research, 76, 718–730. https://doi.org/10.2110/jsr.2006.073

Shanmugam, G. 2021. Mass Transport, Gravity Flows, and Bottom Currents. Elsevier. doi:10.1016/C2019-0-03665-5.

Shiki, T., & Cita, M.B. (2008) Chapter thirteen - Tsunami-related sedimentary properties of Mediterranean homogenites as an example of deep-sea tsunamiite. In: T. Shiki, Y. Tsuji, T. Yamazaki, K. Minoura (Eds.) Tsunamiites. Elsevier, 203-215. https://doi.org/10.1016/B978-0-444-51552-0.00013-8

Shiki, T., Tachibana, T., Fujiwara, O., Goto, K., Nanayama, F.,& Yamazaki, T. (2008). Characteristic Features of Tsunamiites. In T. Shiki, Y. Tsuj, K. Minoura, & T. Yamazaki (Eds.), Tsunamiites - Features and Implications (1st ed). Elsevier. 319–340.

Shiki, T., and T. Yamazaki. 2008. 'The Term "Tsunamiite"'. In Tsunamiites, Elsevier, 5–7. https://doi.org/10.1016/B978-0-12-823939-1.00002-1

Shipp, R. C., Nott, J. A., & Newlin, J. A. (2004). Physical characteristics and impact of mass transport complexes on deepwater jetted conductors and suction anchor piles. Offshore Technology Conference. https://doi.org/10.4043/16751-MS

Skaberne, D. (1987). Geological investigations in the Anhovo area, western Slovenia. In E. Colizza, R. Costa, F. Cucchi, & N. Pugliese (Eds.), International Symposium on the Evolution of the Karstic Carbonate Platform (pp. 123–130). Udine: Università di Trieste.

Silver, E.A., & Beutner, E.C. (1980) Mélanges. Geology, 8, 32-34.

Šmuc, A., 2005. Jurassic and Cretaceous Stratigraphy and Sedimentary Evolution of the Julian Alps, NW Slovenia. Založba ZRC Publishing, Ljubljana, Slovenia (98 pp.).

Strasser, M., Moore, G.F., Kimura, G., Kopf, A.J., Underwood, M.B., Guo, J., & Screaton, E.J. (2011). Slumping and mass transport deposition in the Nankai fore arc: Evidence from IODP drilling and 3-D reflection seismic data. Geochemistry Geophysics Geosystems, 12, 2010GC003431. https://doi.org/10.1029/2010GC003431

Tappin, D. R., Watts, P., & Grilli, S. T. (2008). The Papua New Guinea tsunami of 17 July 1998: Anatomy of a catastrophic event. Natural Hazards and Earth System Sciences, 8(2), 243–266. https://doi.org/10.5194/nhess-8-243-2008

Tappin, D. R. 2010. 'Submarine Mass Failures as Tsunami Sources: Their Climate Control'. Philosophical Transactions of the Royal Society A: Mathematical, Physical and Engineering Sciences 368(1919): 2417–34. doi:10.1098/rsta.2010.0079.

Tappin, D.R., Grilli, S.T., Harris, J.C., Geller, R.J., Masterlark, T., Kirby, J.T., Shi, F., Ma, G., Thingbaijam, K.K.S., & Mai, P.M. (2014). Did a submarine landslide contribute to the 2011 Tohoku tsunami? Marine Geology 357, 344–361. https://doi.org/10.1016/j.margeo.2014.09.043

Taramelli, T. (1881). Carta geologica del Friuli. Atti della Reale Accademia dei Lincei, Serie 3, 9, 513–533.

Tellini, A. (1891). Studi geologici sulle Alpi Carniche occidentali. Atti dell'Accademia Gioenia di Scienze Naturali in Catania, Serie 4, 4, 1–104.

Tripsanas, E.K., Piper, D.J.W., Jenner, K.A., & Bryant, W.R. (2008). Submarine mass-transport facies: new perspectives on flow processes from cores on the eastern North American margin. Sedimentology, 55, 97–136. https://doi.org/10.1111/j.1365-3091.2007.00894.x

Tunis, G., & Venturini, C. (1984). Il flysch cretacico del bacino del Natisone (Prealpi Giulie meridionali). Giornale di Geologia, 46(1–2), 69–88.

Tunis, G., & Venturini, C. (1987). Stratigrafia e sedimentologia del Flysch di Grivò (Paleocene sup.–Eocene inf.) delle Valli del Natisone (Prealpi Giulie meridionali). Rendiconti della Società Geologica Italiana, 9, 17–22.

Tunis, G., & Venturini, C. (1988). Evoluzione paleogeografica e tettonica del bacino del Natisone (Alpi Giulie meridionali) durante il Paleogene. Memorie di Scienze Geologiche, 40, 231–241.

Tunis, G., & Venturini, C. (1992). The carbonate megabeds of the Julian Basin (Natisone Valleys, eastern Friuli). Eclogae Geologicae Helvetiae, 85(3), 735–754.

Urgeles, R., Camerlenghi, A., 2013. Submarine landslides of the Mediterranean Sea: Trigger mechanisms, dynamics, and frequency-magnitude distribution. Journal of Geophysical Research, Earth Surface, 118, 2600–2618. https://doi.org/10.1002/2013JF002720

Venzo, S., & Brambati, A. (1969). Il Flysch di Manzano (Friuli orientale). Memorie degli Istituti di Geologia e Mineralogia dell'Università di Padova, 27, 1–40.

Venturini, S., & Tunis, G. (1989). Nuovi dati ed interpretazioni sulla tettonica del settore meridionale delle Prealpi Giulie e della regione al confine tra Italia e Iugoslavia. Memorie di Scienze Geologiche, 41, 411–422.

Venturini, S., & Tunis, G. (1992). Nuovi dati stratigrafici, paleoambientali e tettonici sul Flysch di Cormons (Friuli orientale). Gortania, 13, 23–42.

Venturini, S., & Tunis, G. (1996). Riflessioni sulla fase tettonica mesoalpina nel Sudalpino orientale. Memorie di Scienze Geologiche, 48, 159–170.

Visintini, M. (1980). Elenco delle Pietre Piasentine nel Museo Archeologico Nazionale di Cividale. In Forum Iulii, Annuario del Museo Archeologico Nazionale di Cividale del Friuli, 4, 35–40.

Vlahović, Igor, Josip Tišljar, Ivo Velić, and Dubravko Matičec. 2005. 'Evolution of the Adriatic Carbonate Platform: Palaeogeography, Main Events and Depositional Dynamics'. Palaeogeography, Palaeoclimatology, Palaeoecology 220(3–4): 333–60. doi:10.1016/j.palaeo.2005.01.011.

Vrabec, M., Šmuc, A., Pleničar, M., & Buser, S. (2009). Geological evolution of Slovenia—An overview. In M. Pleničar, O. Nojan, M. Novak, & S. Pirc (Eds.), The Geology of Slovenia. Geološki zavod Slovenije. Chapter 1.

Vuerich, F. (1969). Analisi mineralogica dei flysch del settore orientale del Friuli. Rivista Italiana di Paleontologia e Stratigrafia, 75(4), 1165–1176.

Wagen, L. (1898) Geological Map of the Austro-Hungarian Empire; Geographical area: Northern Adriatic; Serie: Geologische Specialkarte der im Reichsrate Vertretenen Konigreiche und Lander der Osterreichisch - Ungarischen Monarchie neu aufgenommen und herausgegeben durch die k. k. Geologische Reichsanstalt; Institution:K.K Geologischen Reichsanstalt

Weimer, P., & Shipp, R. C. (2004). Mass transport complex: Musing on past uses and suggestions for future directions. Offshore Technology Conference. https://doi.org/10.4043/16752-MS

Zakšek, K., Oštir, K., Kokalj, Ž. (2011). Sky-View Factor as a Relief Visualization Technique. Remote Sensing, 3, 398–415.

Zhang, Y., Pe-Piper, G., Piper, D.J.W., 2013. Sediment geochemistry as a provenance indicator: Unravelling the cryptic signatures of polycyclic sources, climate change, tectonism and volcanism. Sedimentology 61, 383–410.

Geological Map

Geological Map of the Julian Basin MTDs between Iudrio and Isonzo Valleys

Andrea Gianese. PhD thesis

UNIVERSITY OF TRIESTE

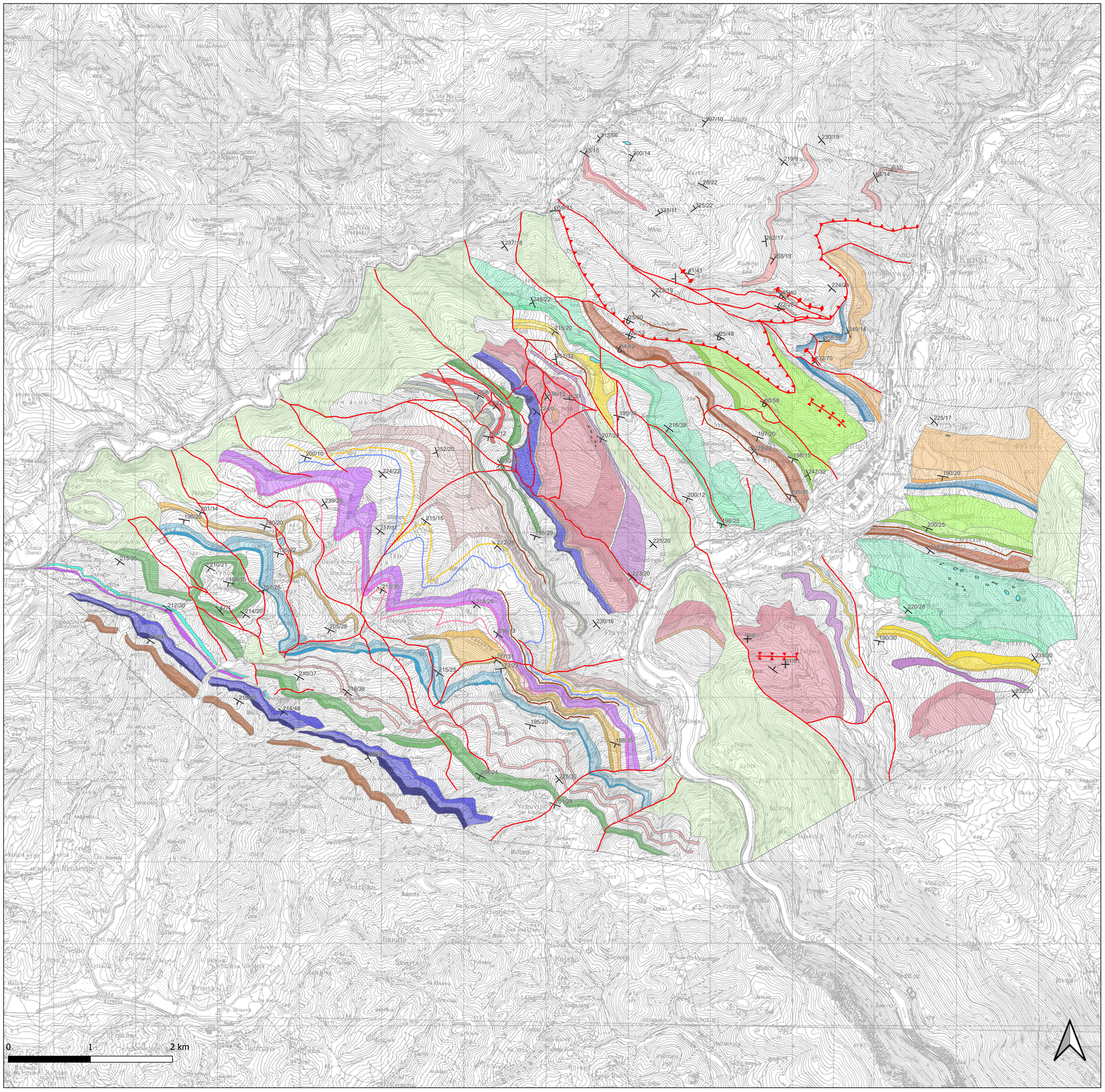

Legend:

MTD 21: U5, U3-4, U1-2
MTD 20: U5, U3-4, U1-2
MTD 19: U1-5
MTD 18: U1-5
MTD 17: U5, U3-4, U1-2
MTD 16: U5, U3-4, U1-2
MTD 15: U5, U3-4, U1-2
MTD 14bis
MTD 14: U5, U3-4, U1-2
MTD 13
MTD 12
MTD 11: U5, U3-4, U1-2
MTD 10: U5, U3-4, U1-2
MTD 9: U1-5, U5, U3-4, U1-2
MTD 8: U5, U3-4, U1-2
MTD 7: U5, U3-4, U1-2
MTD 6: U5, U3-4, U1-2
MTD 5: U1-5, U5, U3-4, U1-2
MTD 4: U5, U3-4, U1-2
MTD 3: U5, U3-4, U1-2
MTD 2bis: U5, U3-4, U1-2
MTD 2: U5, U3-4, U1-2
MTD 1bis: U5, U3-4, U1-2
MTD 1: U5, U3-4, U1-2

Other MTDs: U1-5, U5
Other MTDs: U3-4, U1-2

Others beds from hyperconcentrated flows and turbidites

Olistoliths

Platform and platform margin carbonates (Cretaceous)

Bedding
Horizontal Bedding
Reverse Bedding
Fault
Thrust Surface
Anticlinal Axis
Syncline Fold

Limit of the Area

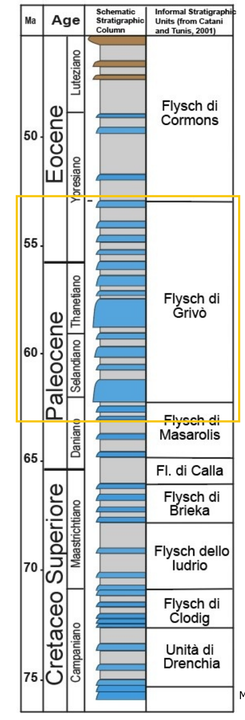

Age of the Main MTDs Sequence

Modified from Ogata et al. (2014)